

# UC Berkeley

## UC Berkeley Electronic Theses and Dissertations

### Title

The Effects of X-Ray Radiation on Epithelial Tissue: Insights from Single-Cell Transcriptomics in *Drosophila melanogaster*

### Permalink

<https://escholarship.org/uc/item/98c6h3sd>

### Author

Cruz, Joyner

### Publication Date

2024

Peer reviewed|Thesis/dissertation

The Effects of X-Ray Radiation on Epithelial Tissue: Insights from Single-Cell  
Transcriptomics in *Drosophila melanogaster*

By

Joyner Cruz

A dissertation submitted in partial satisfaction of the

requirements for the degree of

Doctor of Philosophy

in

Molecular and Cell Biology

and the Designated Emphasis

in

Computational and Genomic Biology

in the

Graduate Division

of the

University of California, Berkeley

Committee in charge:  
Professor Iswar Hariharan, Chair  
Professor Peter Sudmant  
Professor Diana Bautista  
Professor Donald Rio

Fall 2024



## Abstract

# The Effects of X-Ray Radiation on Epithelial Tissue: Insights from Single-Cell Transcriptomics in *Drosophila melanogaster*

by

Joyner Cruz

Doctor of Philosophy in Molecular and Cell Biology

and the Designated Emphasis in Computational and Genomic Biology

University of California, Berkeley

Professor Iswar Hariharan, Chair

X-ray radiation is a damaging form of energy with the potential to disrupt virtually all cellular processes by inflicting broad, indiscriminate damage to the macromolecules that drive them. Despite its relatively non-specific effects, it has long been observed that different cell types, tissues, and organisms have differing responses to X-rays. Mounting evidence suggests that the source of this variability is diverse, and our understanding of its causes remains incomplete.

Some characteristics are generally predictive of the outcome of tissues exposed to X-rays, such as the state of proliferation, oxygenation, and cell cycle status of the cells that comprise them. This knowledge informs the treatment of cancers with radiotherapy which, for example, is thought to disproportionately kill cancers due in part to their abnormal proliferative state. However, these characteristics are inadequate to fully account for the variability of X-ray responses observed in different tissue targets, an observation made yet more complex by the fact that tissues frequently consist of heterogeneous cell populations which themselves may have variable X-ray responses.

Cumulative research, particularly in the field of cancer biology, has revealed that this variability is often associated with differences in the transcriptomes of irradiated cells. For example, some cancers that are resistant to killing by radiotherapy have been shown to have elevated expression of damage ameliorating genes involved in processes such as DNA damage repair. Moreover, tumors consisting of heterogeneous cell populations may grow resistant to irradiation during fractionated therapy through the unintended selection of cells with bolstered expression of radiation protective genes.

Collectively, much work has been conducted on X-ray induced changes in gene expression in several systems ranging from human tumors to fruit fly embryos. However, the limitations of the sequencing methodologies employed in these studies prevented deep analysis of intratissue differences in X-ray response and the transcriptional states associated with them. The rise of single-cell RNA sequencing (scRNA-seq) technologies has made it possible to perform these analyses by allowing for the single-cell origin of transcripts to be retained during sequencing. In this work, we use the wing imaginal disc, a simple epithelial tissue found within the larvae of *Drosophila melanogaster*, to study the effects of X-rays on the transcriptomes of different cells within the same tissue.

In Chapter 1, I provide a summary of conserved molecular pathways that are integral to X-ray response, centered around DNA damage, and provide an overview of the factors that influence the sensitivity of cells to irradiation. I then place the work presented here within the context of past studies on the transcriptomic changes that occur after X-ray exposure in *Drosophila* and more recent scRNA-seq studies in mammalian tissues. Finally, I summarize the technology of scRNA-seq and its relevance to this work.

In Chapter 2, I present our primary findings. We use scRNA-seq to describe the major transcriptional changes induced by X-ray irradiation in different regions of the tissue and uncover two categories of transcriptional states present in the wing disc that are associated with variable X-ray induced gene expression. First, we find that transcriptional states associated with cell location in the proximodistal axis of the tissue are associated with the induction of different genes. Second, we find that transcriptional states defined by cell cycle genes are associated with varying levels of X-ray induced gene expression, with those cells likely invoking a G2/M cell-cycle arrest having the largest average X-ray gene induction. We also adapt the Herfindahl-Hirschman Index, a measure used in the field of economics to assess market concentration, to rank genes in terms of their expression homogeneity. Using this method, we find that genes involved in core damage response pathways are relatively homogeneous across cell clusters when compared to certain ligands and transcription factors.

# Table of Contents

Abstract.....	1
Table of Contents.....	i
List of Figures.....	iii
List of Tables.....	iv
Acknowledgement.....	v
Author Contributions.....	viii
<b>1 Introduction.....</b>	<b>1</b>
1.1 Molecular Mechanisms of X-Ray Response.....	2
1.2 IR Induced p53 Dependent Transcriptional Changes.....	8
1.3 General Variation in X-ray response.....	9
1.4 Transcriptomic Studies on the Effects of Ionizing Radiation in <i>Drosophila</i> .....	11
1.5 Overview of scRNA-Seq.....	13
1.6 Findings from scRNA-seq in Irradiated Mammalian Tissues.....	14
1.7 Significance of the Present Study.....	16
1.8 Chapter 1 References.....	18
<b>2 Single cell transcriptomics of X-ray irradiated <i>Drosophila</i> wing discs reveal heterogeneity related to cell-cycle status and cell location.....</b>	<b>30</b>
2.1 Abstract.....	31
2.2 Introduction.....	32
2.3 Results.....	34
2.3-1 X-ray irradiation induces widespread DNA damage and reduced mitoses and DNA synthesis in the wing disc.....	34
2.3-2 Cells of irradiated and unirradiated wing discs are transcriptomically stratified across its proximodistal axis.....	37
2.3-3 X-ray induced genes involved in apoptosis, DNA damage response, and reaction to reactive oxygen species are relatively homogeneous across the disc after irradiation.....	42
2.3-4 PDGF/VEGF, Toll, and JAK/STAT pathway ligands are enriched heterogeneously in the wing disc after X-ray irradiation.....	53
2.3-5 Transcription factors <i>Dif</i> and <i>Ets21C</i> are enriched heterogeneously in the wing disc, while <i>p53</i> , <i>Irbp18</i> , and <i>Xrp1</i> are relatively homogenous.....	61
2.3-6 Cell cycle centric clustering of cells reveals an emergent, high <i>trbl</i> cell cycle state with enriched expression of several secreted signaling genes.....	66
2.3-7 Simultaneously visualizing two levels of heterogeneity.....	75
2.4 Discussion.....	77
2.5 Materials and Methods.....	82

2.6 Acknowledgements .....	87
2.7 Chapter 2 References.....	88

# List of Figures

## Chapter 1, Introduction:

<b>Figure A:</b> <i>Drosophila</i> Wing Imaginal Disc and Adult Structures .....	10
--	----

## Chapter 2, Paper Title:

<b>Figure 1:</b> Effects of X-ray irradiation of DNA damage, apoptosis and cell-cycle progression.....	36
<b>Figure 2:</b> Territories of the wing disc shown by immunofluorescence and UMAP plots .....	39
<b>Figure S2_1:</b> UMAP plots of Top Cluster Markers by Region .....	41
<b>Figure 3:</b> Heterogeneity of gene expression across the wing disc following radiation exposure.....	45
<b>Figure S3_1:</b> Histogram of cluster HHI scores, Broad Region HHI scores, and Euclidean Expression Distance scores.....	47
<b>Figure S3_2:</b> Proportion mRNA heatmaps of Ligands and Transcription Factors .....	48
<b>Figure S3_3:</b> Proportion mRNA heatmaps of Apoptosis, ROS, Cell Cycle, and DDR Genes.....	49
<b>Figure S3_4:</b> Proportion mRNA heatmaps of Kinase, Phosphatase, and Receptor Genes.....	51
<b>Figure S3_5:</b> Examples of Genes Spanning Range of Expression Distance Score .....	52
<b>Figure 4:</b> X-ray-induced expression of genes encoding ligands.....	56
<b>Figure S4_1:</b> Toll and PDGF/VEGF ligands and receptors.....	58
<b>Figure S4_2:</b> JAK/STAT receptors and TNF ligands and receptors .....	60
<b>Figure 5:</b> X-ray Induced Expression of Transcription Factors.....	63
<b>Figure S5_1:</b> High mag images of dysf HCR and increased p53 and Xrp1 gain.....	65
<b>Figure 6:</b> Visualization of expression changes using cell-cycle-based clustering .....	69
<b>Figure S6_1:</b> Cluster tree showing cluster composition at different clustering resolutions .....	71
<b>Figure S6_2:</b> Dendrogram of cell cycle based cluster relationships.....	73
<b>Figure 7:</b> Differences in gene expression between cell cycle clusters .....	74
<b>Figure 8:</b> HHI scoring of categorical genes in standard clusters vs cell cycle clusters .....	76
<b>Figure 9:</b> Two types of heterogeneity following X-ray irradiation.....	81

## List of Tables

All tables in this thesis, other than Table A, are associated with Chapter 2 and can be downloaded as supplementary files on the Biovrix webpage hosting our preprint:

DOI: <https://doi.org/10.1101/2024.12.10.627868>

**Table A:** Studies examining genome wide transcriptomic changes in *Drosophila* after exposure to ionizing radiation..... 12

**Table S2\_T1:** Top Markers for each subcluster

**Supplement S3\_T1.** DEG 4000 rads vs 0 rads

**Supplement S3\_T2.** Apoptosis, DNA damage response (DDR), response to reactive oxygen species (ROS), cell cycle regulation, transcription factors (TFs), phosphatases, kinases, ligands, and receptors genes considered for SC-HHI comparison (pre-filter)

**Supplement S3\_T3.** Apoptosis, DNA damage response (DDR), response to reactive oxygen species (ROS), cell cycle regulation, transcription factors (TFs), phosphatases, kinases, ligands, and receptors genes considered for SC-HHI comparison (post-filter)

**Table S6\_T1.** Cell Cycle Gene Markers for Cell Cycle Based Clusters

**Table S7\_T1.** X-ray Induced Gene Markers for Cell-Cycle Based Clusters

## **Acknowledgements**

### **Support from Iswar Hariharan**

During my time with Iswar, I have seen him handle a number of considerable challenges. During the pandemic, he re-situated his lab to operate virtually and in a supportive capacity, with the well being of his trainees as priority. During his time as co-chair, during which a heated university wide strike took place, he supported his trainees' personal decisions in the matter, and kept his word. These are not to mention the challenges inherent to the academic career, which are stressful to an extent that cannot be understated. In all cases, I have seen him act with integrity and consideration for those impacted by his decisions, something which I greatly respect.

As for science, I would say his approach contains a layer of humility. When discussing unknowns, he seems to take for granted that he indeed could be wrong, and someone else right. This invites discussion. He does not expect perfection from his trainees, for his awareness of mistakes that he himself or others have made in the past; I have not once felt uncomfortable telling him of my mistakes or shortcomings in the work. This, in my opinion, is a powerful thing.

In addition to the above, I would also like to thank Iswar for his flexibility and understanding. Like everyone else, life has at times presented me with obstacles that are far outside of the realm of my occupation. Even in such cases, Iswar has extended compassion to my circumstances and accommodated how he could, which I am deeply grateful for.

### **Support from past members of the Hariharan Lab**

Danielle Spitzer: Danielle was a great source of support and reassurance during graduate school. I consider her a wise and honorable person. She thought deeply about many issues and would take the time to offer me advice when asked.

Nicholas Everetts: When I joined the lab, I soon knew that I wanted to do what Nick did. He has a great ability to convey complicated concepts simply, and I consider him a great teacher. I still call upon his explanations in my current work.

Sophia Friesen: Sophie was a kind and encouraging presence in lab and always took the time to find out what was going on in other's lives. I am grateful to have had them as a more senior graduate student in lab during my thesis work.

Melanie Worley: Melanie has always offered thoughtful and enthusiastic feedback on my work in the lab.

Jamie Lahvic: Jamie was my rotation mentor in the Hariharan lab and committed herself to it completely. I appreciate her support.

### **Those who worked with me on this project**

William Sun: William began working with me during my last year as a graduate student. William brought much needed new energy to the project at its later stages and worked hard to bring new knowledge to our endeavor.

Alexandra Verbeke: Alex also began working with me during my last year of graduate school. Her work validated many of our single-cell results, significantly bolstering findings in Chapter 2

I also thank William and Alex for making work more pleasant and giving me plenty to laugh about.

### **Support from other peers during my graduate career:**

Shaina Carroll and Justin Williams: Shaina and Justin are my dear friends. Sometimes, they feel like family away from home. I thank them for all their support throughout the years.

Stephan Uwe Gerlach: Stephan is one of the most thoughtful people I know. I thank him for his support during some rocky times in graduate school.

### **Support from other faculty during my graduate career:**

Diana Bautista: Diana was one of my interviewers for entry into the MCB program. Since then, she has been a kind of role model for me. Diana has offered me advice on career, teaching, and life more generally. I admire her for her approach to teaching.

Peter Sudmant: Peter has generously offered support and advice regarding graduate school, and was exceptionally open to my technical questions regarding computational analyses. Much of what I learned during his course on quantitative approaches to biology I put into practice, and influenced the work in Chapter 2.

I also thank Don Rio for his input on the work in Chapter 2 and for generously sharing reagents with me.

**Support from those before my graduate work:**

Linda Huang: Linda, at UMass Boston, was the first faculty member to believe in me and advocate for my success. She introduced me to research biology. I thank her for all of her support. I admire her skeptical approach to science.

Stephanie Cronin: Stephanie was my first direct mentor as an undergraduate. She has offered support through the years, even after I finished my undergraduate studies.

Paul Garrity: Paul, at Brandeis, was one of my first role models in science. I deeply admire his way with people. I still carry with me some of his approach to science.

**I thank those dear to me outside of work**

My Brother: For his generosity, kind heart, and endless support.

My Mother: For supporting me through college and showing me that change is possible at any stage in life, even when what you're given makes that hard.

Robin: For taking me in during uncertain times. For showing me a gentler way of looking at life.

Lisa: For being herself. For encouraging me to take better care of myself and for being there thick or thin.

I would also like to thank Nic, Trevor, and Keeana for their valued support and care.

## Author Contributions

The primary conceptual design of the work and manuscript described in Chapter 2 was a collaboration between **Iswar Hariharan** and **Joyner Cruz**.

**William Sun** conducted most experiments reported in figure 2.1 (2.1D-2.1M). William also conducted many experiments not reported here that contributed to the direction of this project.

**Alexandra Verbeke** conducted hybridization chain reaction experiments reported in Chapter 2. Alexandra also made significant proofreading contributions the manuscript reproduced in Chapter 2.

Chapter 2 is a reproduction of the following preprint, and includes significant contributions from all its authors:

*Single cell transcriptomics of X-ray irradiated Drosophila wing discs reveals heterogeneity related to cell-cycle status and cell location*

Joyner Cruz<sup>1</sup> , Willam Y. Sun<sup>1</sup> , Alexandra Verbeke<sup>1</sup> , and Iswar K. Hariharan<sup>1</sup> \*  
DOI: <https://doi.org/10.1101/2024.12.10.627868>

# **Chapter 1**

## **Introduction**

## 1.1 Molecular Mechanisms of X-Ray Response

Ionizing radiation (IR) is a damaging form of energy present in trace amounts in many environments and which is used at high doses in the form of X-rays to treat cancers (Baskar et al., 2012). X-rays damage living tissues and the cells comprising them in two ways. First, X-rays can ionize integral components of the cell through direct incidence. Second, X-rays can split water, thereby generating reactive oxygen species (ROS) which go on to participate in destructive reactions throughout the cell. Both means of damage can result in DNA breaks and protein damage (Hubenak et al., 2014) that have the potential to disrupt virtually every system in a cell. At the cellular level, there are four broad processes integral to X-ray response: 1) Sensing: The cell senses damage inflicted upon it. 2) Pausing: The cell pauses normal processes, such as proliferation 3) Repair/Homeostatic Restoration: The cell repairs inflicted damage and restores its milieu. 4) Resolution: The cell resumes its normal activities, becomes senescent, or undergoes apoptosis. In this section, I will summarize the key molecules and processes involved in the sensing, repair/homeostatic restoration, pausing, and resolution of IR response that are conserved in *Drosophila melanogaster*. There are many excellent review papers more comprehensively covering the pathways briefly covered in Chapter 1.1. I have drawn heavily upon their syntheses to guide the summaries below. These primarily include the following: (Baonza et al., 2022; Fuchs & Steller, 2011; Ingaramo et al., 2018; Pakos-Zebrucka et al., 2016; Sekelsky, 2017; Wyatt & West, 2014).

### **Sensing:**

#### *Sensing of DNA Damage and Immediate Response*

##### *Double Strand Breaks*

A particularly dangerous form of lesion inflicted upon DNA by X-ray radiation is the double strand break. When the ends of broken double stranded DNA (dsDNA) are exposed, a protein complex consisting of Mre11, Rad50, Nbs1 (the “MRN” complex) is recruited to the site. The interaction between the MRN complex and dsDNA breaks are sufficient to activate two key kinases, ATM and ATR, that act as the first transducers in a breadth of signaling cascades. Once activated, ATM kinase phosphorylates the histone variant H2AX over large stretches of the DNA flanking the break. This phosphorylation triggers the recruitment of DNA repair proteins to the surrounding area.

ATM activates the kinase Chk1, and ATR activates the kinase Chk2. In *Drosophila* The ATR/Chk2 axis modulates several important processes, such as cell death and DNA repair, by activating the master regulator p53 (discussed below) via phosphorylation. It is primarily the ATM/Chk1 axis that regulates cell cycle, though it does not directly interact with p53, unlike it does in mammals (Ingaramo et al., 2018). For review of DNA damage repair, used in this summary, see (Baonza et al., 2022).

### *Other forms of DNA damage*

In addition to double-strand breaks, several other forms of X-ray induced DNA damage with well characterized repair pathways are known to exist. X-rays also generate a variety of single-strand breaks and lesions (Abbotts & Wilson, 2017). Pathways known to repair these forms of damage include the base and nucleotide excision repair pathways, which involve the complete removal and replacement of damaged nucleotides (Huang & Zhou, 2021). These pathways require their own set of specific proteins for their execution, many of which are conserved in *Drosophila*, which I will not cover here. For relevant reviews on single-strand break repair see the following (Abbotts & Wilson, 2017; Huang & Zhou, 2021; Sekelsky, 2017).

### **Pausing:**

#### *Cell Cycle Delay*

In order to allow for sufficient repair to occur after exposure to IR, cells may pause their cycles of replication. Advancement through the cell cycle is centrally controlled by a class of proteins known as cyclins and their catalytic counterparts, the cyclin dependent kinases (CDKs). CDKs are thought to be constitutively expressed throughout the cell cycle, however they remain inactive without their bound cyclins. It is the cyclins themselves that are regulated in their expression, with specific cyclins peaking and depleting at different phases of the cell cycle, reviewed generally in (Vermeulen et al., 2003). In *Drosophila*, Cdk1 together with Cyclin B drives the transition from G2 into mitosis during normal cell cycle progression, but are inhibited by the kinase myt1, which is thought to be dependent on Chk1 (Baonza et al., 2022). This Chk1 dependent delay allows cells to undergo DNA repair processes before entering mitosis. ATM/Chk1 are also required for the intra-S-phase delay induced after irradiation, at least in the larval brain (Jaklevic & Su, 2004).

#### *Pausing of Normal Translation: The Integrated Stress Response*

In addition to a cell cycle pause, cells may change their targets of translation in response to IR. *Drosophila*, like many eukaryotes, are able to rapidly overhaul their translational programs in response to different stressors including IR through the phosphorylation of a single translation initiation factor, eIF2 $\alpha$ ; This translational overhaul is known as the Integrated Stress Response (ISR), wherein cells globally reduce the translation of genes that are non-essential for immediate survival and simultaneously increase the translation of genes that are involved in damage control. The ISR is reviewed in (Pakos-Zebrucka et al., 2016), used in this summary. In unstressed conditions, eIF2 $\alpha$  forms a ternary complex containing the amino acid methionine, which is required to start the translation of a protein. This ternary complex forms part of the preinitiation complex (PIC) that interacts with the 5' caps of mRNA in order to ultimately

load methionine at the start codon, which begins a common form of translation called cap-dependent translation.

eIF2 $\alpha$  is the target of several stress responsive kinases, including those conserved in *Drosophila*: PERK (*PEK* in flies) which responds to stress in the endoplasmic reticulum, and *Gcn2* which responds to amino acid starvation (Pakos-Zebrucka et al., 2016; Pomar et al., 2003). In conditions of stress, eIF2 $\alpha$  is phosphorylated, which prevents the formation of the ternary complex, reducing its overall availability, and therefore reducing overall cap-dependent translation. However, in these very same conditions a small subset of mRNAs that contain interspersed upstream open reading frames (uORFs) simultaneously have an increase in the translation of their gene products. One example of this class of mRNA is that of ATF4 (*crc* in flies), which encodes for a transcription factor with targets involved in stress response. ATF4 contains two uORFs: One uORF overlaps with the ATF4 coding sequence, and the other is further upstream. In unstressed conditions, translation begins at the first uORF, and is able to reinitiate at the second uORF due to the available ternary complex. Because the second uORF overlaps with the coding sequence of the gene product, its translation precludes the translation of the gene product. In stressed conditions, when the availability of the ternary complex is reduced, reinitiation of translation at this second uORF is less likely, allowing instead for reinitiation to occur at the gene coding sequence itself. For another review on the ISR see also (Costa-Mattioli & Walter, 2020).

Though IR has been observed to generate an ISR in mammalian systems, e.g. (Das et al., 2020; B. Zhang et al., 2010), no work examining the effects of IR on the canonical ISR in *Drosophila* have been published. However, there are some findings consistent with the hypothesis that IR may trigger the canonical ISR in *Drosophila*. The *Drosophila* transcription factor *Xrp1* shows increased transcript and protein levels across the wing disc 4h after exposure to IR (Khan & Baker, 2022). *Xrp1* was also found to be induced in “minute” cells that carried mutations in ribosomal subunit genes (Baillon et al., 2018), and in other experiments it was shown that minute clones in the wing disc had reduced levels of overall translation (C.-H. Lee et al., 2018) and highly increased levels of phosphorylated eIF2 $\alpha$ , and that these increased levels of phosphorylated eIF2 $\alpha$  required *Xrp1* (Kiparaki et al., 2022). These data show that *Xrp1* is important for the ISR in conditions of disrupted ribosome biogenesis, which it may also be involved in after IR exposure, where it is highly induced.

Interestingly, some of the IR induced genes known to be p53 dependent (Akdemir et al., 2007) were also found to be *Xrp1* dependent in qRT-PCR experiments after IR. These genes were the ROS gene *GstD1* and the DNA repair genes *rad50*, *mus205*, *Lig4*, *Ku80* (Khan & Baker, 2022). It was also found that overexpression of *Xrp1* itself was

sufficient to drive the expression of the p53 target genes *rpr*, *hid* and *GstD1*, and that disruption of normal *Xrp1* function reduced cell death 2-4h after irradiation, as did disruption of *p53*. These findings suggest that *p53* and *Xrp1* may act together on shared transcriptional targets.

## **Repair/Homeostatic Restoration:**

### **DNA damage repair**

There are two conserved major pathways involved in the repair of double stranded breaks: homologous recombination, and non-homologous end joining. For review in *Drosophila*, used as a reference in this summary, see (Sekelsky, 2017).

#### *Non-Homologous End Joining*

Non-homologous end joining (NHEJ) occurs independently of a repair template through the ligation of two ends of broken DNA, and is relatively low fidelity. NHEJ can occur throughout the cell cycle, though it is thought to be the primary means of repair in the G1 phase of the cell cycle, when repair through HR is unavailable. In NHEJ, the ends of broken DNA are brought together by Ku70 (known as *Irpb* in flies) and Ku80, which together form a protein kinase. The ends of the DNA are then ligated by a complex formed from Lig4, XRCC4 (*CG3448* in flies), and XLF (*CG12728* in flies). Ku80, Ku70, Lig4, XRCC4, and XLF are conserved in humans, however the fly has no known orthologs to human genes involved in end processing, an important step for the ligation of DNA ends that are damaged or contain incompatible overhangs. Despite this, there is evidence for end processing in flies (Sekelsky, 2017).

#### *Homologous Recombination*

During homologous recombination (HR), regions of damaged DNA are repaired using a sister chromatid as a template. Because this process requires a proximal sister chromatid, it is thought to be restricted to the S and G2 phases of the cell cycle. This process is considered relatively high fidelity due to its templated repair. Repair by HR is started with resectioning of the break ends, during which their 5' ends are chewed back to create 3' single stranded overhangs. The MRN complex as well as CtIP (*CG5872* in flies) are required for an initial resectioning phase, which is followed by a longer resectioning phase requiring *Exo1* (*tos* in flies) or *Dna2* and *Blm*. Resection is thought to indicate a commitment to HR over NHEJ. Following resection, the strands undergo a search for homologous sequences along the template DNA which is mediated in *Drosophila* by *Rad51* (*spn-A* in flies) and its paralogs RAD51C and XRCC3 (*spn-D* and *mus301* in flies). Two other *Rad51* paralogs found in flies, *Rad51D* and *Xrcc2*, may be involved as well, though as of 2017 no genetic studies had been conducted to confirm this. Another protein involved in this process is the helicase *Rad54* (*Okr* in flies).

There are several possibilities for how the final structure of interwoven broken DNA ends and template DNA are arranged and ultimately resolved. In holliday junction models, one type of resolution depends upon resolvases that are required to nick both the template and broken DNA at regions of intersection in order for them to be ligated together. In *Drosophila*, *Gen* and *mus81* are resolvases involved in this form of repair. Notably, this type of resolution can create crossing over between template and repaired DNA, which can result in the loss of heterozygosity if a homologous chromosome is used as the repair template. In another form of resolution called dissolution, a topoisomerase complex, composed of Blm and TOP3 $\alpha$  in *Drosophila*, allows for the complementary strands of template and repaired DNA to be pulled apart without the need for DNA nicking. Notably, this can not result in crossover. For visualization of these processes, see (Wyatt & West, 2014).

#### *Factors influencing HR vs NHEJ for DNA Repair*

There are several factors that influence the use of HR vs NHEJ in DNA repair. In one *Drosophila* study, researchers found that age, sex, and tissue type impacted the frequency of HR vs NHEJ events after the induction of double strand breaks (Graham et al., 2024). It was found that tissues that contain populations of cells undergoing a canonical cell cycle (late-stage embryos, wing discs, larval brains) had higher proportions of HR compared to those with non-canonically cycling cells (salivary glands, early embryo) or mostly terminally differentiated cells (adult heads). Authors also found that sex impacts the use of HR vs NHEJ in some cases, as females had reduced relative HR in their premeiotic germline compared to males. Despite the different proportions of HR vs NHEJ undergone in each tissue, both forms of repair were present in every tissue tested.

#### *HR and NHEJ in the Drosophila Transcriptome After Irradiation*

Because genome-wide transcriptomic studies conducted on irradiated tissues in *Drosophila* often did not report all observed changes in gene expression, it is difficult to draw strong conclusions on the absence of HR or NHEJ gene enrichment in different contexts. In one study, 2.5h-5h old embryos were enriched at  $\geq 1.6$  fold with transcripts corresponding to NHEJ (*Ku70*, *Ku80*, *CG3448*), but not those corresponding to HR, 1.5h after exposure to 4000 rads. Because gene changes  $<1.6$  fold were not reported, it is conservative to assume that at the very least, genes involved with NHEJ underwent stronger induction after irradiation than those involved with HR (Akdemir et al., 2007). Another study that was conducted on similarly aged embryos (3h-4h old, 4000 rads, 3h recovery), and reported all changes in transcript abundance, is consistent with these findings. However, certain HR genes such as *Rad51* were also reported to be induced after irradiation at less than 1.6 fold change, with p values  $>0.05$  (C.-Y. Lee et al., 2003). In another study, *Drosophila* wing discs exposed to 4000 rads showed an enrichment of both HR (*Rad51*) and NHEJ (*Ku70*, *Ku80*, *Lig4*) transcripts of greater than 1.5 fold change p values  $<0.005$  at 2 and 18 hours after irradiation. Because the aforementioned

studies on HR vs NHEJ repair rates, as well as transcriptomic studies, were conducted in a bulk fashion on entire tissues, it remains unclear to what extent NHEJ and HR are mutually exclusive at the cellular level.

### **Resolution:**

How the fate of a cell is determined after exposure to IR (and damaging stimuli generally) remains an intensely researched topic. After being damaged by IR, cells may undergo regulated (e.g. apoptosis) or unregulated (e.g. necrosis) cell death, or survive to regain their pre-exposure function. Also described (but sparsely so in *Drosophila*), normally proliferating cells may enter a state of senescence after IR exposure, wherein they cease proliferation and acquire properties normally associated with aging.

### *Apoptosis*

In *Drosophila*, p53 is one of many transcription factors known to converge upon and regulate the transcription of the pro-apoptotic genes *rpr* and *hid*, which trigger a core downstream apoptotic signaling cascade. Indeed, *rpr* and *hid* were found to be upregulated in the hours following a high acute dose of irradiation in the embryo (Akdemir et al., 2007; Brodsky et al., 2004; C.-Y. Lee et al., 2003) and larval wing disc (Van Bergeijk et al., 2012). The products of *rpr* and *hid* inhibit Diap1, a ubiquitin ligase that suppresses the activity of a class of proteases integral to apoptosis known as caspases. The inhibition of Diap1 allows for the derepression of the caspase *Dronc* and its association with *Ark*, which together cleave the caspases *Drice* and *Dcp-1*. *Drice* and *Dcp-1* go on to drive the widespread changes required to carry out apoptosis by cleaving a variety of targets throughout the cell. This general apoptotic program is similar to that found in mammals, with some important distinctions, reviewed here (Denton et al., 2013; Fuchs & Steller, 2011; Steller, 2008; Umargamwala et al., 2024).

Though the cleavage of caspases were thought to be a point of no return in apoptosis, work in the *Drosophila* (as well as work in other systems) has shown that some of the cells that undergo caspase cleavage do not execute apoptosis fully, and go on to survive (Colon Plaza & Su, 2024; G. Sun et al., 2020). In the wing disc, it was found that many of the cells that comprised the tissue one day after irradiation had survived caspase activation, and that their survival depended upon the gene *Ciz1* (G. Sun et al., 2020). It was found in another study that wing disc cells that survive IR induced caspase activation are capable of proliferating and go on to contribute to the adult tissue, and that these cells may repair their DNA more efficiently than cells which had not activated their caspases (Colon Plaza & Su, 2024). These results indicate that the transcript levels of *rpr* and *hid*, and the activation of their downstream targets is not sufficient to predict apoptotic outcome after irradiation.

## 1.2 IR Induced p53 Dependent Transcriptional Changes

A primary means of transcriptomic control occurs at the level of transcription - that is, the regulation of the *amounts* of mRNA created from coding loci across the genome. Integral to this process are transcription factors, proteins which directly bind to gene regulatory sequences and promote or suppress the transcription of certain, often proximal, genes. p53 is an intensely studied transcription factor important for generating a variety of responses to diverse stressors, and is at the center of transcriptional control in response to IR. Important *p53* regulation occurs at the post-translational level, and in *Drosophila* *p53* can be modified via phosphorylation, ubiquitination, and sumoylation. *Chk2* activates *p53* by directly phosphorylating it. The role of p53 in *Drosophila* is reviewed in (Ingaramo et al., 2018), used to guide this summary.

In *Drosophila* embryos, a study utilizing microarrays revealed that the induction/depletion of 76 genes after exposure to gamma radiation depended upon p53 with moderate to strong consistency (Akdemir et al., 2007). Genes that required p53 for normal induction after irradiation included activators of apoptosis (e.g. *rpr*, *egr*, *hid*), negative regulators of apoptosis (*Corp*), DNA repair genes (e.g. *mre11*, *ku70*), those involved in detoxification of reactive oxygen species (*GstD5*), and even p53 itself. Interestingly, the authors found no inter-replicate consistency when examining irradiation induced gene changes in p53 mutants, suggesting p53 is an integral part of coordinated irradiation response. In *Drosophila*, p53 encodes four protein isoforms. Work exploring the effects of two of these isoforms in the wing disc showed that one isoform variant preferentially induced *rpr*, while the other preferentially induced *hid*, suggesting that isoform production provides another layer of p53 regulation in flies (Dichtel-Danjoy et al., 2013).

In mammals, p53 is negatively regulated by the ubiquitin ligase *MDM2*, which tags it for degradation and export from the nucleus. *Drosophila* have no known ortholog to *MDM2*, however expression of the ubiquitin ligase *sip3* was shown to reduce elevated p53 protein levels and apoptosis induced by *p53* overexpression in the wing disc (Yamasaki et al., 2007). *Corp*, which itself depends on *p53* for its induction after IR exposure, is another negative regulator of p53 found in *Drosophila*. In the eye imaginal disc, it was shown that concurrent expression of *Corp* reduced cell death caused by overexpression of *p53*, and that *Corp* mutants had levels of cell death in areas of p53 overexpression that were greater than in wildtype backgrounds. Likewise, when p53 was overexpressed in the eye disc, simultaneous *Corp* expression greatly reduced p53 protein levels, and when p53 was overexpressed in *Corp* mutant backgrounds, p53 protein levels were even more elevated than observed in a wildtype background (Chakraborty et al., 2015).

## 1.3 General Variation in X-ray response

### *General Characteristics Associated with X-Ray Sensitivity and Resistance*

Despite the non-specific nature of X-ray damage, it has long been observed that different types of cells have different outcomes after X-ray exposure. The most dramatic and generalizable of these observations is that some cells die (a property known as radiosensitivity) and some survive (a property known as radioresistance).

Several characteristics are associated with radiosensitivity generally, though none alone are sufficient to predict how any particular cell type will respond to irradiation. Cells that are rapidly proliferating (that is, undergoing complete cell cycles in quick succession) are understood to be more radiosensitive than those which are not (Vogin & Foray, 2013). This effect has been observed in *Drosophila*, where endocycling tissues (tissues undergoing repeated DNA replication without the completion of a full cell cycle) such as the fat body and salivary gland resist IR induced cell death, while fully proliferating tissues like the wing imaginal disc do not (Baonza et al., 2022; Halme et al., 2010). The particular cell cycle phase a cell is in at the time of irradiation is also relevant, with cells in M-phase being most radiosensitive while cells in S-phase are least radiosensitive (Sinclair, 2012; Syljuåsen, 2019).

In addition, higher oxygenation levels increase radiosensitivity, as oxygen readily accepts the electrons liberated from water radiolysis and derivative ROS, which transforms it into destructive superoxide radicals (Holley et al., 2014). These general principles inform the application of X-rays to treat cancer. X-rays are thought to disproportionately kill tumorous tissue, which undergoes accelerated and aberrant proliferation, relative to adjacent healthy tissue. Irradiation is also applied in fractionated doses over several sessions, so as to allow the cells in a tumor to redistribute themselves into radiosensitive cell cycle phases between exposures. Because internal tumor environments are often hypoxic and therefore provide protection to cells within from irradiation, fractionated dosing is also thought to allow surviving tumor cells to redistribute to areas of increased oxygenation between exposures (Pajonk et al., 2010).

### *Genetic Variance and Radiosensitivity*

Of course, the complete set of factors that can contribute to radiation response, alone or together, are far more abundant and complex than those described above. Variation in the sequence or state of DNA at any of the gene or regulatory loci (and by extension, the proteome and transcriptome) involved in x-ray response pathways can alter the outcome to exposure. This type of variation can be found intrinsically between cells, tissues, organs, and organisms, or it can be induced in aberrant cancers.

In the case of many human cancers, abnormal regulation of the transcript abundance of certain genes is associated with the radioresistant properties of the cancer (Balbous et al., 2016; Fu et al., 2019; Z. Sun et al., 2021; Toy et al., 2021; Yard et al., 2016; Young et al., 2014). A central insight from these studies is that genes involved in damage repair/mitigation and the suppression of apoptosis are often more highly expressed in radioresistant cancers than in their radiosensitive counterparts.

### *Other Observations of Heterogeneity in X-Ray Response in Drosophila*

The *Drosophila* wing disc is an example of a tissue that displays intrinsic inter-regional heterogeneity in IR response that can not obviously be attributed to cell cycle status. The wing disc is a larval tissue composed primarily of a simple epithelial layer that develops into the adult wing (Fig. 1.1). After exposure to IR, the distribution of cell death in younger larval discs (from ~4 day old larvae) is unevenly distributed. When assays measuring cell death are performed on the disc after exposure to IR, some contiguous regions have high indicators of death, while some are nearly void of it.

In an exploration of this phenomenon, one group found that IR resistance in one of these death free regions depended on the JAK/STAT and wg signaling pathways normally active in that area. It was also found that *rpr*, but not *hid*, was repressed in a JAK/STAT dependent manner in this region after irradiation, and that ectopically expressing it there reduced radioresistance. Interestingly, the authors demonstrated with lineage tracing experiments that the cells in this region can translocate to another, less resistant part of the disc to compensate for losses there (Verghese & Su, 2016). Though radioresistant heterogeneity can be observed in many studies on wing discs e.g. (Oikemus et al., 2004), the former was the first to explore it as its central focus.

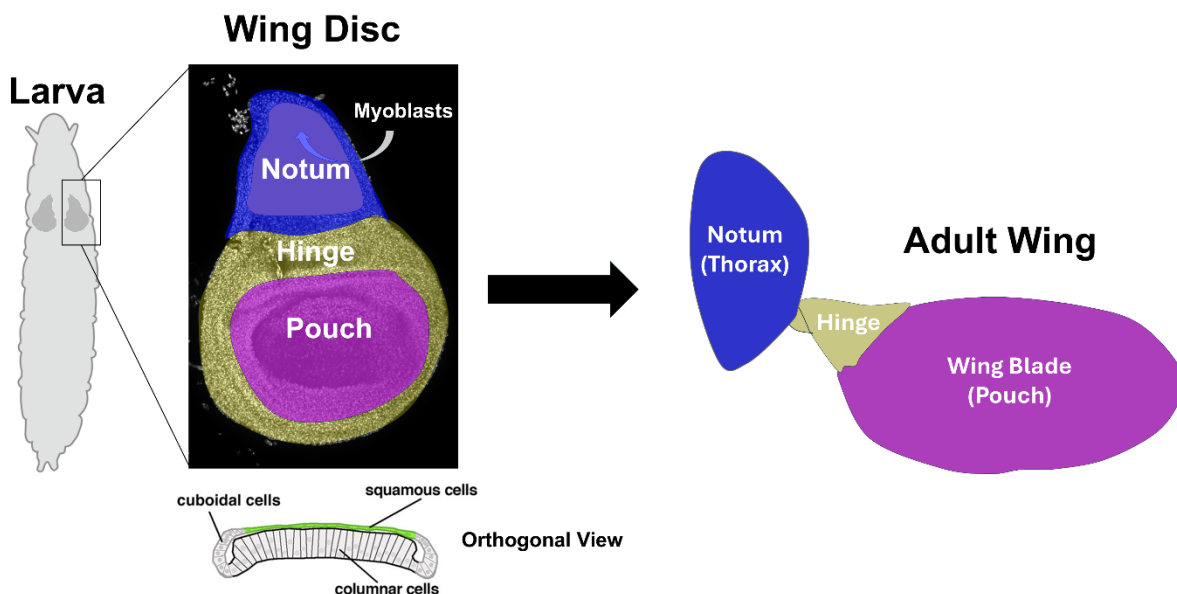


**Figure A** *Drosophila Wing Imaginal Disc and Adult Structures*. The wing disc is an epithelial sac composed of two opposing monolayers found in larvae. The majority of the disc consists of a layer of pseudostratified columnar epithelial cells known as the “disc proper.” The notum, the hinge, and the pouch are the three major regions of the disc proper which contribute to the notum of the adult thorax, wing hinge, and wing blade, respectively. A second, thin layer of squamous epithelial cells opposes the disc proper (see orthogonal view). The wing disc also contains a population of myoblasts that reside under the basal side of the notum and generate the adult flight muscles. Image Credits: Orthogonal illustration of the wing disc comes from (Aldaz et al., 2010) and larval drawing from biorender.com.

## 1.4 Transcriptomic Studies on the Effects of Ionizing Radiation in *Drosophila*

A fundamental apparatus of control used by cells to adapt and respond to their environment is the regulation of their transcriptomes (the totality of mRNAs present in the cell). This regulation can be summarized as the selective increase of the availability of some mRNAs to translation, and the reduction of others. A snapshot of the average transcriptome of cells comprising a tissue can be generated by sampling the total mRNA present in the tissue, determining which gene each encodes for, and counting them. This can be done by directly sequencing cDNA generated from captured mRNA, or by hybridizing it to complementary oligonucleotides of known gene sequences organized in a microarray. In *Drosophila*, both of these approaches have been used to survey the transcriptomic changes that occur after exposure to IR a variety of tissues. Collectively, these studies have shown IR to be a potent inducer of genes involved in the control of cell death, DNA damage repair, detoxification of ROS, and other pathways involved in stress response, repair, and regeneration.

### *Genome Wide Transcriptional Profiling Studies in Drosophila*

At the time of this writing, I am aware of 18 publications that include the generation and analysis of genome-wide changes in transcription induced by IR in *Drosophila*. Across these studies, x-rays, gamma rays, and UV-C were used as sources of IR. One study examined the effects of background radiation, but this is an exception (Zarubin et al., 2021). Of these 18 studies, five were conducted on whole embryos, six on whole adults, two on larval wing discs, two on whole larvae, one on larval brains, one on pupal retinæ, and one on whole adult heads. All experiments were conducted in a bulk fashion using either microarrays or RNA-seq, examining total changes across the entire tissue or organism. In one exception, a subregion of the larval wing disc was first sorted using FACS, allowing for the analysis of subregional changes in gene expression (Ledru et al., 2022). The methods of these studies are summarized in the table below.

Radiation Type	Dose (Rads) Or other	Tissue Sequenced	Type	Recovery Time	Method	Genotype	Reference
X-rays	4000	Larval Wing Disc	Single-Cell	4h	Single-Cell mRNA Sequencing	Wildtype	This Study, 2024
X-rays	4000	Larval Wing Disc	FACS Sorted	24h 48h	RNA seq	Wildtype*	(Ledru et al., 2022)
Cesium Gamma Rays	1000, 40, 40 + 1000	Larval Brain	Bulk	Chronic Low Dose, 4h Challenging Dose	RNA seq	Wildtype, Assumed	(Porrazzo et al., 2022)
Negative Background Radiation	Negative Background Radiation	Whole Adult	Bulk	NA	RNA seq	Wildtype	(Zarubin et al., 2021)
Gamma Rays	4000	Whole Embryo, Adult Heads	Bulk	1.5h	RNA seq	Wildtype, P53 Mutant	(Kurtz et al., 2019)
Gamma Rays	14,400 36,000 86,400	Whole Adult	Bulk	Immediate/ Undescribed	RNA Seq	Wildtype	(Moskalev et al., 2015)
Gamma Rays	10	Whole Larvae	Bulk	Immediate/ Undescribed	Genome Wide Microarray	Wildtype	(Kim et al., 2015)
Cesium Gamma Rays	10 1,000 5,000 10,000 20,000	Whole Adult	Bulk	2 days 10 days 20 days	RNA seq	Wildtype	(Antosh et al., 2014)
Radium Source Gamma Rays	20	Whole Adult	Bulk	Immediate/ Undescribed	RNA seq	Wildtype	(Moskalev et al., 2014)
Cesium	90,656	Whole Adult	Bulk	48h	RNA seq	Wildtype*	(Landis et al., 2012)
X-rays	4000	Larval Wing Disc	Bulk	2h 18h	Genome Wide Microarray	Wildtype, P53 mutant	(Van Bergeijk et al., 2012)
Cesium Gamma Rays	20	Whole Adult (Irradiated Embryos)	Bulk	35 Days	Genome Wide Microarray	Wildtype	(Seong et al., 2011)
Co60 Source Gamma Rays	0.05	Whole Embryo	Bulk	5m, 0.5h, 1h, 1.5h	Microarray	Wildtype*	(Ogura et al., 2009)
Gamma Rays	Undisclosed	Whole Embryo	Bulk	0.25h-0.5h	Microarray	Wildtype*	(Y. Zhang et al., 2008)
Gamma Rays	4000	Whole Embryo	Bulk	1.5h	Genome Wide Microarray	Wildtype, P53 mutant	(Akdemir et al., 2007)
X-rays UV-C	4000 (X-rays) 300 J/m2 (UV-C)	Whole Larvae	Bulk	2h (X-rays) 4h (UV-C)	Microarray	Wildtype, P53 Mutant	(Ujfaludi et al., 2007)
X-rays	4000	Whole Embryo	Bulk	0.25h, 0.5h, 1h, 2h, 4h	Genome Wide Microarray	Wildtype P53 mutant Mnk Mutant	(Brodsky et al., 2004)
Co60 Source	4000	Whole Embryo	Bulk	3h or 4h	Genome Wide Microarray	Wildtype	(C.-Y. Lee et al., 2003)
UV-C	40 000 $\mu$ J/cm2	Pupal Retinae	Bulk	1.5h	Microarray	Wildtype, Assumed	(Jassim, 2003)

**Table A.** *Studies examining genome wide transcriptomic changes in Drosophila after exposure to ionizing radiation.* Blue highlight indicates studies that used similar dosing and recovery periods to those used in the present study. This study is highlighted in gray. Asterisks next to wildtype genotypes indicate that these flies carried mutations or transgenes not expected to impact radiation response.

Five of these studies followed a similar experimental design to our own, administering an acute dose of penetrating IR (x-rays or gamma rays) and examining gene expression in the immediate hours (0.25h-4h recovery) following irradiation. (Akdemir et al., 2007; Brodsky et al., 2004; Kurtz et al., 2019; C.-Y. Lee et al., 2003; Van Bergeijk et al., 2012). Repeatedly, genes involved in apoptotic regulation, DNA damage repair, detoxification of ROS, and JNK pathway regulation were induced in the hours following irradiation, a theme substantiated in our present work.

Importantly, many of the X-ray induced genes uncovered in these studies, even in tissues other than the wing disc, were also found to be induced in our own data, presented at length in Chapter 2. For example, Akdemir et al., 2007 put forth a list of 29 “high stringency” p53 dependent genes that were reproducibly upregulated after X-ray exposure in the embryo. In our own work on the wing disc, 28 of these genes were captured and 21 of them were enriched after X-ray exposure in the wing disc. These included core genes involved in apoptosis (e.g. *hid*, *Corp*) and DNA damage repair (e.g. *mre11*, *Irbp18*, and *Xrp1*). The 7 remaining genes that were not enriched in our own data after irradiation likely reflect differences in the tissues examined or recovery times used.

## 1.5 Overview of scRNA-Seq

### *scRNA-Seq Library Generation*

In recent years, single-cell sequencing technologies have allowed researchers to sample the transcriptomes of tissues while preserving information on the single-cell origin of each transcript. Currently, the most common way to accomplish this is by using droplet-based technologies that utilize microfluidics to separate cells into individual reactions (the most popular likely distributed by 10x Genomics, described here). In brief, tissues are first dissociated into single cells using enzymatic digests. Optionally, this suspension may be FACS sorted to remove unwanted cell populations (e.g. dead cells). This single cell suspension is combined with a master mix required for reverse transcription and loaded into a microfluidics device that aims to generate well-spaced, single-file streams of cells.

These streams of cells meet another stream, this one containing beads in single-file that are coated with the oligonucleotides required to capture and prime the mRNA released from a cell. Importantly, these oligonucleotides contain a cell ID sequence unique to the

bead, and a molecular identifier sequence unique to each oligonucleotide that is incorporated into the final cDNA product. At the confluence of these streams, a single cell and a single bead join, and are partitioned downstream using oil, in which the initial reverse transcription and labeling reaction will take place. Through reverse transcription and PCR amplification, a library of cDNA sequences is generated from across the tissue, each containing a barcode identifying its cell and transcript of origin. This library can then be sequenced at a desired read depth. For a more complete review of single sequencing methods, see (Potter, 2018).

#### *scRNA-Seq Computational Processing*

Once the library is sequenced, sequences are aligned to the transcriptome and counted, generating the basic workable format of scRNA-seq data, the cell by gene count matrix. Each column of the matrix corresponds to one cell, and each row corresponds to each gene. At the intersection of the rows and columns are the total number of transcripts captured of a given gene in each cell.

Typically, the gene counts in this matrix are normalized to the total transcripts captured within each corresponding cell, which helps to eliminate any stochastic variation in the efficiency of transcript capture across cells. To make sense of this matrix, dimensionality reduction is performed (e.g. principal component analysis, scVI), typically on a scaled subset of the most variable genes. The cells are then clustered with various algorithms (e.g. Louvain) in this reduced space, such that cells of the same cluster are more transcriptionally similar to each other than cells of another cluster. If different cell types are present in the data, they will often be grouped into different clusters, which can then be compared to find genes that are differentially expressed between cell types. To visualize cells, their assigned clusters, and their gene expression, another dimensionality reduction technique (e.g. tSNE, UMAP) is applied that is suited for the ample separation of clusters on a two-dimensional plot.

## **1.6 Findings from scRNA-seq in Irradiated Mammalian Tissues**

#### *scRNA-seq of Irradiated Mammalian Tissues and Culture*

To date, no scRNA-seq experiments on irradiated *Drosophila* tissues or cultures have been published, however, several scRNA-seq experiments have been described in irradiated mammalian tissues and culture. These include those conducted on dissociated epithelial tissues, including the scRNA-sequencing of mouse intestines (Ayyaz et al., 2019; Han et al., 2022; Lu et al., 2023; Morral et al., 2024; Sheng et al., 2020; Yuan et al., 2023), fibrotic lungs (Mukherjee et al., 2021), ovaries (Mills et al., 2024), and rat skin (Tu et al., 2022; Y. Zhang et al., 2024), and an experiment on microglia isolated from irradiated mouse brains (Osman et al., 2020). Studies have also

been conducted on cancerous lung tissue and gliomas collected from human patients (Cha et al., 2023; Filbin et al., 2018; Liang et al., 2024) and human cancer derived cell culture lines (Wu et al., 2019).

#### *Heterogeneous Response to IR in the Mouse Ovary*

Mills et al., 2024 examined changes in gene expression in the mouse ovary 6h after exposure to a relatively low dose of 50 rad. Authors recovered 11 cell types in their scRNA-seq data including oocytes, which made up only 1-2% of cells. Their analyses revealed highly heterogeneous IR responses in different cell types within the ovary. Strikingly, though accounting for a small fraction of total cells, oocytes had the greatest reaction to IR, differentially expressing 86 genes in response to X-rays. For comparison, the cell type with the next greatest number of highly IR responsive genes were ovarian epithelial cells, with only 20 enriched/depleted genes. Moreover, when examining the most differentially expressed genes uncovered in previous bulk-seq of the ovary, authors found that the vast majority of them were most differentially expressed in oocyte cells in their irradiated scRNA-seq data. Together, these results show that a small cell population can have an outsized impact on IR induced changes in gene expression when considering the tissue as whole that are obscured in bulk-seq. This is loosely analogous to our own findings in Chapter 2, where we identify cells of a transcriptional state likely associated with cell-cycle arrest has the greatest expression of most X-ray induced genes.

#### *Stem Cell Based Regeneration in the Mouse Gut*

scRNA-seq experiments on irradiated mouse intestines revealed an undifferentiated quiescent cell type termed “revival stem cells (revSCs)” that emerge in the days following acute exposure to IR. revSCs were recognized due to their unique gene expression signatures that were not present in the intestine prior to irradiation (Ayyaz et al., 2019; Lu et al., 2023; Morral et al., 2024). These revSCs were found to be required for intestinal regeneration (Ayyaz et al., 2019), to contribute to the regenerated tissue in lineage tracing experiments, and to depend upon p53 for their generation (Morral et al., 2024). revSCs are derived from and ultimately regenerate crypt base columnar cells, a bonafide stem cell population present in the intestine that sustains the relatively high turnover rate found in the tissue in unstressed conditions (Ayyaz et al., 2019). Together, these findings exemplify a mode of tissue regeneration in the mouse intestine that is largely dependent on a specialized subset of stem/stem-derived cells with distinct transcriptional profiles.

#### *Stem Cell Independent Regeneration of the Wing Disc*

The existence of a true stem cell population in the *Drosophila* wing disc is debatable (for one argument in favor of their existence in resident myoblasts, see (Gunage et al.,

2014)). Regardless, some “stem-cell like” properties are induced in the disc after irradiation; After exposure to x-rays, cells in the hinge of the wing disc can change fate and translocate to help reconstitute other parts of the tissue, especially the pouch (Verghese & Su, 2016, 2018). Though hinge cells are able to change fate in a way that is “stem cell like,” the regenerated wing disc is largely composed of cells that are not derived from this hinge region, suggesting the presence of multiple regenerative cell sources. For instance, the progenitor hinge cells that contribute to the pouch after irradiation contribute only minimally to the notum, a region which makes up a significant portion of the disc (Verghese & Su, 2018). See Fig. 1 for illustration of wing disc regions. In one study, hinge cells were FACS sorted, sequenced, and compared to other cells in the wing disc after irradiation. It was found that hinge cells were enriched for genes involved in ribosome biogenesis and that these genes were required for the translocation of hinge cells into the pouch (Ledru et al., 2022). Beyond this, no unique gene markers clearly demarcating an IR induced stem-cell like population in the hinge were reported. These data are consistent with the notion that the wing disc utilizes a mode of regeneration that does not require a bonafide stem cell population, and which is facilitated by multiple regions throughout the tissue.

## 1.7 Significance of the Present Study

Though scRNA-seq has not yet been conducted on irradiated *Drosophila* tissues, it has been successfully applied to wing discs in the past (Bageritz et al., 2019; Deng et al., 2019; Everetts et al., 2021; Floc’hlay et al., 2023; Worley et al., 2022; Zappia et al., 2020). These studies were conducted on normally developing discs or on discs stressed with genetically induced tumors or blastemas. The only other scRNA-seq study on damaged wing discs examined the transcriptional changes associated with genetically induced cell death targeted to the center of the pouch, with the majority of the tissue not directly impacted by this manipulation (Worley et al., 2022). Many of the transcriptional changes thought to be involved in regeneration occurred almost exclusively in the proximal tissue surrounding the targeted cell death but not elsewhere in the disc. Genes induced in these surrounding tissues include the pro-regenerative transcription factor *Ets21C*, JAK/STAT ligands *upd1*, *upd2*, *upd3*, and *Pvf1*, a ligand involved in wound healing. This form of manipulation generates localized damage, loosely analogous to directed physical wounding, which largely depends upon the surrounding unmanipulated tissue for regeneration.

In the present study, we perform scRNA-seq on normally developing wing imaginal discs and discs irradiated with 4000 rads of x-rays to examine IR induced transcriptional changes across the tissue in the immediate hours following exposure. In contrast to work using the genetic ablation model, our current experiments represent the first scRNA-seq study conducted on wing discs uniformly and ubiquitously damaged by an

exogenous agent. This form of damage challenges the wing disc to recover in its entirety without an available pool of unaffected tissue, a feat which likely requires regulatory mechanisms that are distinct from those induced by localized damage. We focus our attention on the heterogeneity of gene induction after X-ray exposure.

In principle, there are at least two categories of transcription states within tissues that may be associated with heterogeneous irradiation response and should be discernible with scRNA-seq of the wing disc. First, there exist different cell states that define distinct cell types or regions of the tissue. Second, there are states that are common to all cell types and regions of the tissue but are nonsynchronous or present only in a subset of total cells, such as those related to cell cycle. In the present study, we find evidence that both types of transcription states are associated with heterogeneous X-ray response in the wing disc.

First, we find cell states that define different regions of the proximodistal (PD) axis are associated with the induction of different genes. For example, the stress induced transcription factor (TF) *Ets21C*, is preferentially induced in cells belonging to the future wing hinge. Second, using a cell cycle centric clustering approach we also find that cell states related to cell cycle phases, which are interspersed throughout the disc, are associated with the induction of specific genes. In particular, we find that a cell state consistent with G2/M arrested cells is associated with the induction of several secreted proteins, while cell states consistent with S-phase have relatively low expression of many X-ray induced genes. To aid in our analysis of gene expression heterogeneity, we utilize a measure similar to the Herfindahl-Hirschman Index (HHI), typically used in economics to gauge market concentration. We focus our attention on several X-ray induced ligands and TFs belonging to the JAK/STAT, Toll, and PDGF/VEGF related pathways, which are revealed by HHI to be relatively concentrated in their expression pattern.

Our experiments offer insight into the initial transcriptional changes that occur in an undifferentiated, simple epithelial tissue after exposure to IR. This approach provides insight that is distinct from previous scRNA-seq experiments in mammals, which focused on differentiated tissues containing distinct cell types days after exposure to IR. Our findings demonstrate that even across a relatively homogenous tissue, IR induces swift, heterogeneous changes in gene expression, and provides ample targets for genetic manipulation in experiments that can be quickly brought to fruition in *Drosophila*.

## 1.8 Chapter 1 References

- Abbotts, R., & Wilson, D. M. (2017). Coordination of DNA single strand break repair. *Free Radical Biology and Medicine*, *107*, 228–244. <https://doi.org/10.1016/j.freeradbiomed.2016.11.039>
- Akdemir, F., Christich, A., Sogame, N., Chapo, J., & Abrams, J. M. (2007). P53 directs focused genomic responses in *Drosophila*. *Oncogene*, *26*(36), 5184–5193. <https://doi.org/10.1038/sj.onc.1210328>
- Aldaz, S., Escudero, L. M., & Freeman, M. (2010). Live imaging of *Drosophila* imaginal disc development. *Proceedings of the National Academy of Sciences*, *107*(32), 14217–14222. <https://doi.org/10.1073/pnas.1008623107>
- Antosh, M., Fox, D., Hasselbacher, T., Lanou, R., Neretti, N., & Cooper, L. N. (2014). *Drosophila Melanogaster* Show a Threshold Effect in Response to Radiation. *Dose-Response*, *12*(4), dose-response.1. <https://doi.org/10.2203/dose-response.13-047.Antosh>
- Ayyaz, A., Kumar, S., Sangiorgi, B., Ghoshal, B., Gosio, J., Ouladan, S., Fink, M., Barutcu, S., Trcka, D., Shen, J., Chan, K., Wrana, J. L., & Gregorieff, A. (2019). Single-cell transcriptomes of the regenerating intestine reveal a revival stem cell. *Nature*, *569*(7754), 121–125. <https://doi.org/10.1038/s41586-019-1154-y>
- Bageritz, J., Willnow, P., Valentini, E., Leible, S., Boutros, M., & Teleman, A. A. (2019). Gene expression atlas of a developing tissue by single cell expression correlation analysis. *Nature Methods*, *16*(8), 750–756. <https://doi.org/10.1038/s41592-019-0492-x>
- Baillon, L., Germani, F., Rockel, C., Hilchenbach, J., & Basler, K. (2018). Xrp1 is a transcription factor required for cell competition-driven elimination of loser cells. *Scientific Reports*, *8*(1), 17712. <https://doi.org/10.1038/s41598-018-36277-4>
- Balbous, A., Cortes, U., Guilloteau, K., Rivet, P., Pinel, B., Duchesne, M., Godet, J., Boissonnade, O., Wager, M., Bensadoun, R. J., Chomel, J.-C., & Karayan-Tapon, L. (2016). A radiosensitizing effect of RAD51 inhibition in glioblastoma stem-like cells. *BMC Cancer*, *16*(1), 604. <https://doi.org/10.1186/s12885-016-2647-9>

- Baonza, A., Tur-Gracia, S., Pérez-Aguilera, M., & Estella, C. (2022). Regulation and coordination of the different DNA damage responses in *Drosophila*. *Frontiers in Cell and Developmental Biology*, *10*, 993257. <https://doi.org/10.3389/fcell.2022.993257>
- Baskar, R., Lee, K. A., Yeo, R., & Yeoh, K.-W. (2012). Cancer and Radiation Therapy: Current Advances and Future Directions. *International Journal of Medical Sciences*, *9*(3), 193–199. <https://doi.org/10.7150/ijms.3635>
- Brodsky, M. H., Weinert, B. T., Tsang, G., Rong, Y. S., McGinnis, N. M., Golic, K. G., Rio, D. C., & Rubin, G. M. (2004). *Drosophila melanogaster* MNK/Chk2 and p53 Regulate Multiple DNA Repair and Apoptotic Pathways following DNA Damage. *Molecular and Cellular Biology*, *24*(3), 1219–1231. <https://doi.org/10.1128/MCB.24.3.1219-1231.2004>
- Cha, Y. J., Kim, E. Y., Choi, Y. J., Kim, C. Y., Park, M. K., & Chang, Y. S. (2023). Accumulation of plasmacytoid dendritic cell is associated with a treatment response to DNA-damaging treatment and favorable prognosis in lung adenocarcinoma. *Frontiers in Immunology*, *14*, 1154881. <https://doi.org/10.3389/fimmu.2023.1154881>
- Chakraborty, R., Li, Y., Zhou, L., & Golic, K. G. (2015). Corp Regulates P53 in *Drosophila melanogaster* via a Negative Feedback Loop. *PLOS Genetics*, *11*(7), e1005400. <https://doi.org/10.1371/journal.pgen.1005400>
- Colon Plaza, S., & Su, T. T. (2024). Ionizing radiation induces cells with past caspase activity that contribute to the adult organ in *Drosophila* and show reduced Loss of Heterozygosity. *Cell Death Discovery*, *10*(1), 6. <https://doi.org/10.1038/s41420-023-01769-4>
- Costa-Mattioli, M., & Walter, P. (2020). The integrated stress response: From mechanism to disease. *Science*, *368*(6489), eaat5314. <https://doi.org/10.1126/science.aat5314>
- Das, S., Joshi, M. B., Parashiva, G. K., & Rao, S. B. S. (2020). Stimulation of cytoprotective autophagy and components of mitochondrial biogenesis / proteostasis in response to ionizing radiation as a credible pro-survival strategy. *Free Radical Biology and Medicine*, *152*, 715–727. <https://doi.org/10.1016/j.freeradbiomed.2020.01.015>

- Deng, M., Wang, Y., Zhang, L., Yang, Y., Huang, S., Wang, J., Ge, H., Ishibashi, T., & Yan, Y. (2019). Single cell transcriptomic landscapes of pattern formation, proliferation and growth in *Drosophila* wing imaginal discs. *Development*, dev.179754. <https://doi.org/10.1242/dev.179754>
- Denton, D., Aung-Htut, M. T., & Kumar, S. (2013). Developmentally programmed cell death in *Drosophila*. *Biochimica et Biophysica Acta (BBA) - Molecular Cell Research*, 1833(12), 3499–3506. <https://doi.org/10.1016/j.bbamcr.2013.06.014>
- Dichtel-Danjoy, M.-L., Ma, D., Dourlen, P., Chatelain, G., Napoletano, F., Robin, M., Corbet, M., Levet, C., Hafsi, H., Hainaut, P., Ryoo, H. D., Bourdon, J.-C., & Mollereau, B. (2013). *Drosophila* p53 isoforms differentially regulate apoptosis and apoptosis-induced proliferation. *Cell Death & Differentiation*, 20(1), 108–116. <https://doi.org/10.1038/cdd.2012.100>
- Everetts, N. J., Worley, M. I., Yasutomi, R., Yosef, N., & Hariharan, I. K. (2021). Single-cell transcriptomics of the *Drosophila* wing disc reveals instructive epithelium-to-myoblast interactions. *eLife*, 10, e61276. <https://doi.org/10.7554/eLife.61276>
- Filbin, M. G., Tirosh, I., Hovestadt, V., Shaw, M. L., Escalante, L. E., Mathewson, N. D., Neftel, C., Frank, N., Pelton, K., Hebert, C. M., Haberler, C., Yizhak, K., Gojo, J., Egervari, K., Mount, C., Van Galen, P., Bonal, D. M., Nguyen, Q.-D., Beck, A., ... Suvà, M. L. (2018). Developmental and oncogenic programs in H3K27M gliomas dissected by single-cell RNA-seq. *Science*, 360(6386), 331–335. <https://doi.org/10.1126/science.aao4750>
- Floc'hlay, S., Balaji, R., Stanković, D., Christiaens, V. M., Bravo González-Blas, C., De Winter, S., Hulselmans, G. J., De Waegeneer, M., Quan, X., Koldere, D., Atkins, M., Halder, G., Uhlirova, M., Classen, A.-K., & Aerts, S. (2023). Shared enhancer gene regulatory networks between wound and oncogenic programs. *eLife*, 12, e81173. <https://doi.org/10.7554/eLife.81173>
- Fu, S., Li, Z., Xiao, L., Hu, W., Zhang, L., Xie, B., Zhou, Q., He, J., Qiu, Y., Wen, M., Peng, Y., Gao, J., Tan, R., Deng, Y., Weng, L., & Sun, L.-Q. (2019). Glutamine Synthetase Promotes Radiation Resistance via Facilitating Nucleotide Metabolism and Subsequent DNA Damage Repair. *Cell Reports*, 28(5), 1136-1143.e4. <https://doi.org/10.1016/j.celrep.2019.07.002>

- Graham, E. L., Fernandez, J., Gandhi, S., Choudhry, I., Kellam, N., & LaRocque, J. R. (2024). The impact of developmental stage, tissue type, and sex on DNA double-strand break repair in *Drosophila melanogaster*. *PLOS Genetics*, *20*(4), e1011250.  
<https://doi.org/10.1371/journal.pgen.1011250>
- Gunage, R. D., Reichert, H., & VijayRaghavan, K. (2014). Identification of a new stem cell population that generates *Drosophila* flight muscles. *eLife*, *3*, e03126. <https://doi.org/10.7554/eLife.03126>
- Halme, A., Cheng, M., & Hariharan, I. K. (2010). Retinoids Regulate a Developmental Checkpoint for Tissue Regeneration in *Drosophila*. *Current Biology*, *20*(5), 458–463.  
<https://doi.org/10.1016/j.cub.2010.01.038>
- Han, X., Chen, Y., Zhang, N., Huang, C., He, G., Li, T., Wei, M., Song, Q., Mo, S., & Lv, Y. (2022). Single-cell mechanistic studies of radiation-mediated bystander effects. *Frontiers in Immunology*, *13*, 849341. <https://doi.org/10.3389/fimmu.2022.849341>
- Holley, A. K., Miao, L., St. Clair, D. K., & St. Clair, W. H. (2014). Redox-Modulated Phenomena and Radiation Therapy: The Central Role of Superoxide Dismutases. *Antioxidants & Redox Signaling*, *20*(10), 1567–1589. <https://doi.org/10.1089/ars.2012.5000>
- Huang, R., & Zhou, P.-K. (2021). DNA damage repair: Historical perspectives, mechanistic pathways and clinical translation for targeted cancer therapy. *Signal Transduction and Targeted Therapy*, *6*(1), 254. <https://doi.org/10.1038/s41392-021-00648-7>
- Hubenak, J. R., Zhang, Q., Branch, C. D., & Kronowitz, S. J. (2014). Mechanisms of Injury to Normal Tissue after Radiotherapy: A Review. *Plastic and Reconstructive Surgery*, *133*(1), 49e–56e.  
<https://doi.org/10.1097/01.prs.0000440818.23647.0b>
- Ingaramo, M. C., Sánchez, J. A., & Dekanty, A. (2018). Regulation and function of p53: A perspective from *Drosophila* studies. *Mechanisms of Development*, *154*, 82–90.  
<https://doi.org/10.1016/j.mod.2018.05.007>

- Jaklevic, B. R., & Su, T. T. (2004). Relative Contribution of DNA Repair, Cell Cycle Checkpoints, and Cell Death to Survival after DNA Damage in *Drosophila* Larvae. *Current Biology*, *14*(1), 23–32. <https://doi.org/10.1016/j.cub.2003.12.032>
- Jassim, O. W. (2003). Dmp53 protects the *Drosophila* retina during a developmentally regulated DNA damage response. *The EMBO Journal*, *22*(20), 5622–5632. <https://doi.org/10.1093/emboj/cdg543>
- Khan, C., & Baker, N. E. (2022). *The DNA Damage response and cell competition are p53- and Xrp1-dependent processes that suppress hyperplastic aneuploidy*. <https://doi.org/10.1101/2022.06.06.494998>
- Kim, C. S., Seong, K. M., Lee, B. S., Lee, I. K., Yang, K. H., Kim, J.-Y., & Nam, S. Y. (2015). Chronic low-dose -irradiation of *Drosophila melanogaster* larvae induces gene expression changes and enhances locomotive behavior. *Journal of Radiation Research*, *56*(3), 475–484. <https://doi.org/10.1093/jrr/rru128>
- Kiparaki, M., Khan, C., Folgado-Marco, V., Chuen, J., Moulos, P., & Baker, N. E. (2022). The transcription factor Xrp1 orchestrates both reduced translation and cell competition upon defective ribosome assembly or function. *eLife*, *11*, e71705. <https://doi.org/10.7554/eLife.71705>
- Kurtz, P., Jones, A. E., Tiwari, B., Link, N., Wylie, A., Tracy, C., Krämer, H., & Abrams, J. M. (2019). *Drosophila* p53 directs nonapoptotic programs in postmitotic tissue. *Molecular Biology of the Cell*, *30*(11), 1339–1351. <https://doi.org/10.1091/mbc.E18-12-0791>
- Landis, G., Shen, J., & Tower, J. (2012). Gene expression changes in response to aging compared to heat stress, oxidative stress and ionizing radiation in *Drosophila melanogaster*. *Aging*, *4*(11), 768–789. <https://doi.org/10.18632/aging.100499>
- Ledru, M., Clark, C. A., Brown, J., Verghese, S., Ferrara, S., Goodspeed, A., & Su, T. T. (2022). Differential gene expression analysis identified determinants of cell fate plasticity during radiation-induced regeneration in *Drosophila*. *PLOS Genetics*, *18*(1), e1009989. <https://doi.org/10.1371/journal.pgen.1009989>

- Lee, C.-H., Kiparaki, M., Blanco, J., Folgado, V., Ji, Z., Kumar, A., Rimesso, G., & Baker, N. E. (2018). A Regulatory Response to Ribosomal Protein Mutations Controls Translation, Growth, and Cell Competition. *Developmental Cell*, *46*(4), 456-469.e4.  
<https://doi.org/10.1016/j.devcel.2018.07.003>
- Lee, C.-Y., Clough, E. A., Yellon, P., Teslovich, T. M., Stephan, D. A., & Baehrecke, E. H. (2003). Genome-Wide Analyses of Steroid- and Radiation-Triggered Programmed Cell Death in *Drosophila*. *Current Biology*, *13*(4), 350–357. [https://doi.org/10.1016/S0960-9822\(03\)00085-X](https://doi.org/10.1016/S0960-9822(03)00085-X)
- Liang, J., Bi, G., Huang, Y., Zhao, G., Sui, Q., Zhang, H., Bian, Y., Yin, J., Wang, Q., Chen, Z., & Zhan, C. (2024). MAFF confers vulnerability to cisplatin-based and ionizing radiation treatments by modulating ferroptosis and cell cycle progression in lung adenocarcinoma. *Drug Resistance Updates*, *73*, 101057. <https://doi.org/10.1016/j.drug.2024.101057>
- Lu, H., Yan, H., Li, X., Xing, Y., Ye, Y., Jiang, S., Ma, L., Ping, J., Zuo, H., Hao, Y., Yu, C., Li, Y., Zhou, G., & Lu, Y. (2023). Single-cell map of dynamic cellular microenvironment of radiation-induced intestinal injury. *Communications Biology*, *6*(1), 1248. <https://doi.org/10.1038/s42003-023-05645-w>
- Mills, M., Emori, C., Kumar, P., Boucher, Z., George, J., & Bolcun-Filas, E. (2024). *Single-cell and bulk transcriptional profiling of mouse ovaries reveals novel genes and pathways associated with DNA damage response in oocytes*. <https://doi.org/10.1101/2024.02.02.578648>
- Morral, C., Ayyaz, A., Kuo, H.-C., Fink, M., Verginadis, I. I., Daniel, A. R., Burner, D. N., Driver, L. M., Satow, S., Hasapis, S., Ghinnagow, R., Luo, L., Ma, Y., Attardi, L. D., Koumenis, C., Minn, A. J., Wrana, J. L., Lee, C.-L., & Kirsch, D. G. (2024). P53 promotes revival stem cells in the regenerating intestine after severe radiation injury. *Nature Communications*, *15*(1), 3018.  
<https://doi.org/10.1038/s41467-024-47124-8>
- Moskalev, A., Shaposhnikov, M., Snezhkina, A., Kogan, V., Plyusnina, E., Peregudova, D., Melnikova, N., Uroshlev, L., Mylnikov, S., Dmitriev, A., Plusnin, S., Fedichev, P., & Kudryavtseva, A. (2014). Mining Gene Expression Data for Pollutants (Dioxin, Toluene, Formaldehyde) and Low

- Dose of Gamma-Irradiation. *PLoS ONE*, 9(1), e86051.  
<https://doi.org/10.1371/journal.pone.0086051>
- Moskalev, A., Zhikrivetskaya, S., Krasnov, G., Shaposhnikov, M., Proshkina, E., Borisoglebsky, D., Danilov, A., Peregudova, D., Sharapova, I., Dobrovolskaya, E., Solovev, I., Zemskaya, N., Shilova, L., Snezhkina, A., & Kudryavtseva, A. (2015). A comparison of the transcriptome of *Drosophila melanogaster* in response to entomopathogenic fungus, ionizing radiation, starvation and cold shock. *BMC Genomics*, 16(S13), S8. <https://doi.org/10.1186/1471-2164-16-S13-S8>
- Mukherjee, A., Epperly, M. W., Shields, D., Hou, W., Fisher, R., Hamade, D., Wang, H., Saiful Huq, M., Bao, R., Tabib, T., Monier, D., Watkins, S., Calderon, M., & Greenberger, J. S. (2021). Ionizing irradiation-induced Fgr in senescent cells mediates fibrosis. *Cell Death Discovery*, 7(1), 349. <https://doi.org/10.1038/s41420-021-00741-4>
- Ogura, K., Magae, J., Kawakami, Y., & Koana, T. (2009). Reduction in Mutation Frequency by Very Low-Dose Gamma Irradiation of *Drosophila melanogaster* Germ Cells. *Radiation Research*, 171(1), 1–8. <https://doi.org/10.1667/RR1288.1>
- Oikemus, S. R., McGinnis, N., Queiroz-Machado, J., Tukachinsky, H., Takada, S., Sunkel, C. E., & Brodsky, M. H. (2004). *Drosophila atm/telomere fusion* is required for telomeric localization of HP1 and telomere position effect. *Genes & Development*, 18(15), 1850–1861. <https://doi.org/10.1101/gad.1202504>
- Osman, A. M., Sun, Y., Burns, T. C., He, L., Kee, N., Oliva-Vilarnau, N., Alevyzaki, A., Zhou, K., Louhivuori, L., Uhlén, P., Hedlund, E., Betsholtz, C., Lauschke, V. M., Kele, J., & Blomgren, K. (2020). Radiation Triggers a Dynamic Sequence of Transient Microglial Alterations in Juvenile Brain. *Cell Reports*, 31(9), 107699. <https://doi.org/10.1016/j.celrep.2020.107699>
- Pajonk, F., Vlashi, E., & McBride, W. H. (2010). Radiation Resistance of Cancer Stem Cells: The 4 R's of Radiobiology Revisited. *Stem Cells*, 28(4), 639–648. <https://doi.org/10.1002/stem.318>

- Pakos-Zebrucka, K., Koryga, I., Mnich, K., Ljubic, M., Samali, A., & Gorman, A. M. (2016). The integrated stress response. *EMBO Reports*, *17*(10), 1374–1395.  
<https://doi.org/10.15252/embr.201642195>
- Pomar, N., Berlanga, J. J., Campuzano, S., Hernández, G., Elías, M., & De Haro, C. (2003). Functional characterization of *Drosophila melanogaster* PERK eukaryotic initiation factor 2 $\alpha$  (eIF2 $\alpha$ ) kinase. *European Journal of Biochemistry*, *270*(2), 293–306. <https://doi.org/10.1046/j.1432-1033.2003.03383.x>
- Porrazzo, A., Cipressa, F., De Gregorio, A., De Pittà, C., Sales, G., Ciapponi, L., Morciano, P., Esposito, G., Tabocchini, M. A., & Cenci, G. (2022). Low dose rate  $\gamma$ -irradiation protects fruit fly chromosomes from double strand breaks and telomere fusions by reducing the esi-RNA biogenesis factor Loquacious. *Communications Biology*, *5*(1), 905.  
<https://doi.org/10.1038/s42003-022-03885-w>
- Potter, S. S. (2018). Single-cell RNA sequencing for the study of development, physiology and disease. *Nature Reviews Nephrology*, *14*(8), 479–492. <https://doi.org/10.1038/s41581-018-0021-7>
- Sekelsky, J. (2017). DNA Repair in *Drosophila*: Mutagens, Models, and Missing Genes. *Genetics*, *205*(2), 471–490. <https://doi.org/10.1534/genetics.116.186759>
- Seong, K. M., Kim, C. S., Seo, S.-W., Jeon, H. Y., Lee, B.-S., Nam, S. Y., Yang, K. H., Kim, J.-Y., Kim, C. S., Min, K.-J., & Jin, Y.-W. (2011). Genome-wide analysis of low-dose irradiated male *Drosophila melanogaster* with extended longevity. *Biogerontology*, *12*(2), 93–107.  
<https://doi.org/10.1007/s10522-010-9295-2>
- Sheng, X., Lin, Z., Lv, C., Shao, C., Bi, X., Deng, M., Xu, J., Guerrero-Juarez, C. F., Li, M., Wu, X., Zhao, R., Yang, X., Li, G., Liu, X., Wang, Q., Nie, Q., Cui, W., Gao, S., Zhang, H., ... Yu, Z. (2020). Cycling Stem Cells Are Radioresistant and Regenerate the Intestine. *Cell Reports*, *32*(4), 107952. <https://doi.org/10.1016/j.celrep.2020.107952>
- Sinclair, W. K. (2012). Cyclic X-Ray Responses in Mammalian Cells *in Vitro*<sup>1</sup>. *Radiation Research*, *178*(2), AV112–AV124. <https://doi.org/10.1667/RRAV09.1>

- Steller, H. (2008). Regulation of apoptosis in *Drosophila*. *Cell Death & Differentiation*, *15*(7), 1132–1138. <https://doi.org/10.1038/cdd.2008.50>
- Sun, G., Ding, X. A., Argaw, Y., Guo, X., & Montell, D. J. (2020). Akt1 and dCIZ1 promote cell survival from apoptotic caspase activation during regeneration and oncogenic overgrowth. *Nature Communications*, *11*(1), 5726. <https://doi.org/10.1038/s41467-020-19068-2>
- Sun, Z., Wang, X., Wang, J., Wang, J., Liu, X., Huang, R., Chen, C., Deng, M., Wang, H., & Han, F. (2021). Key radioresistance regulation models and marker genes identified by integrated transcriptome analysis in nasopharyngeal carcinoma. *Cancer Medicine*, *10*(20), 7404–7417. <https://doi.org/10.1002/cam4.4228>
- Syljuåsen, R. G. (2019). Cell Cycle Effects in Radiation Oncology. In F. Wenz (Ed.), *Radiation Oncology* (pp. 1–8). Springer International Publishing. [https://doi.org/10.1007/978-3-319-52619-5\\_101-1](https://doi.org/10.1007/978-3-319-52619-5_101-1)
- Toy, H. I., Karakulah, G., Kontou, P. I., Alotaibi, H., Georgakilas, A. G., & Pavlopoulou, A. (2021). Investigating Molecular Determinants of Cancer Cell Resistance to Ionizing Radiation Through an Integrative Bioinformatics Approach. *Frontiers in Cell and Developmental Biology*, *9*, 620248. <https://doi.org/10.3389/fcell.2021.620248>
- Tu, W., Tang, S., Yan, T., Feng, Y., Mo, W., Song, B., Wang, J., Cheng, S., Geng, F., Shi, Y., Yu, D., & Zhang, S. (2022). Integrative multi-omic analysis of radiation-induced skin injury reveals the alteration of fatty acid metabolism in early response of ionizing radiation. *Journal of Dermatological Science*, *108*(3), 178–186. <https://doi.org/10.1016/j.jdermsci.2023.01.001>
- Ujfaludi, Z., Boros, I., & Bálint, É. (2007). Different sets of genes are activated by P53 upon UV or ionizing radiation in *Drosophila melanogaster*. *Acta Biologica Hungarica*, *58*(Supplement 1), 65–79. <https://doi.org/10.1556/ABiol.58.2007.Suppl.6>
- Umargamwala, R., Manning, J., Dorstyn, L., Denton, D., & Kumar, S. (2024). Understanding Developmental Cell Death Using *Drosophila* as a Model System. *Cells*, *13*(4), 347. <https://doi.org/10.3390/cells13040347>

- Van Bergeijk, P., Heimiller, J., Uyetake, L., & Su, T. T. (2012). Genome-Wide Expression Analysis Identifies a Modulator of Ionizing Radiation-Induced p53-Independent Apoptosis in *Drosophila melanogaster*. *PLoS ONE*, *7*(5), e36539. <https://doi.org/10.1371/journal.pone.0036539>
- Vergheze, S., & Su, T. T. (2016). *Drosophila* Wnt and STAT Define Apoptosis-Resistant Epithelial Cells for Tissue Regeneration after Irradiation. *PLOS Biology*, *14*(9), e1002536. <https://doi.org/10.1371/journal.pbio.1002536>
- Vergheze, S., & Su, T. T. (2018). Ionizing radiation induces stem cell-like properties in a caspase-dependent manner in *Drosophila*. *PLOS Genetics*, *14*(11), e1007659. <https://doi.org/10.1371/journal.pgen.1007659>
- Vermeulen, K., Van Bockstaele, D. R., & Berneman, Z. N. (2003). The cell cycle: A review of regulation, deregulation and therapeutic targets in cancer. *Cell Proliferation*, *36*(3), 131–149. <https://doi.org/10.1046/j.1365-2184.2003.00266.x>
- Vogin, G., & Foray, N. (2013). The law of Bergonié and Tribondeau: A nice formula for a first approximation. *International Journal of Radiation Biology*, *89*(1), 2–8. <https://doi.org/10.3109/09553002.2012.717732>
- Worley, M. I., Everetts, N. J., Yasutomi, R., Chang, R. J., Saretha, S., Yosef, N., & Hariharan, I. K. (2022). Ets21C sustains a pro-regenerative transcriptional program in blastema cells of *Drosophila* imaginal discs. *Current Biology*, *32*(15), 3350-3364.e6. <https://doi.org/10.1016/j.cub.2022.06.040>
- Wu, H., Yu, J., Kong, D., Xu, Y., Zhang, Z., Shui, J., Li, Z., Luo, H., & Wang, K. (2019). Population and single-cell transcriptome analyses reveal diverse transcriptional changes associated with radioresistance in esophageal squamous cell carcinoma. *International Journal of Oncology*. <https://doi.org/10.3892/ijo.2019.4897>
- Wyatt, H. D. M., & West, S. C. (2014). Holliday Junction Resolvases. *Cold Spring Harbor Perspectives in Biology*, *6*(9), a023192–a023192. <https://doi.org/10.1101/cshperspect.a023192>

- Yamasaki, S., Yagishita, N., Sasaki, T., Nakazawa, M., Kato, Y., Yamadera, T., Bae, E., Toriyama, S., Ikeda, R., Zhang, L., Fujitani, K., Yoo, E., Tsuchimochi, K., Ohta, T., Araya, N., Fujita, H., Aratani, S., Eguchi, K., Komiya, S., ... Nakajima, T. (2007). Cytoplasmic destruction of p53 by the endoplasmic reticulum-resident ubiquitin ligase 'Synoviolin.' *The EMBO Journal*, *26*(1), 113–122. <https://doi.org/10.1038/sj.emboj.7601490>
- Yard, B. D., Adams, D. J., Chie, E. K., Tamayo, P., Battaglia, J. S., Gopal, P., Rogacki, K., Pearson, B. E., Phillips, J., Raymond, D. P., Pennell, N. A., Almeida, F., Cheah, J. H., Clemons, P. A., Shamji, A., Peacock, C. D., Schreiber, S. L., Hammerman, P. S., & Abazeed, M. E. (2016). A genetic basis for the variation in the vulnerability of cancer to DNA damage. *Nature Communications*, *7*(1), 11428. <https://doi.org/10.1038/ncomms11428>
- Young, A., Berry, R., Holloway, A. F., Blackburn, N. B., Dickinson, J. L., Skala, M., Phillips, J. L., & Brettingham-Moore, K. H. (2014). RNA-seq profiling of a radiation resistant and radiation sensitive prostate cancer cell line highlights opposing regulation of DNA repair and targets for radiosensitization. *BMC Cancer*, *14*(1), 808. <https://doi.org/10.1186/1471-2407-14-808>
- Yuan, T., Zhang, J., Zhao, Y., Guo, Y., & Fan, S. (2023). Single-cell RNA sequencing of intestinal crypts reveals vital events in damage repair and the double-edged sword effect of the Wnt3/ $\beta$ -catenin pathway in irradiated mice. *Redox Biology*, *68*, 102942. <https://doi.org/10.1016/j.redox.2023.102942>
- Zappia, M. P., De Castro, L., Ariss, M. M., Jefferson, H., Islam, A. B., & Frolov, M. V. (2020). A cell atlas of adult muscle precursors uncovers early events in fibre-type divergence in *Drosophila*. *EMBO Reports*, *21*(10), e49555. <https://doi.org/10.15252/embr.201949555>
- Zarubin, M., Gangapshev, A., Gavriljuk, Y., Kazalov, V., & Kravchenko, E. (2021). First transcriptome profiling of *D. melanogaster* after development in a deep underground low radiation background laboratory. *PLOS ONE*, *16*(8), e0255066. <https://doi.org/10.1371/journal.pone.0255066>

- Zhang, B., Wang, Y., Pang, X., Su, Y., Ai, G., & Wang, T. (2010). ER stress induced by ionising radiation in IEC-6 cells. *International Journal of Radiation Biology*, *86*(6), 429–435.  
<https://doi.org/10.3109/09553001003668014>
- Zhang, Y., Lin, N., Carroll, P. M., Chan, G., Guan, B., Xiao, H., Yao, B., Wu, S. S., & Zhou, L. (2008). Epigenetic Blocking of an Enhancer Region Controls Irradiation-Induced Proapoptotic Gene Expression in Drosophila Embryos. *Developmental Cell*, *14*(4), 481–493.  
<https://doi.org/10.1016/j.devcel.2008.01.018>
- Zhang, Y., Yan, T., Mo, W., Song, B., Zhang, Y., Geng, F., Hu, Z., Yu, D., & Zhang, S. (2024). Altered bile acid metabolism in skin tissues in response to ionizing radiation: Deoxycholic acid (DCA) as a novel treatment for radiogenic skin injury. *International Journal of Radiation Biology*, *100*(1), 87–98. <https://doi.org/10.1080/09553002.2023.2245461>

Chapter 2 is a reproduction of the following preprint,  
and includes significant contributions from all its authors:

*Single cell transcriptomics of X-ray irradiated Drosophila wing discs reveals  
heterogeneity related to cell-cycle status and cell location*

Joyner Cruz<sup>1</sup> , Willam Y. Sun<sup>1</sup> , Alexandra Verbeke<sup>1</sup> , and Iswar K. Hariharan<sup>1</sup> \*  
DOI: <https://doi.org/10.1101/2024.12.10.627868>

## **Chapter 2**

Single-cell transcriptomics of X-ray irradiated *Drosophila* wing discs reveal  
heterogeneity related to cell-cycle status and cell location

## 2.1 Abstract

Even seemingly homogeneous populations of cells can express phenotypic diversity in response to environmental changes. Thus, the effects of X-ray irradiation on tissues composed of diverse cell types is likely to be complex. We have used single-cell RNA sequencing to study the effects of X-ray radiation on the wing-imaginal disc of *Drosophila*, a relatively simple tissue that is mostly composed of epithelial cells. Transcriptomic clustering of cells collected from the wing disc generates clusters that are mainly grouped based on cell location in the proximodistal axis. To quantify heterogeneity of gene expression among clusters, we adapted a metric used to study market concentration, the Herfindahl-Hirschman Index. We show that genes involved in DNA damage repair, alleviation of reactive oxygen species, cell-cycle progression, and apoptosis are expressed relatively uniformly. In contrast, genes encoding a subset of ligands, notably cytokines that activate the JAK/STAT pathway, transcription factors implicated in regeneration such as Ets21C, and some signaling proteins are expressed in more restricted territories. Several of these genes are still expressed in a p53-dependent manner indicating that regional and radiation-induced factors combine to regulate their expression. We similarly examined heterogeneity within territories by using a clustering approach based on cell-cycle gene expression. Using this method, we identified a subpopulation characterized by high levels of *tribbles* expression that is mostly found in irradiated discs. Remarkably, this subpopulation accounts for a considerable fraction of radiation-induced gene expression, indicating that cellular responses are non-uniform even within territories. Thus, both inter-regional and intra-regional heterogeneity are important features of tissue responses to X-ray radiation.

## 2.2 Introduction

Ionizing radiation (IR) is a damaging form of energy present in trace amounts in many environments and is commonly used at high doses in the form of X-rays to treat cancers. Worldwide, it is estimated that radiation therapy is an important component of treatment for more than 50% of cancers including those that arise in the brain, breast and prostate. Even in the early years of radiation research, it became apparent that different types of cells varied considerably in their sensitivity to radiation. For example, lymphocytes were rapidly depleted from tissues following radiation, while tissues such as the kidney and liver seemed far more resilient (reviewed by McBride & Schaefer, 2020). In general, tissues that turnover rapidly are more sensitive. Furthermore, within tissues, stem cells are most sensitive while differentiated cells are relatively radioresistant. Even within tissues composed of relatively homogenous populations of cells, cells at particular stages of the cell cycle (e.g. G2/M) are more radiosensitive and cells that are more hypoxic tend to be radioresistant (Withers, 1975).

Most of our mechanistic understanding of how cells react to ionizing radiation comes from genetic studies of the DNA damage response (DDR) in yeast and from biochemical studies of cultured mammalian cells (Harper & Elledge, 2007; Pizzul et al., 2022). These studies have identified the sequence of biochemical reactions that are activated by double-stranded breaks in DNA and culminate in DNA Damage repair. They have also highlighted the importance of the reactive oxygen species (ROS) generated by ionizing radiation that contribute to the damage inflicted on cellular macromolecules. Importantly, cellular damage can result in the activation of mechanisms that arrest the cell cycle to enable a restoration of cellular homeostasis or, failing that, to activate pathways that promote apoptotic cell death. A key player in mammalian cells is the p53 protein which is stabilized following DNA damage and activates the transcription of genes that promote both cell cycle arrest and apoptosis (Levine, 2020).

Studies in *Drosophila* have made important contributions to our understanding of the deleterious effects of ionizing radiation. Indeed, the discovery that X-rays generated mutations in a dose-dependent manner was first discovered in *Drosophila* (Muller, 1927). Subsequent genetic studies identified loci that made flies more susceptible to the effects of DNA-damaging agents – many of these genes encode proteins now known to function in DDR (Sekelsky, 2017). The wing imaginal disc, the larval precursor of the adult wings and part of the thorax (Tripathi & Irvine, 2022), emerged as an attractive model for studying the effects of IR on a relatively simple tissue (Haynie & Bryant, 1977; James & Bryant, 1981). The wing disc derives from a precursor population of approximately 30 cells in the embryo (Worley et al., 2013) and, because of cell proliferation, is composed of more than 30,000 cells by the end of the larval stages (Martín et al., 2009). Most of the wing disc is composed of epithelial cells and a small

fraction of myoblasts which are precursors of the adult flight muscles. (Gunage et al., 2014).

Haynie and Bryant (1977) irradiated larval imaginal discs and used clone marking techniques to show that IR at a dose of 1000 rad (10Gy) kills 40-60% of cells and irradiation with 4000 rad kills approximately 85% of cells. Despite this, compensatory proliferation allowed for the development of wings of normal size and shape. In a study using gamma irradiation (James and Bryant, 1981), it was shown that cell death is observed as soon as 4 h after irradiation and continues for up to 44 h. In parallel, there is a dramatic decrease in the number of cells undergoing mitosis within 1 h with a resumption after 8 h. More recent studies using flow cytometry and FUCCI have shown that cells accumulate preferentially in the G2 phase of the cell cycle after irradiation (Ruiz-Losada et al., 2022). Thus, as in mammalian cells, the two obvious cellular responses to IR are cell-cycle arrest and apoptosis. A key difference, however, is that unlike in mammalian cells where p53 functions in both pathways, *Drosophila* p53 promotes apoptosis but does not seem to function in arresting the cell cycle (Brodsky et al., 2000; Ollmann et al., 2000). In p53 mutants, the expression of genes that function in a wide variety of cellular responses to DNA damage is reduced and apoptosis within 4 h of exposure to IR does not occur. Instead, there is a delayed phase of cell death that involves multiple pathways and aneuploid cells persist in the tissue even into the pupal phase (Akdemir et al., 2007; Brodsky et al., 2004; Brown et al., 2020; Wells et al., 2006; Wells & Johnston, 2012; Wichmann et al., 2006).

Even in a relatively simple tissue such as the wing disc, cells display considerable heterogeneity in their response to radiation. While high levels of cell death are observed in the wing pouch, the dorsal hinge shows reduced levels. The relative radioresistance of this region is dependent upon Wnt and STAT signaling (Verghese & Su, 2016). In more mature discs, more cell death is observed in the intervein regions of the pouch than in regions fated to generate veins (Moon et al., 2005). Thus, even in regions of the disc where there are no obvious morphological differences between cells, the response to radiation can differ considerably. Several studies have documented transcriptional changes at a genome wide level in *Drosophila* embryos (Akdemir et al., 2007; Brodsky et al., 2004; Kurtz et al., 2019; Lee et al., 2003; Ogura et al., 2009; Zhang et al., 2008) and in imaginal discs (Ledru et al., 2022; Van Bergeijk et al., 2012) following irradiation. However, because these studies have prepared RNA either from whole embryos, entire discs or from cells from specific regions without retaining the single-cell origin of transcripts, they cannot be used to assess the heterogeneity of transcriptional responses throughout the disc.

We and others have used single-cell transcriptomics to characterize differences in the transcriptome of cells from different parts of the wing disc (Bageritz et al., 2019; Deng et

al., 2019; Everetts et al., 2021; Zappia et al., 2020). Since the dominant sources of transcriptional variability between cells, or stratifying factors, reflect differences in cell location along the proximodistal (PD) axis, cells from different regions of the disc can easily be identified. Additionally, we and others have characterized transcriptional changes at the single-cell level after ablation of the wing pouch using the tumor necrosis factor (TNF) ortholog *eiger* (*egr*) (Floc'hlay et al., 2023; Worley et al., 2022) and we have previously identified a pathway downstream of the Ets21C transcription factor that functions during regeneration but not during wing disc development (Worley et al., 2022). These studies provide a foundation for characterizing transcriptional responses of the wing disc to IR and to examine the level of transcriptional heterogeneity between cells.

Here we present a comparison, at the single-cell level, of the transcriptomes of unirradiated and irradiated wing discs from late third-instar larvae. Our studies reveal heterogeneity at two different levels – between territories in the disc and between cells in individual territories. We show that regional heterogeneity is more a feature of some classes of genes over others and use quantitative approaches to investigate heterogeneity more generally.

## 2.3 Results

### 2.3-1 X-ray irradiation induces widespread DNA damage but apoptosis and cell-cycle arrest occur nonuniformly

The wing disc consists of three major regions that span its PD axis: The notum, which generates most of the adult thorax, the hinge, which develops into the hinge which connects the wing blade to the thorax, and the pouch, which develops into the wing blade (Fig. 1A). We first characterized the primary effects of X-rays on these regions. In order to confirm that X-rays induce DNA damage in each of the major PD regions, we used immunofluorescence to visualize phosphorylated histone H2Av (p-H2Av), a modified histone variant generated after DNA damage that serves as an early mark of double-strand break repair (Madigan et al., 2002).

We found that in unirradiated discs, p-H2Av fluorescence was present in relatively low levels throughout the tissue (Fig. 1B). Thirty minutes after irradiation, a time point conducive to capturing an initial response to DNA damage, we observed a global increase in p-H2Av signal, with little inter-regional variability (Fig. 1C). To test for X-ray induced cell death, we performed immunofluorescence (IF) staining using an antibody that targets cleaved Dcp-1, an effector caspase that is active during apoptosis (Song et al., 1997). Unirradiated discs showed low levels of Dcp-1 signal likely associated with normal development (Fig. 1D). Four hours after X-ray exposure, discs showed a marked

increase in Dcp-1 signal in each of the major regions of the disc (Fig. 1E). In contrast to p-H2Av fluorescence, anti-DCP1 signal is non-uniform. High levels of apoptosis were observed in the wing pouch but cells along the dorsoventral boundary were spared. Additionally apoptosis is reduced in portions of the wing hinge as has been observed previously (Verghese & Su, 2016).

To examine the proliferative effects of X-ray exposure, we used IF staining against phosphohistone H3 (PHH3), a modified H3 histone state associated with chromatin condensation during mitosis (Hendzel et al., 1997). PHH3 signal was observed across all regions of unirradiated discs (Fig. 1F). In irradiated discs, we observed a global reduction of PHH3 signal as soon as 15 minutes after exposure (Fig. 1G) with greater reduction at 2 and 4 hours after exposure (Fig. 1H-1I). This is consistent with prior observations that cells accumulate in G2 following IR exposure and fail to enter mitosis (Ruiz-Losada et al., 2022). As an additional measure of proliferation, we visualized DNA synthesis using EdU labeling, where positive labeling is associated with an active S-Phase (Salic & Mitchison, 2008). Like PHH3 staining, EdU labeling was observed across all regions of the tissue in unirradiated discs (Fig. 1J). Up to two hours after irradiation, the distribution of EdU labeling resembled that of unirradiated discs (Fig. 1K-1L), while at four hours after exposure, there was a consistent reduction in EdU labeling in the notum and pouch regions of the tissue, while the hinge was largely spared from this reduction (Fig. 1M, Fig. S1\_1-S1\_2). The persistence of EdU incorporation in the hinge could either indicate that a proportion of cells in this region continue to enter S-phase or, alternatively, that there are higher levels of DNA synthesis related to DNA repair in this region. Taken together, our observations indicate that different regions of the disc show differences in response to radiation both in terms of parameters related to cell-cycle progression and to apoptosis.

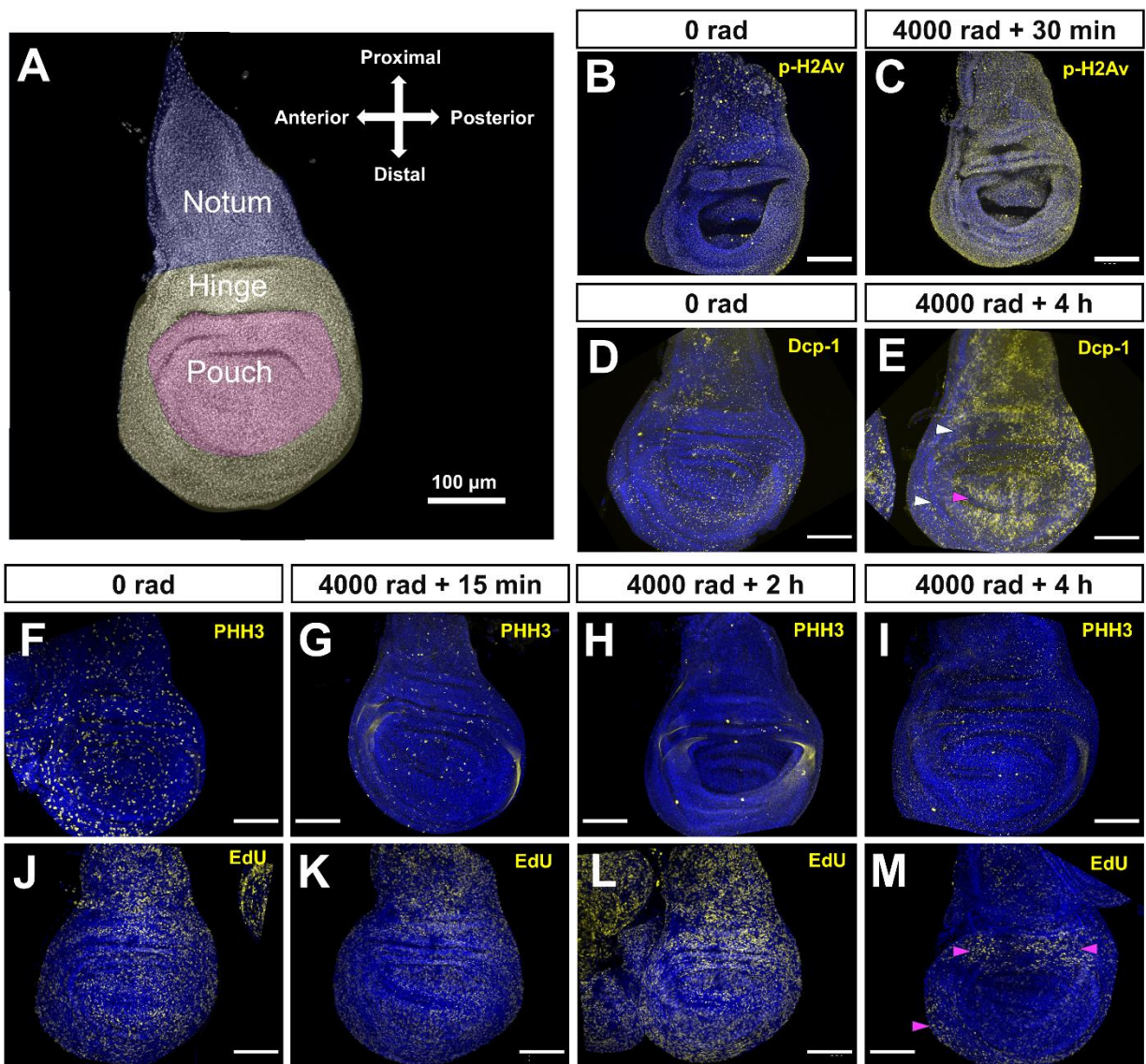


**Figure 1. Effects of X-ray irradiation of DNA damage, apoptosis and cell-cycle progression**

**(A)** Cartoon overlay of wing disc showing the PD regions. **(B, C)** IF of p-H2AX at 0 rad **(B)** and 4000 rad of irradiation, 30 min after exposure **(C)**. **(D, E)** IF of cleaved Dcp-1 at 0 rad **(D)** and 4000 rad 4 h after exposure **(E)**. Magenta arrowhead points to the DV boundary and white arrowheads point to regions of the hinge, regions with less Dcp-1

signal. **(F - I)** IF of PHH3 at 0 rad **(F)** and 4000 rad 15 min **(G)**, 2 h **(H)**, and 4 h **(I)** after exposure. **(J - M)** EdU incorporation at 0 rad **(J)** and 4000 rad 15 min **(K)**, 2 h **(L)** and **(M)** 4 h after exposure. Magenta arrowheads point to regions of high EdU staining at 4 h. All scale bars are 100  $\mu$ m.

### **2.3-2 Cells of unirradiated and irradiated wing discs show similar patterns of expression of many regionally-expressed genes**

Since we have observed differences in cell death and DNA synthesis across the disc, it is likely that there are transcriptomic differences between regions. To explore changes in gene expression on a genome-wide basis across the disc, we used scRNAseq. Previous scRNAseq studies of the disc have shown that genes with patterns of expression restricted to different regions of the PD axis can be used as markers to estimate the approximate anatomical location of cell clusters (Bageritz et al., 2019; Deng et al., 2019; Everetts et al., 2021; Zappia et al., 2020). These include *zfh2* expressed in the hinge (1A, A'') and *nubbin* (*nub*) expressed in the pouch (Fig. 1A', 1A''). In irradiated discs, we found no major changes in the general expression pattern of either gene (Fig. 1B-B''). This suggests that these two marker genes can be used to accurately identify hinge and pouch cells in both conditions.

To examine gene expression on a genome-wide scale, we performed single-cell RNA sequencing (scRNA-seq) on wing discs collected from late third instar larvae 4h after exposure to 4000 rad X-rays, and from larvae of the same stage that were unexposed to irradiation. For both samples two replicates were collected. To generate datasets containing high-quality cells, several filtering steps were applied. In brief, cells that were positively stained with propidium iodide, indicating a compromised cell membrane, were removed via FACS. After sequencing, cells within each dataset that had low numbers of captured genes were removed from further analysis. For analysis, all four datasets were integrated using Seurat V5's anchor-based canonical correlation analysis (CCA) integration process (see methods for details). Cells were grouped into clusters in the integrated dataset using the Louvain algorithm (default in Seurat V5) with a resolution parameter of 2, resulting in 35 clusters (Fig. 2C).

We found that each dataset was individually stratified across its PD axis, as well as when integrated, as indicated by a separation of PD markers between clusters (Fig. 2D-2H). Clusters were classified as belonging to one of seven broad PD regions based on marker expression: The pouch, hinge-pouch, hinge, hinge-notum, notum, PE, and Myoblasts. For the pouch, hinge-pouch, and hinge: *nub*<sup>+</sup>, *zfh2*<sup>-</sup> positive clusters were annotated as pouch, *nub*<sup>+</sup>, *zfh2*<sup>+</sup> clusters as hinge-pouch, and *nub*<sup>-</sup>, *zfh2*<sup>+</sup> as hinge. For the hinge-notum and notum: *tup*<sup>+</sup> (or *eyg*<sup>+</sup>, Fig. S2\_1A), *zfh2*<sup>-</sup> clusters were

annotated as notum, and *tup+* (or *eyg+*), *zfh2+* as hinge-notum. The one *twi+* cluster was annotated as Myoblasts (Fig. S2\_1B). The classification of clusters into broad regions is imperfect, as there are some examples of clusters expressing moderate levels of marker genes belonging to the region that neighbors the one they were classified into (e.g. *zfh2* is expressed at moderate levels in some cells belonging to P2).

To identify unique cluster markers, we performed differential gene expression (DGE) analysis on each individual cluster compared to all other clusters, and compared to all other clusters within the same broad region (Fig. S2\_1C, Table S2\_T1). Unique markers indicated that many clusters likely correspond to contiguous places in the wing disc with regionally restricted gene expression of one or more genes, e.g. pouch 5, marked by *Optix*, a gene restricted in expression to a small region of the anterior pouch (Seimiya & Gehring, 2000). Other clusters likely correspond to noncontiguous regions in the wing disc with restricted gene expression of one or more genes, e.g. pouch 7, marked by *Doc1*, a gene expressed in two separate locations of the dorsal and ventral pouch (Butler et al., 2003). In two cases, clusters did not correspond to specific regions of restricted gene expression: pouch cluster 9 (P9), which was enriched for cells with S-phase markers, and pouch cluster 3 (P3), which was enriched in irradiated cells expressing the cell cycle gene *trbl* (later discussed at length). In sum, we interpret cluster identity to be primarily associated with genes of restricted, though not necessarily contiguous, regional patterns of expression in the disc with some additional contributions from other parameters such as cell-cycle state.

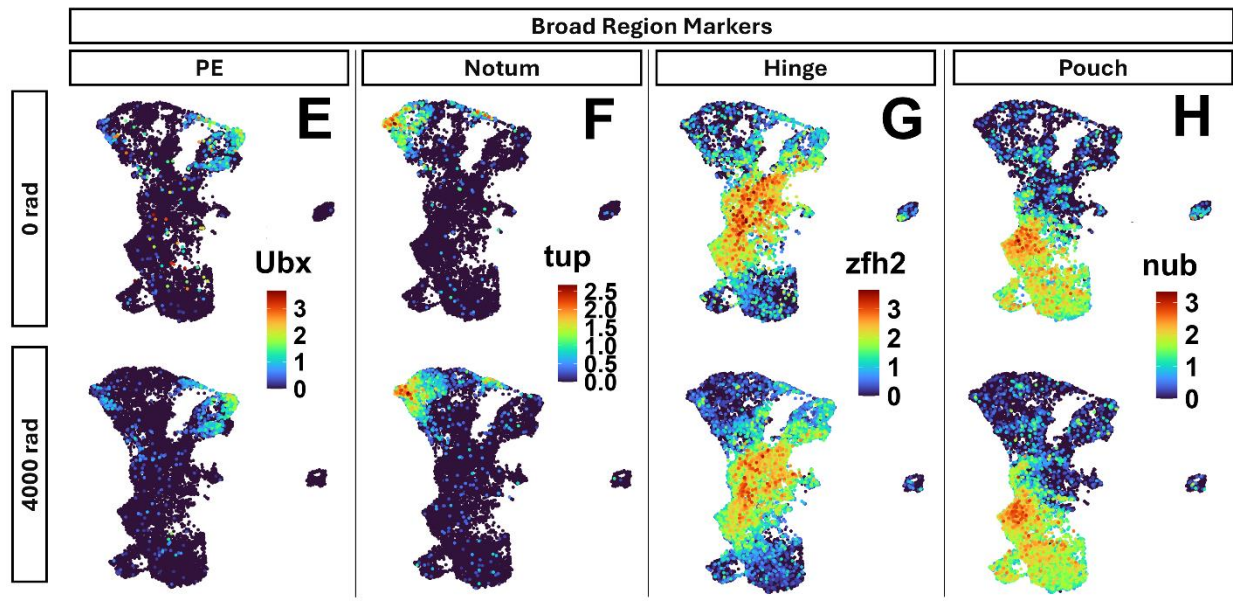
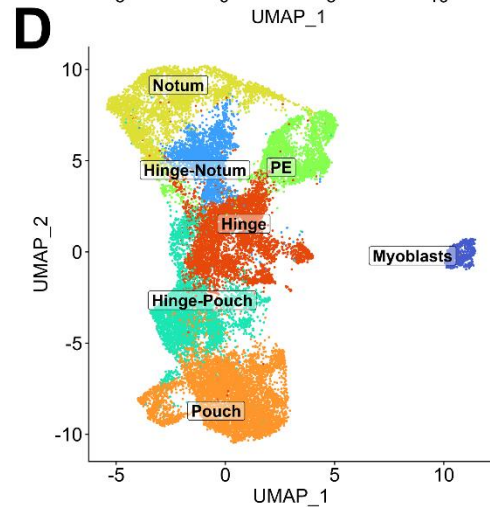
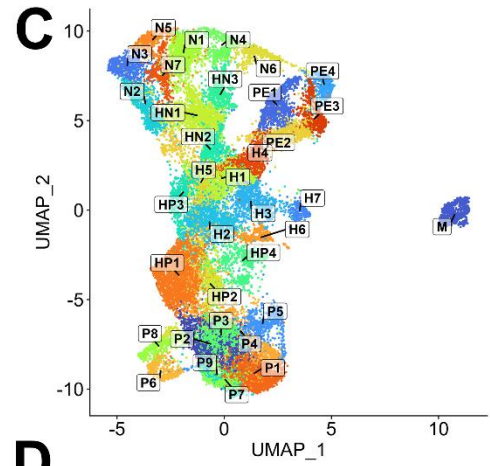
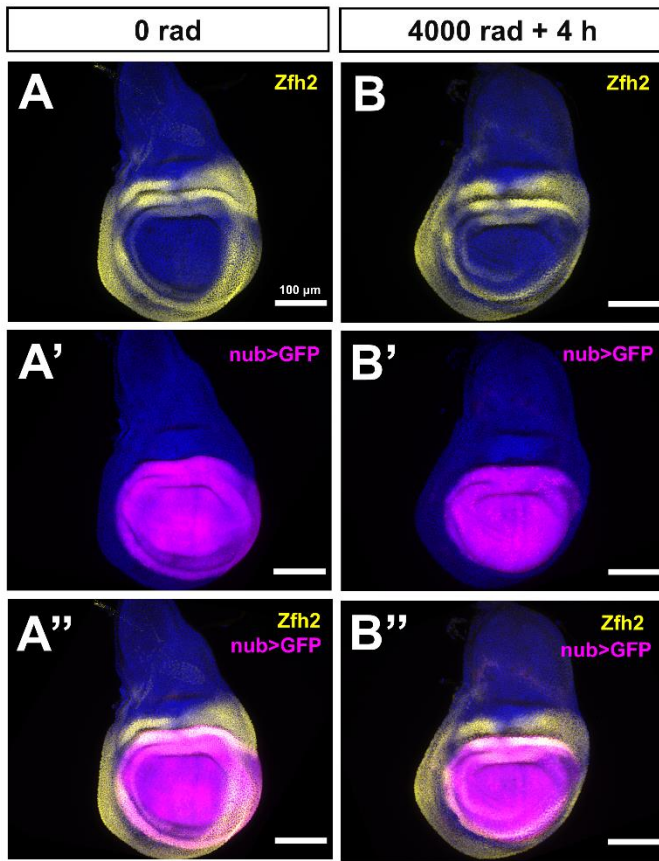


**Figure 2. Territories of the wing disc shown by immunofluorescence and UMAP plots.**

IF of *Zfh2* (**A, B**), *nub>GFP* (**A', B'**), and merged images of both (**A'', B''**) at 0 rad (**A - A''**) or 4 h after exposure to 4000 rad (**B-B''**). All scale bars are 100  $\mu$ m. (**C**) UMAP showing 35 cluster annotations with cluster designations based on PD region. (**D**) UMAP showing broad epithelial region annotations. (**E-H**) UMAP plots showing the expression of markers used to annotate specific epithelial regions at 0 rad (top row) and 4000 rad (bottom row); *Ubx* for PE (**E**), *tup* for notum (**F**), *zfh2* for hinge (**G**), *nub* for pouch (**B**). Combinations were used to determine hinge-notum and hinge-pouch regions. Plots for *eyg* (also used for the notum) and *twi* (used for the myoblasts) are shown in Figure S2\_1.

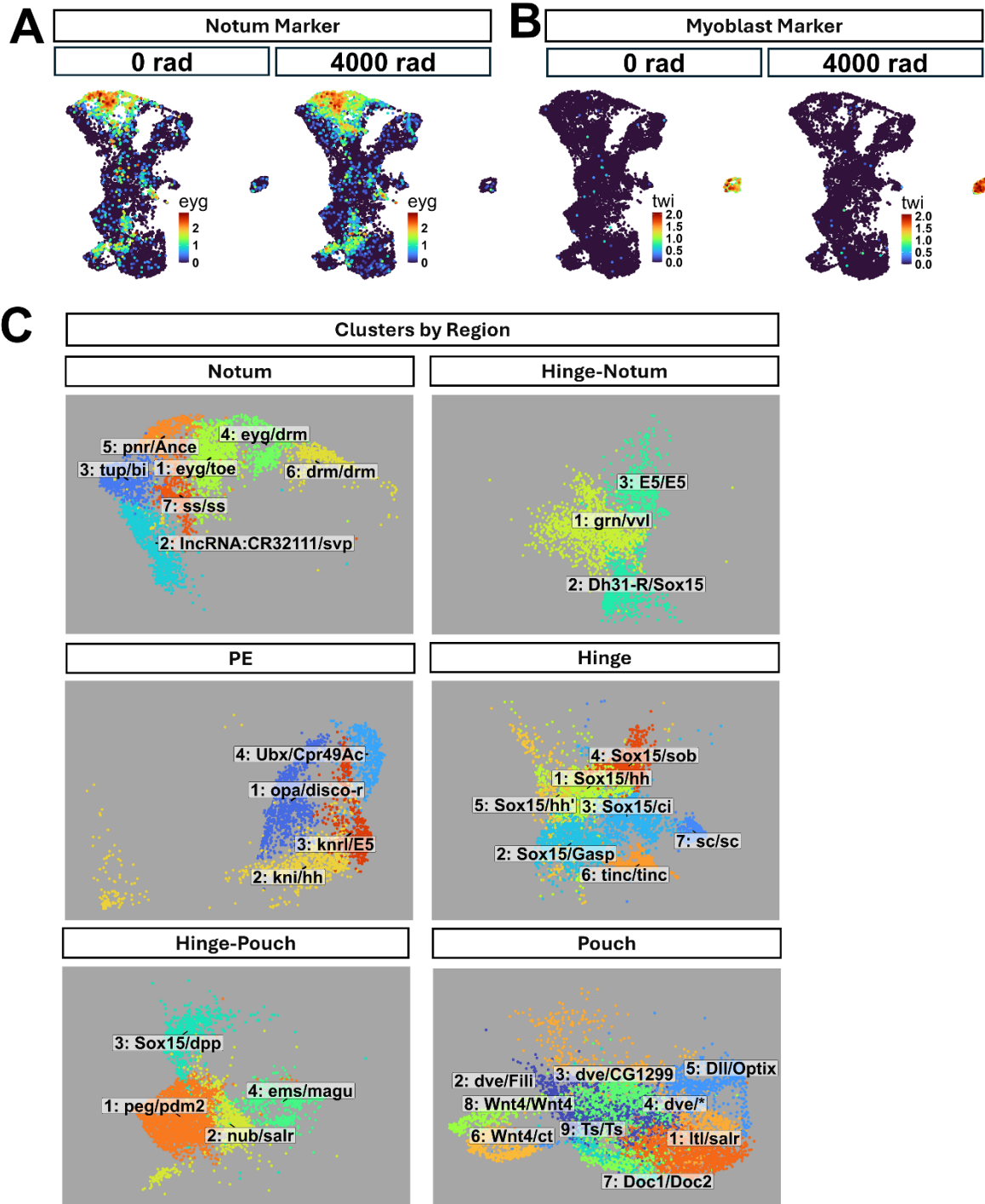


**Figure S2\_1. UMAP plots of Top Cluster Markers by Region.**

**(A)** Expression UMAPs of *eyg* at 0 rad (left) and 4000 rad (right). **(B)** Expression

UMAPs of *twi* at 0 rad (**left**) and 4000 rad (**right**). **(C)** Cropped and zoomed in UMAP plots of clusters belonging to each of the major PD regions. Each cluster is labeled by its cluster number and the genes that are most highly expressed in it when compared to all clusters (left of the slash) and when compared to other clusters within the same PD region (right of the slash).

### **2.3-3 X-ray induced genes involved in apoptosis, DDR, and reaction to ROS are relatively homogeneous across the disc after irradiation**

For an initial broad survey of changes in gene expression after irradiation, we compared the gene expression of all cells of the irradiated condition to all cells of the unirradiated condition. We applied lenient filters, retaining genes that were present in  $\geq 1\%$  of cells in either condition, had an absolute  $\log_2FC \geq 0.1$ , and an adjusted  $p$  value  $< 0.05$ , resulting in 3,767 genes with increased expression in the irradiated condition and 1,122 genes with decreased expression. Among genes with increased expression were many of those described in previous genome-wide analyses on embryos and wing discs, including genes involved in apoptotic regulation (e.g. *rpr*, *hid*, *Corp*, *egr*) and genes involved in DDR and repair (e.g. *Irpb18*, *Xrp1*, *p53*, *Ku80*, *Irpb*, *mre11*, *rad50*) (Akdemir et al., 2007; Brodsky et al., 2004; Van Bergeijk et al., 2012). Similarly, among genes with decreased expression were many described previously in wing discs, including those involved in DNA replication (e.g. *PCNA*, *dup*, *Mcm3*, *geminin*, *Pole2*) (Van Bergeijk et al., 2012). For all changes, see Table S3\_T1.

There are currently few methods used routinely to assess the heterogeneity of gene expression across cell clusters. There are a variety of ways that heterogeneity is quantified in economics and the social sciences (reviewed in Steele et al., 2022). In order to quantify the heterogeneity of X-ray induced genes across cell clusters, we implemented a variation of the formula used in the Herfindahl-Hirschman Index (HHI), a measure of market concentration used in economics (Herfindahl, 1950; Hirschman, 1945) (here used to measure the “concentration” of gene expression across clusters). If the share of total expression in each cluster is calculated and if those numbers are simply all added, the overall total would be 1. If however, the share of expression in each cluster is squared and then those numbers are added, the total would depend upon the distribution of expression between the clusters. If expression was distributed evenly among  $N$  clusters, then each cluster would have  $1/N$  of the total expression. In that case the HHI would be  $1/N$  which is the lowest possible value. In contrast, if all expression was concentrated in one cluster, then the HHI would be 1 which would be the highest possible value and which would be indicative of maximal heterogeneity between clusters. To calculate the HHI score for a given gene, the average gene expression under the irradiated condition for each of the 35 clusters was individually divided by the sum of all average expressions across clusters, squared, and then added

together (Fig. 3A, formula on top). Thus, in the case of 35 clusters, the minimum possible score is 0.0286 and the maximum possible score is 1. We consider HHI scoring to be a useful heuristic method for ranking expression concentration in clustered data. However, the interpretation of HHI is limited by the quality and meaning of clusters. Despite its limitations, HHI applied to clusters here, which are primarily defined by genes of spatially restricted expression, allows us to rank genes in terms of their spatial heterogeneity.

To see if there were differences in expression concentration between classes of genes that may be important for X-ray response, we applied HHI using the 35 clusters to 521 genes enriched at 4000 rad that belonged to one of nine categories: Apoptosis, DDR, response to ROS, cell cycle regulation, transcription factors (TFs), phosphatases, kinases, ligands, and receptors (see S3\_T2 for complete list of genes used before filtering to 521). The mean HHI for all included genes was 0.037 with a minimum value of 0.029 (*eff*) and a maximum value of 0.25 (*tup*), the theoretical range being between 0.0286 (least concentrated) and 1 (most concentrated). The classes of genes that have been studied most intensively in the context of cellular responses to radiation (apoptosis, DDR, ROS, cell cycle) are all expressed relatively homogeneously with HHI values less than 0.06. We found that most genes with the highest HHI scores tended to encode either ligands or transcription factors, indicating their concentrated expression in relatively few clusters. A small number of genes that encoded phosphatases, kinases or receptors were also expressed relatively heterogeneously. Another way to visualize the relative heterogeneity of expression is to show the proportion of mRNA of each gene in each of the 35 clusters. Genes with the highest HHI from six different classes are shown demonstrating greater spatial expression concentration of the TFs and Ligands than the other categories. (Fig. 3B). Likewise, expression UMAPS of low HHI genes (Fig. 3D-3F) showed less concentrated patterns of expression when compared to high scoring genes (Fig. 3G).

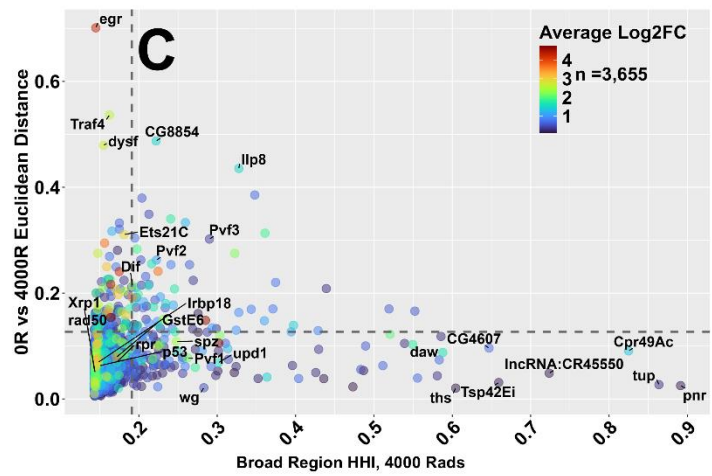
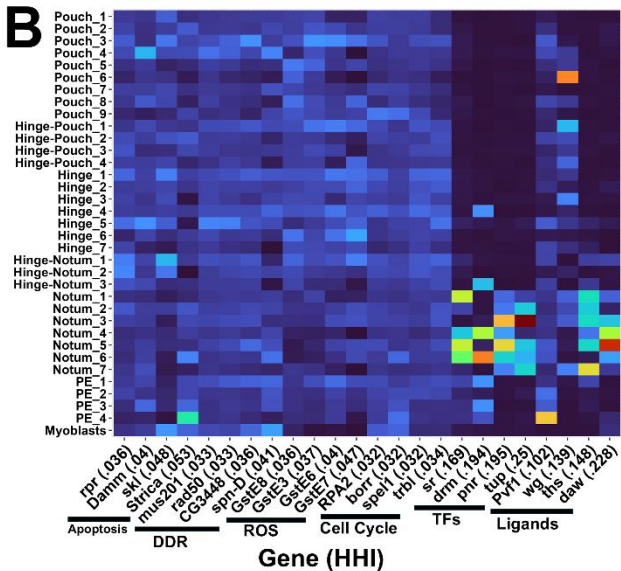
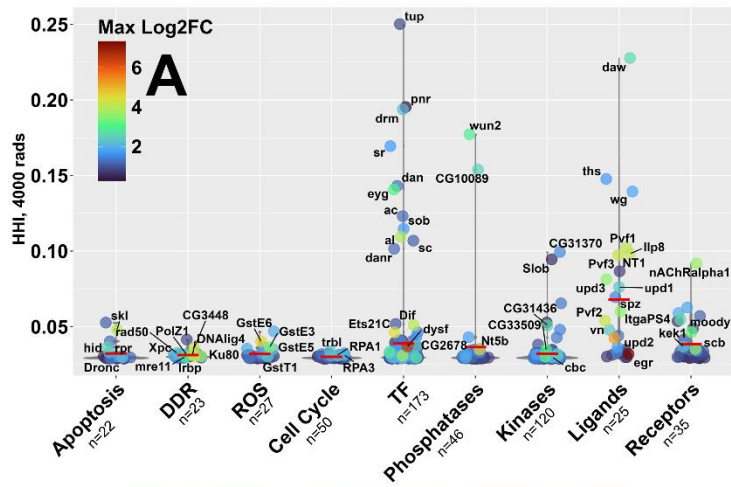
High scoring ligands (95th+ percentile of included genes, HHI>0.066, n=27) included JAK/STAT pathway activators *upd1* (concentrated in clusters of the hinge, hinge-notum, and PE) and *upd3* (concentrated in clusters of the pouch, hinge-pouch, and hinge). Expression of the VEGF/PDGF orthologs *Pvf1* and *Pvf3*, which bind to the Pvr receptor tyrosine kinase, is most concentrated in clusters of the PE). Expression of *llp8*, which encodes a member of the insulin/relaxin family and regulates systemic responses to disc injury is concentrated in the hinge-pouch. All of these genes are known to be upregulated in response to various types of disc injury (Blanco et al., 2010; Floc'hlay et al., 2023; Katsuyama et al., 2015; Worley et al., 2022). Given that radiation induces damage uniformly, the relatively localized expression of these genes was unexpected. The four transcription factors with the highest HHI scores, *stripe (sr)*, *drumstick (drm)*,

*pannier* (*pnr*) and *tailup* (*tup*) are all known to function in cell fate determination. For HHI scores on all genes included in this analysis, see S3\_2-S3\_4 and table S3\_T3.

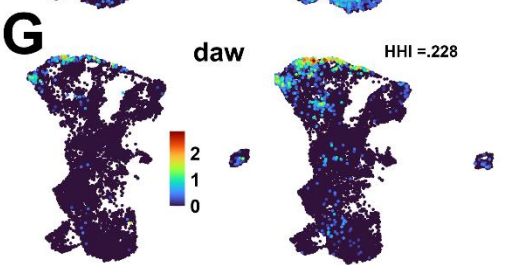
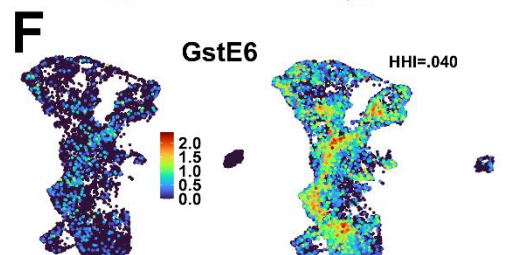
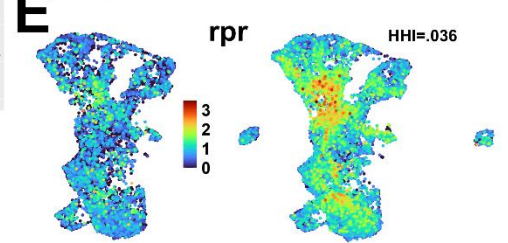
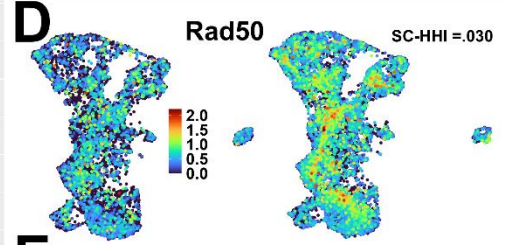
When examining gene expression using HHI, we noticed that many X-ray induced genes with concentrated expression at 4000 rad had a lower, but similar pattern of expression at 0 rad (e.g. *daw*, fig. 3G and *upd1*, fig. 4B-4C). To assess whether this property applied to many genes, we implemented a measure of the difference in the pattern of gene expression between conditions on the 3,767 x-ray induced genes. To reduce noise, we further removed genes not found in at least 1% of cells in both conditions, resulting in 3,655 genes. For each gene, we calculated the proportion of mRNA found in each of the seven PD regions (PE, notum, hinge-notum, hinge, hinge-pouch, pouch and myoblasts) under each condition. We chose to use the seven PD regions rather than the 35 clusters to determine large, strong changes in gene expression across the PD axis. Thus each gene could be represented as a point in seven-dimensional space in each of the two conditions. We then calculated the Euclidean distance (“expression distance”) between these points. Gene scores for this measure ranged from 0 to 0.7, with higher scores indicating a greater difference in the overall pattern of expression between conditions (Fig. 3C).

Scores formed a right skewed distribution, with the vast majority of genes (>95%) scoring <0.13 (Fig. S3\_1C). We found that genes below this threshold, when inspected using expression UMAPs (Fig. S3\_5), displayed some level of conserved expression patterns between conditions, with lower scoring genes having more conserved patterns of expression. Examples from this category include the DNA repair protein Rad50 (Fig. 2D), the proapoptotic gene reaper (*rpr*) (Fig. 2E), *GstE6* which responds to oxidative stress (Fig. 2F) and activin-like ligand *dawdle* (*daw*) (Fig. 2G). The genes with the most marked changes in expression pattern, accounting for the top 5% of genes with the highest Euclidean distance between the two conditions, included the TNF ortholog *eiger* (*egr*) and the transcription factor *dysfusion* (*dysf*) (Fig. 3H, 3I). To examine the relationship between expression distance and expression concentration in the seven broad regions, we also calculated the HHI score of genes using the proportion of mRNA in each (“BR-HHI”) and plotted them against expression distance (Fig. 3C). Genes with high BR-HHI scores in the 4000 rad condition tended to have relatively low expression distance scores (e.g., *daw*, *tup*, *pnr*), indicating that they shared a similar pattern of expression at 0 rad. The reason for this similarity of expression pattern under the two conditions is not obvious. One possible explanation is that genes that are transcriptionally active under unirradiated conditions in some regions of the disc have more accessible chromatin configurations in those cells and are therefore more easily induced in those same cells following irradiation. Another is that induction of these genes occurs by the combined action of region-specific transcription factors and those that are induced by radiation.

$$HHI = \left( \frac{\text{Cluster 1 Average Expression}}{\text{Sum Average Cluster Expression}} \right)^2 + \left( \frac{\text{Cluster 2 Average Expression}}{\text{Sum Average Cluster Expression}} \right)^2 \dots + \left( \frac{\text{Cluster n Average Expression}}{\text{Sum Average Cluster Expression}} \right)^2$$



0 rad      4000 rad  
Expression Distance < 95<sup>th</sup> pth



Expression Distance > 95<sup>th</sup> pth

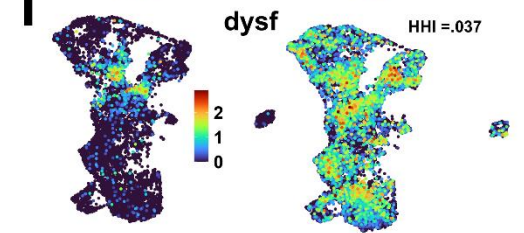
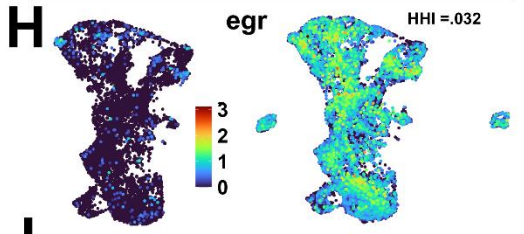


### Figure 3. Heterogeneity of gene expression across the wing disc following radiation exposure

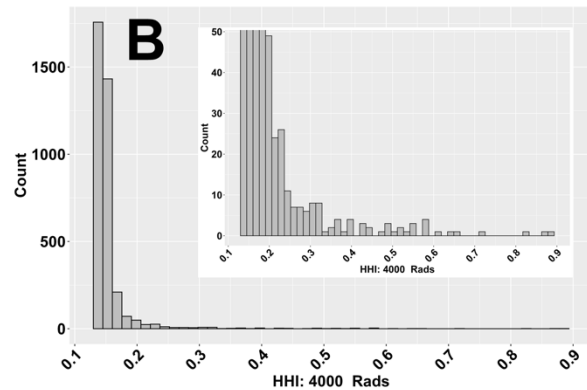
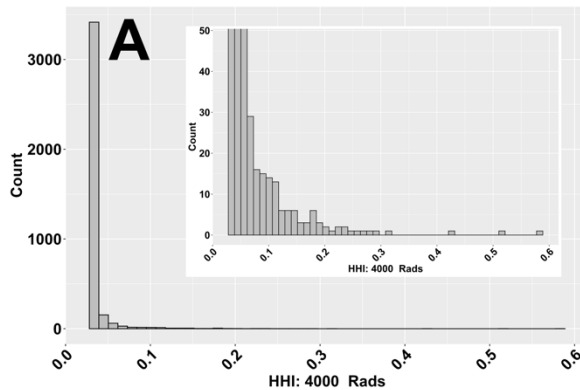
**(A)** 521 genes across 9 functional categories plotted as points by their HHI score at 4000 rad. Point color represents the  $\log_2FC$  between conditions in the cluster that has the highest  $\log_2FC$ . The horizontal red bar represents the mean HHI score for the genes of that category. Genes with  $\max \log_2FC > 2$  or  $HHI > 0.075$  were labeled where space permitted. The equation used to calculate the Herfindahl-Hirschman Index (HHI) is shown above the panel. **(B)** Heat map of 4 highest HHI scoring genes in apoptosis, DDR, ROS, cell cycle (low HHI scoring categories), and TF and ligands (categories with high HHI scoring genes). Box colors represent the proportion of mRNA found in each subregion relative to the sum of all mRNA found in all clusters (the values used to calculate HHI). **(C)** X-ray induced genes plotted by their HHI score (calculated on 7 broad regions, not the 35 clusters) and the Euclidean distance in gene expression in seven-dimensional space at 0 rad vs 4000 rad (calculated using the 7 broad regions as described in the text). Color represents the  $\log_2FC$  of each gene when comparing all cells from the 4000 rad condition to all cells of the 0 rad condition. The dotted lines are drawn at the 95th percentile of each of the two parameters. **(D-G)** Gene expression UMAPs of example genes with <95th percentile Euclidean distance score belonging to the DDR **(D)**, apoptosis **(E)**, ROS **(F)**, and ligand **(G)** groups. **(H-I)** Gene expression UMAPs of two genes with large differences in expression pattern between 0 rad and 4000 rad identified by a Euclidean distance in the top 5%. Genes in **(D-I)** are arranged from high (top) to low (bottom) HHI score.

Adjusted p value <0.05, Average log<sub>2</sub>FC>0.1 Percent expressed either condition ≥0.01, n=3,767

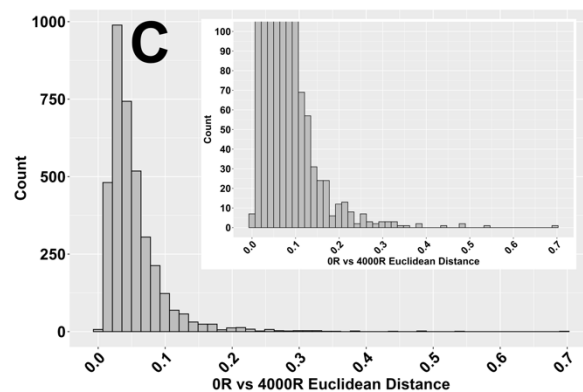
Adjusted p value <0.05, Average log<sub>2</sub>FC>0.1 Percent expressed 0 Rads >=0.01, Percent Expressed 4000 Rads ≥0.01, n=3,655

**Subcluster HHI**

**Broad Region HHI**

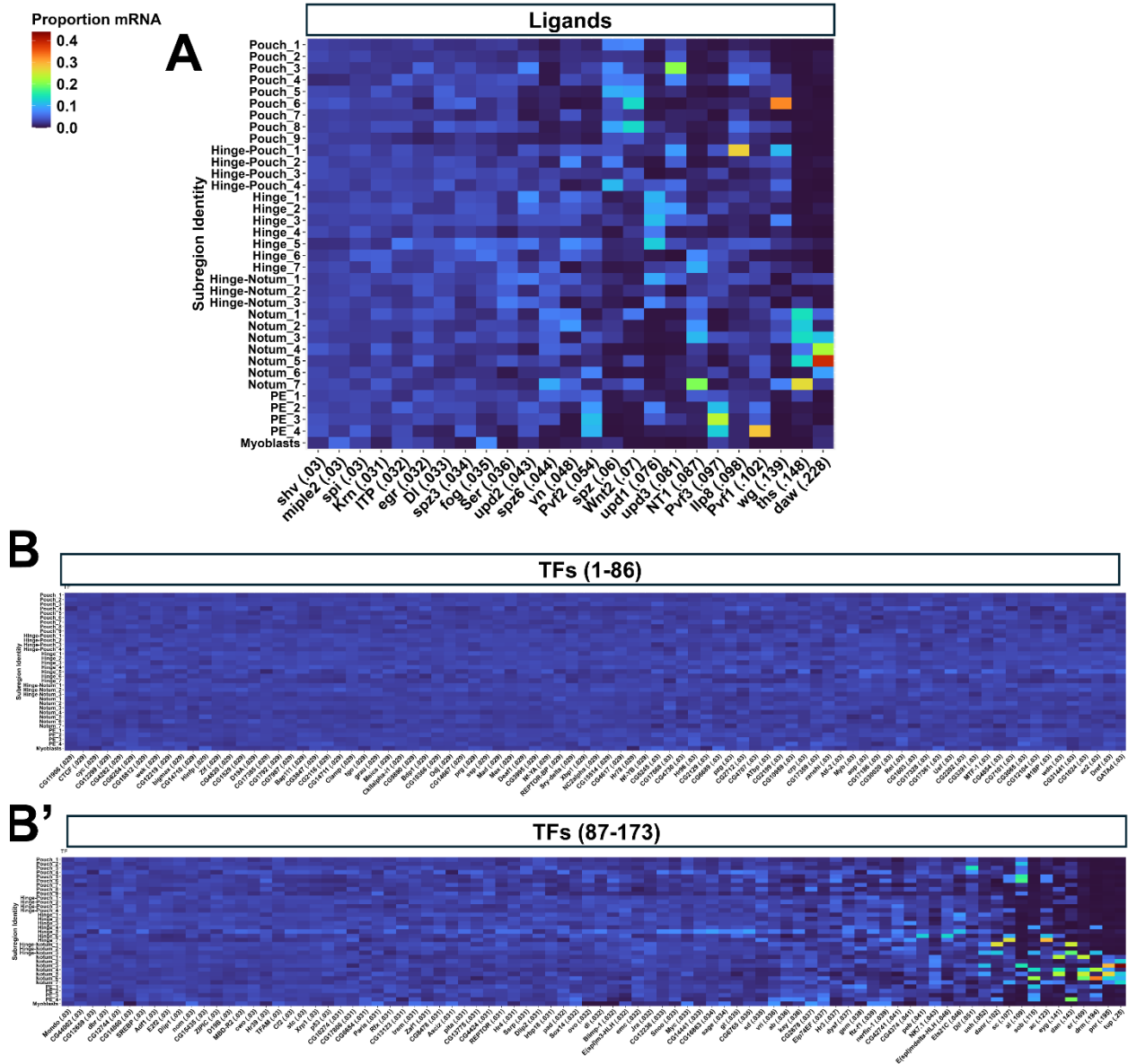


**Broad Region 0R vs 4000R Expression Distance**



**Supplement S3\_1. Histogram of cluster HHI scores, Broad Region HHI scores, and Euclidean Expression Distance scores.**

**(A)** Histogram of cluster HHI scores of 3,767 X-ray induced genes that pass the following filters: Adjusted p value < 0.05, Average log<sub>2</sub>FC > 0.1, Percent expressed *either* condition ≥ 0.01. Inset is the same histogram cropped on the y-axis to better view the distribution. **(B)** Histogram of Broad Region HHI scores of 3,655 X-ray induced genes that pass the following filters: Adjusted p value < 0.05, Average log<sub>2</sub>FC > 0.1, Percent of cells expressing in *both* conditions ≥ 1%. Inset is the same histogram cropped on the y-axis to better view the distribution. **(C)** Histogram of Expression Euclidean Distances for the same 3,655 genes as in **(B)**. Inset is the same histogram cropped on the y-axis to better view the distribution.



**Supplement S3\_2. Proportion mRNA heatmaps of Ligands and Transcription Factors**

Heatmaps showing the proportion of mRNA found in each of the 35 clusters in the 4000 rad condition for all genes in the Ligand (**A**) and TF (**B-B'**) gene categories.



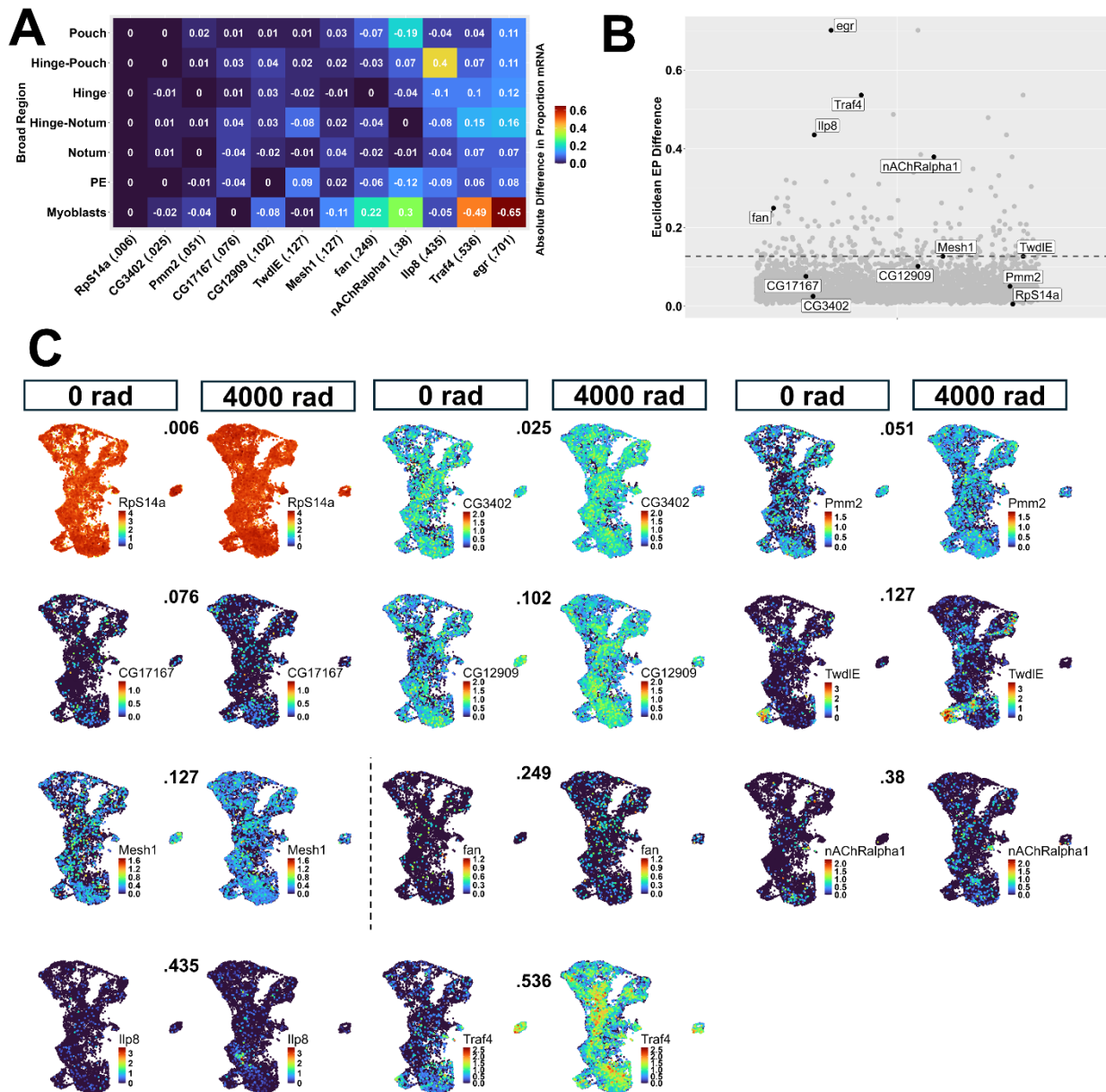
**Supplement S3\_3. Proportion mRNA heatmaps of Apoptosis, ROS, Cell Cycle, and DDR Genes**

Heatmaps showing the proportion of mRNA found in each cluster in the 4000 rad condition for all genes in the Apoptosis **(A)** ROS **(B)**, Cell Cycle **(C)** , and DDR **(D)** gene categories.



## Supplement S3\_4. Proportion mRNA heatmaps of Kinase, Phosphatase, and Receptor Genes.

Heatmaps showing the proportion of mRNA found in each cluster in the 4000 rad condition for all genes in the Kinase (A-A'), Phosphatase (B), and Receptor (C) gene categories.



### Supplement S3\_5. Examples of Genes Spanning Range of Expression Distance Score

**(A)** Heat map showing the difference in the proportion of each PD region between 4000 and 0 rad. Numbers in the tiles are the numeric values of this difference, with positive values indicating a higher proportion at 4000 rad for a given region, and negative values indicating a lower proportion at 4000 rad. Euclidean distance was calculated on the absolute values of these differences. Genes were selected to span the range of Expression Distances. **(B)** Plot showing the distribution of Expression Distances for the 3,655 genes plotted in Fig. 3C. The dotted line is drawn at the 95th percentile of scores. Genes from panel A are highlighted. **(C)** Expression UMAPs of genes spanning the range of Expression Distance scores, ordered in ascending order of Expression Distance (number above UMAPs). The dotted line separates genes below (left of the line) and above (right of the line) the 95th percentile.

### 2.3-4 The TNF ortholog *eiger* is expressed in most cells while ligands of the Toll, PDGF/VEGF and JAK/STAT pathway show regionally induced expression

To examine differences in the expression of genes with high HHI scores more closely, we focused on the 14 ligands with the highest maximum FC after X-ray exposure in any cluster. Among the top 14 ligands were genes belonging to the TNF pathway, the Toll pathway, PDGF/VEGF related pathway, and the JAK/STAT pathway.

The most highly induced and uniformly expressed ligand was the tumor necrosis factor (TNF) pathway activator *eiger* (*egr*), increasing more than 16 fold overall after irradiation (Fig. 4A left). In the 4000 rad condition, *egr* had the lowest HHI score among ligands, with expression in all major regions of the PD axis (Fig. 4A right). The two genes encoding *egr* receptors, *grnd* and *wgn*, are expressed in the disc in both conditions. *grnd* had an overall positive fold change after X-ray exposure and is expressed relatively uniformly across clusters while *wgn* has an overall negative fold change and is concentrated in the pouch and hinge-pouch (Fig. S4\_2). *Eiger* activates the JNK pathway which was previously shown to function in promoting p53-independent cell death (McNamee & Brodsky, 2009).

The Toll pathway is well known as a branch of innate immunity in *Drosophila* that is also important in wound healing (Capilla et al., 2017; Carvalho et al., 2014). Two of six Toll pathway ligands were enriched after X-ray exposure, with *Spz* being among the top 14 induced ligands (the second ligand being *Spz3*, not shown in Fig. 4). The clusters of highest FC belonged to the pouch and hinge-pouch (Fig. 4A left), with expression in the 4000 rad condition being concentrated in these regions (Fig. 4A right). Seven of nine Toll receptors in *Drosophila* were also detected in the wing disc. Toll receptor genes

*18w*, *Tl*, *Toll-7*, and *Tollo* were detected at high levels, *Toll-9* at low levels, and *Tehao* and *Toll-6* at barely detectable levels. *18w*, *Tl*, *Toll-7* and *Tollo* were expressed in varying patterns across clusters and had overall reduced expression after X-ray exposure (Fig. S4\_1).

PDGF/VEGF related signaling in *Drosophila* is known to function in cell migration and wound closure (Tsai et al., 2022). All three *Drosophila* PDGF/VEGF related ligands, *Pvf1*, *Pvf2*, and *Pvf3*, were among the top 14 enriched after X-ray exposure, with *Pvf1* and *Pvf2* having the highest overall FC (log<sub>2</sub>FC 2.14 and 1.07, respectively, Fig. 5A left). All three ligands showed a relatively high level of expression at 0 rad in the PE (Fig. S4\_1) which was maintained at 4000 rad (4A right). At 4000 rad, *Pvf1* and *Pvf2* were expressed at varying degrees in all major PD regions of the disc, while *Pvf3* had lesser expression in most clusters of the pouch and notum (Fig. S4\_1). The sole PDGF/VEGF receptor in *Drosophila*, *Pvr*, is expressed relatively uniformly across all clusters in both conditions, being slightly enriched in the 4000 rad condition, consistent with the possibility that all major regions of the disc are capable of responding to Pvf ligands.

In *Drosophila*, the JAK/STAT pathway is required for normal development but is also known to be important for regeneration of the wing disc (Herrera & Bach, 2019; Katsuyama et al., 2015). All three *Drosophila* JAK/STAT ligands, *upd1* (Harrison et al., 1998), *upd2* (Rajan & Perrimon, 2012), and *upd3* (Romão et al., 2021), were among the top 14 most induced ligands in scRNA-seq: *upd1* was primarily induced in the hinge and hinge-notum after irradiation, with concentrated expression in these regions in the 4000 rad condition that matched a similar, but lesser pattern of expression at 0 rad (Fig. 4A and 4B-4C right). *upd2* and *upd3* were expressed at low levels across all clusters at 0 rad (Fig. 4F and 4J). *upd2* was induced in all regions of the disc epithelium as well as the myoblasts, and *upd3* was primarily induced in the pouch and hinge-pouch after X-ray exposure (Fig. 4G-4K right). To validate these findings, we performed hybridization chain reaction (HCR) on *upd* transcripts in the 0 and 4000 rad conditions. *upd1* displayed a previously characterized pattern of restricted expression in the hinge and hinge-notum that was enhanced after irradiation, which was consistent with its expression UMAP (Fig. 4B, 4C). *upd2* was most highly expressed in the hinge/pouch of the wing disc with low expression in the notum (Fig. 4F-4G). *upd3* was most strongly expressed in the pouch and hinge pouch with low/undetectable expression in the hinge consistent with its expression UMAP (Fig. 4K). The sole JAK/STAT receptor in *Drosophila*, *dome*, is expressed in all clusters at 0 rad with a slight increase in expression at 4000 rad (Fig. S4\_2).

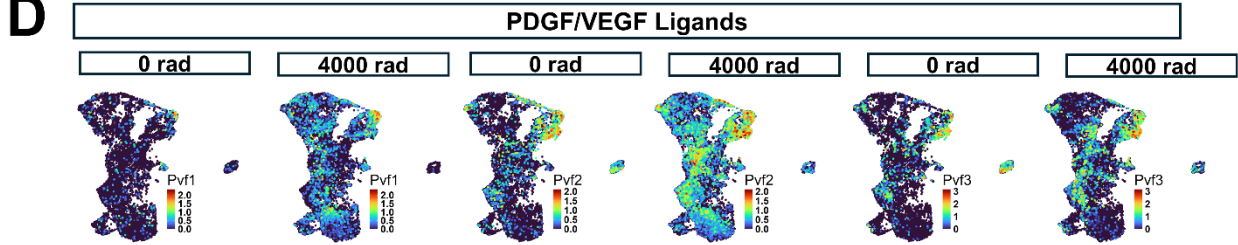
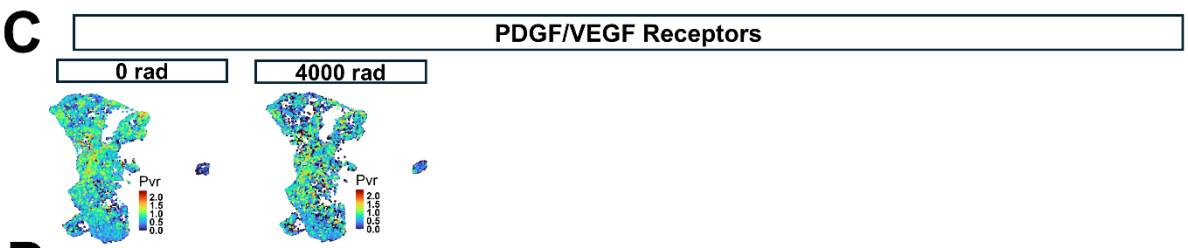
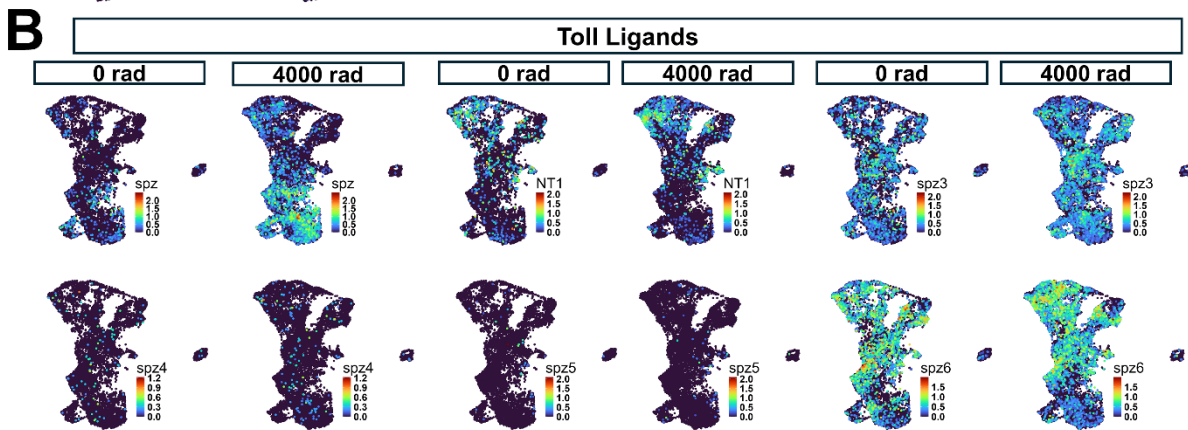
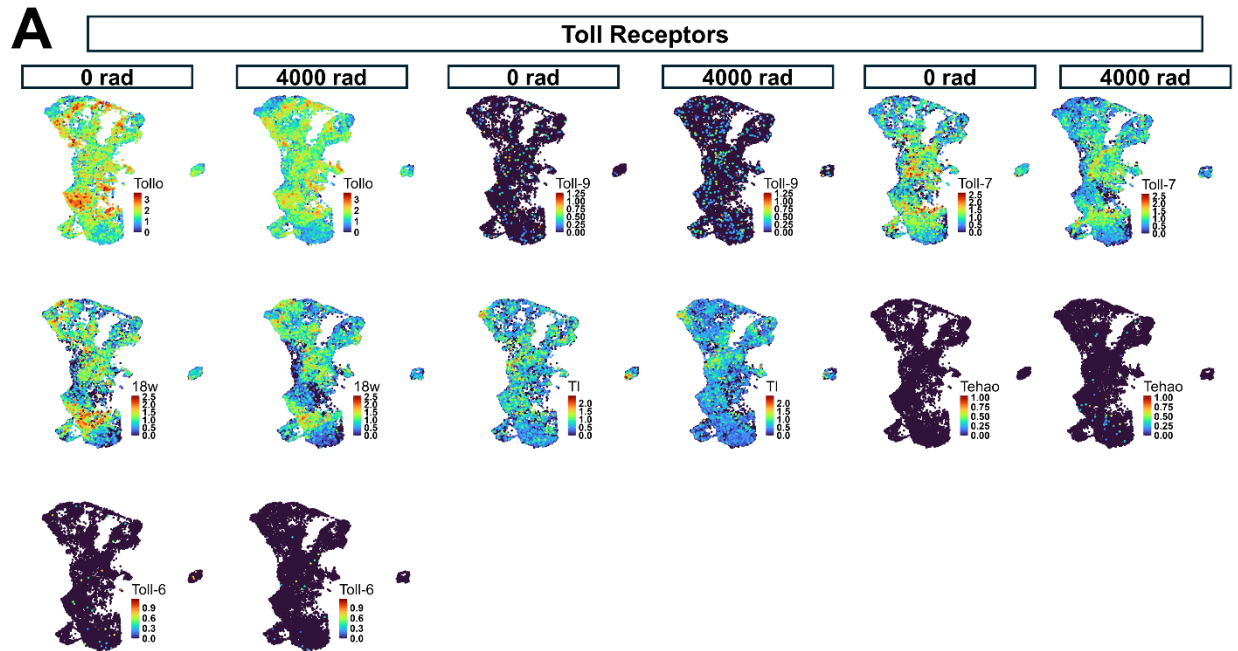
The expression of *upd2* and *upd3* in *RasV12* tumors has been shown to be dependent on p53 and confer tumor radiation resistance in *Drosophila* (Dong et al., 2021). We

therefore sought to determine if radiation induced expression of the upd genes required *p53* in normally developing irradiated wing discs. In wing discs carrying a near-complete deletion of *p53* (Xie & Golic, 2004), *upd2* and *upd3* showed little to no induction after X-ray exposure (Fig. 4H and 4I, 4L and 4M) unlike their wildtype counterparts. However, *upd1* in *p53* mutants had a normal pattern of expression in regions of the hinge before irradiation (Fig. 4D) with an increase of expression after irradiation (Fig. 4E), similar to wild type wing discs. Together, these results indicate that the normal pattern of *upd1* expression, and its induction after irradiation, is independent of *p53*. In contrast, X-ray induced *upd2* and *upd3* expression requires *p53*.



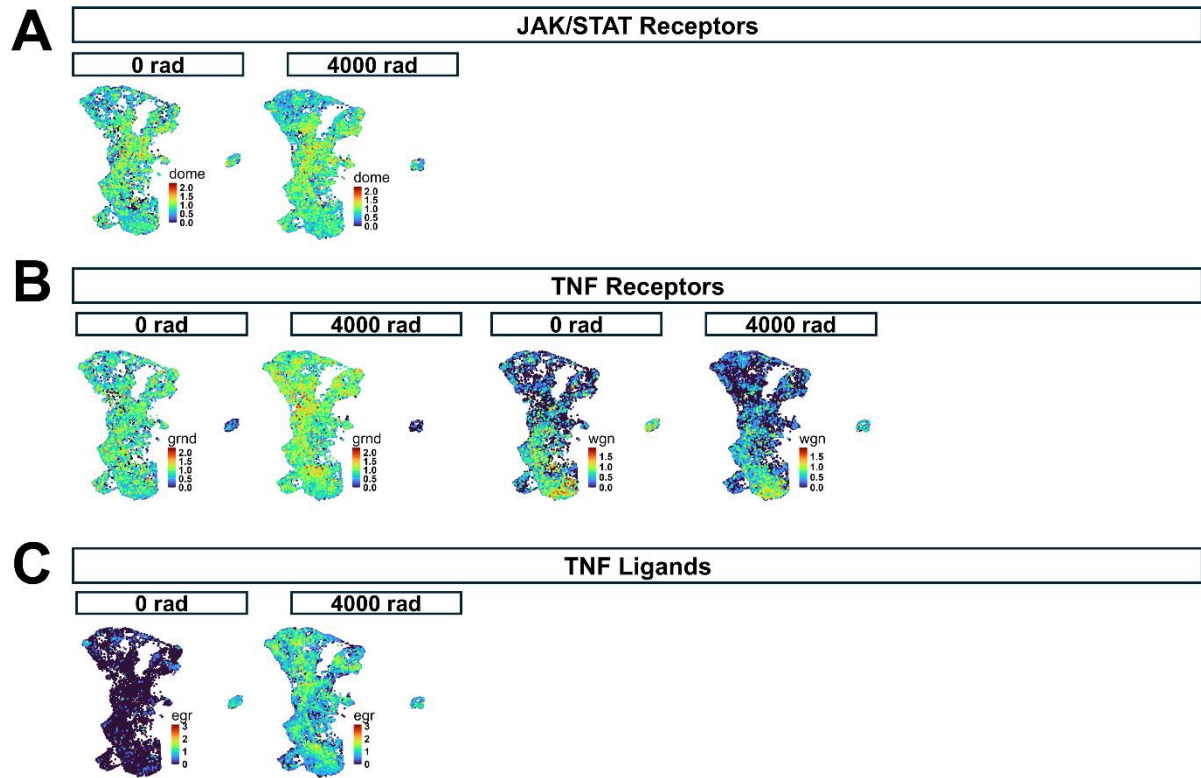
#### Figure 4. X-ray-induced expression of genes encoding ligands

**(A)** Heatmaps showing  $\log_2FC$  between conditions for each cluster (left) and proportion of total mRNA in each cluster at 4000 rad (right) of top 14 ligands ranked by max  $\log_2FC$  in any cluster. **A Left:** Boxes are colored based on the average  $\log_2FC$  from 0 rad to 4000 rad for each cluster. The left number in each box is the percentage of cells in the cluster expressing at least one transcript at 0 rad; the right number is the same at 4000 rad. Dark black numbers indicate that the change is statistically significant in that cluster (adjusted p value < 0.05, Wilcoxon Rank Sum Test, Bonferroni correction), while light gray numbers indicate that it is not (adjusted p value  $\geq 0.05$ ). Genes are sorted from left to right in descending order of the mean  $\log_2FC$  when comparing all cells of 0 rad to all cells of 4000 rad (“overall mean  $\log_2FC$ ”); The overall mean  $\log_2FC$  value is in parentheses next to gene names (all significant). **A Right:** Boxes are colored based on the proportion of mRNA expressed in that cluster vs the total amount of mRNA expressed in all clusters. Genes are sorted from left to right in ascending order of HHI score at 4000 rad. HHI score is noted in parentheses next to gene name. Genes shown in panels **(B-G)** are underlined with gray bars in **(A)**. **(B-M)** In each panel: HCR of *upd1*, *upd2*, *upd3* are in yellow and DAPI in blue at 0 rad **(B, D, F, H, J, L)** or 4000 rad **(C, E, G, I, K, M)**. Wild type discs **(B, C, F, G, J, K)** are compared to p53 mutant discs **(D, E, H, I, L, M)**. To the right of each wild-type HCR image is an expression UMAP of each gene in each condition. The myoblasts were cropped into the UMAP images for space, indicated by the dotted box around them.



**Supplement S4\_1. Toll and PDGF/VEGF ligands and receptors**

Expression UMAPs of Toll receptors **(A)**, Toll ligands **(B)**, PDGF/VEGF receptors **(C)**, and PDGF/VEGF ligands **(D)**.



**Supplement S4\_2. JAK/STAT receptors and TNF ligands and receptors**  
 Expression UMAPs of JAK/STAT receptors (**A**), TNF receptors (**B**), and TNF ligands (**C**).

### **2.3-5 Transcription factors *Dif* and *Ets21C* are expressed heterogeneously in the wing disc, while expression of *p53*, *Irbp18*, and *Xrp1* is relatively homogenous**

Similarly to ligands, we focused our attention on the TFs with the maximum FC in any cluster after x-ray exposure. Among these 14 TFs were those involved in DDR previously shown to be upregulated after IR including *p53*, *Irbp18*, and *Xrp1* (Akdemir et al., 2007; Brodsky et al., 2004; Khan & Baker, 2022), and *dysf*, a TF important for the development of several structures including the trachea (Jiang & Crews, 2003), but yet to be characterized in the context of X-ray response. Also included were genes involved in regeneration (*Ets21C*), immunity (*Dif*), and several predicted TFs with unknown functions (*CG14441*, *CG15435*, *CG2678*, *CG1729*).

*Xrp1* and *Irbp18* are two transcription factors important for DDR that form a heterodimeric unit and are upregulated after irradiation. Both *Irbp18* and *Xrp1* are transcriptional targets of *p53*, a master transcriptional regulator of DDR and apoptosis, which itself is upregulated after exposure to X-rays. *Irbp18*, *Xrp1*, and *p53* were enriched in every scRNA-seq cluster after irradiation, with relatively homogenous expression across them at 4000 rad (Fig. 5A, right). We confirmed the homogenous expression patterns of *p53* and *Xrp1* using HCR in the wing disc at 0 and 4000 rad (Fig. 5B-5C, 5Q-5R, S5\_1B for increased gain at 0 rad), which were indeed evenly expressed across the disc.

Two TFs with heterogeneous enrichment after irradiation were the pro-regenerative TF *Ets21C* (Worley et al., 2022) and the Toll pathway inducer *Dif* (Ip, 1993). In scRNA-seq, *Dif* was expressed most highly in the pouch of the disc, though was also present in other regions in the 4000 rad condition (Fig. 5A right, 5T left). An HCR of *Dif* confirmed this pattern of expression (Fig. 5T Right). *DI*, the other TF inducer of the Toll pathway was present in all scRNA-seq clusters at 4000 rad (Fig. S5\_1A). In the 4000 rad condition, *Ets21C* scRNA-seq expression was concentrated in hinge, with lesser but present expression in other regions of the disc (Fig. 5A right, 5H left). An HCR of *Ets21C* in irradiated wing discs confirmed this, with regions of high expression present in both the dorsal and ventral hinge (Fig. 5H right). We next sought to determine if *Ets21C* required *p53* for its induction after x-ray exposure and performed HCR on *Ets21C* in *p53* mutant wing discs. *Ets21C* showed little to no expression before or after X-ray exposure in *p53* mutant wing discs (Fig. 5J, 5K), indicating its dependence on *p53* for X-ray induction. This is consistent with previous work showing that p53 can activate the JNK pathway (Shlevkov & Morata, 2012), and that *Ets21C* expression is JNK dependent, at least in tissues with overgrowth perturbations (Toggweiler et al., 2016), although it is also possible that p53 directly activates *Ets21C* transcription but only in some regions of the disc.

Another TF that drew our interest was *dysf*, which is required for the development of the larval tracheal system and adult leg joints (Córdoba & Estella, 2018; Jiang & Crews, 2003), but has yet to be described in the context of exogenous stressors. In scRNA-seq, *dysf* was less concentrated in expression across clusters relative to *Ets21C* and *Dif*, but more so than *p53*, *Xrp1*, or *Irbp18* at 4000 rad (Fig. 5A, right). HCR of *dysf* revealed expression in the dorsal and anterior-ventral hinge of the disc at 0 rad (Fig. 5L, left), which was reflected in the scRNA-seq expression pattern (Fig 5L, right). At 4000 rad, *dysf* was additionally induced in all major PD regions (Fig. 5M, right, see left for matched scRNA-seq expression). However, this induction was only observed in a subset of discs, as some irradiated discs showed no additional *dysf* expression after irradiation (Fig. 5N). Importantly, irradiated discs with no induced *dysf* expression did show increased *Ets21C* and *p53* expression similar to those with X-ray induced *dysf* (Fig. 5D, 5I), supporting the fact that they weren't excluded from X-ray exposure. These discs also displayed the developmentally-regulated expression pattern of *dysf* present in unirradiated discs, indicating that the HCR probes used in this experiment were capable of detecting *dysf* RNA. The reason for the dramatic difference in *dysf* induction between discs is not known, but one possible explanation is that discs may vary slightly in maturity and that *dysf* might simply not be induced in discs that are slightly more mature as has been observed for several damage-responsive genes (Harris et al., 2020).

Interestingly, in those discs with additional *dysf* expression at 4000 rad, X-ray induced *dysf* was specifically localized to nuclei (Fig. 5M, Fig. S5\_1B for higher magnification). In contrast, the regions of *dysf* expression present at 0 rad had no discernible biased subcellular localization in either condition. The specific nuclear localization of X-ray induced *dysf* was unique among the genes we visualized with HCR.

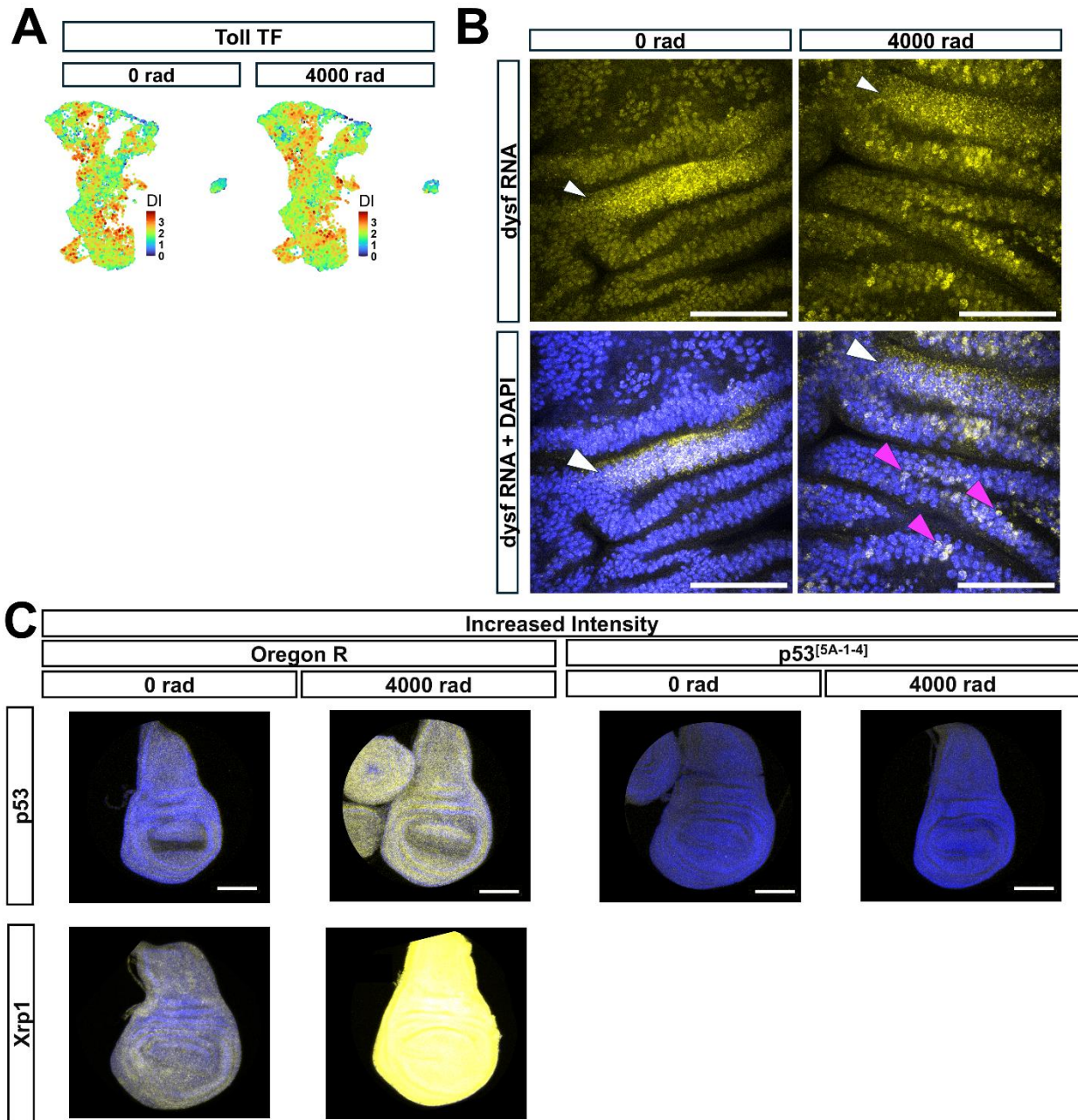
When unirradiated *p53* mutant discs were probed for *dysf*, the wildtype expression pattern was present (Fig. 5O). After X-ray exposure, no *p53* mutant discs were found to have additional *dysf* expression, though the expression pattern found in unirradiated discs was present (Fig. 5P). Together, these results indicate that the pattern of *dysf* expression found in unperturbed wing discs is *p53* independent and the RNA is not restricted to the nucleus. In contrast, X-ray induced *dysf* expression depends upon *p53*, the RNA is mostly localized to the nucleus, and appears to occur in most but not all wild-type discs.

Taken together these results indicate that, for IR-responsive transcription factors, some are induced homogeneously while others are expressed in specific regions. Moreover, at least two of the IR-induced transcription factors, *Ets21C* and *dysf*, require *p53* for their induction as has been shown for *Xrp1* by others (Brodsky et al., 2004; Khan & Baker, 2022). It is therefore likely that *p53* functions in combination with other region-specific factors to enable IR-induced expression of *Ets21C* and *dysf*.



### Figure 5. X-ray Induced Expression of Transcription Factors

**(A)** Heatmaps showing log<sub>2</sub>FC between conditions for each cluster (**left**) and proportion of total mRNA in each cluster at 4000 rad (**right**) of top 14 TFs by max log<sub>2</sub>FC in any cluster. Generated in the same way as figure 5A. Genes shown in figures B-T are underlined with gray bars in A. **(B,G,L,Q,S)** HCR of *p53*, *Ets21C*, *dysf*, *Xrp1*, and *Dif* at 0 rad in Oregon R wing discs. **(C,H,M,R,T)** HCR of the same genes at 4000 rad in Oregon R wing discs. HCR in yellow and DAPI in blue. To the right of 0 rad and left of 4000 rad HCR image is an expression UMAP of each gene in each condition. **(D,I,N)** alternative irradiated wing disc showing non-induction of *dysf* after X-rays. The myoblasts were cropped into the UMAP images for space, indicated by the dotted box around them. **(E,J,O)** HCR of *p53*, *Ets21C* and *dysf* in *p53[5A-1-4]* mutant wing discs at 0 rad. **(F,K,P)** HCR of the same genes at 4000 rad in *p53[5A-1-4]* mutant wing discs. HCR in yellow and DAPI in blue.



**Supplement S5\_1.**

**(A)** Heatmap of the Toll TF *Di*. **(B)** 63X magnification images of *dysf*HCR. White arrowheads point to the location of normal developmental expression of *dysf* in the posterior hinge (pouch is below this location). Magenta arrowheads point to X-ray induced *dysf*RNA which is localized to the nucleus. Scale bars are 50  $\mu$ m. **(C)** HCR of *p53* and *Xrp1* with increased gain. Scale bars are 100  $\mu$ m.

### **2.3-6 Cell cycle centric clustering of cells reveals an emergent, high *trbl* transcriptional state with enriched expression of several secreted signaling genes**

So far, we have characterized heterogeneity at the territorial level. However, for prior studies, we know that there must be heterogeneity in cellular responses to radiation even within territories. This is because, at the dose of radiation used, a majority of cells are expected to die while the remaining cells survive and typically resume proliferation. It is likely that these two classes of cells are interspersed among each other. For clustering thus far, we have used Seurat V5's standard pipeline, which calls upon the 2000 most variable genes in the dataset for clustering and dimensionality reduction, including UMAP. This results in clusters that are stratified based on the greatest sources of transcriptional variation at the global level. In the wing disc, the major sources of variation appear to be in genes that differ in expression along the PD axis and thus the UMAP bears some similarities to the layout of the wing disc itself where individual clusters are drawn from particular regions of the disc. In such a UMAP, cells that differ in response to radiation are likely to be found in each cluster.

We therefore considered other methods of clustering that might emphasize differences in transcriptional response that are not dependent upon the location of the cell within the disc. One approach would be to base the clustering on genes that are known to vary between cells in a location-independent manner. Our previous work has shown that in populations of relatively homogeneous cells, such as the myoblasts of the wing disc, that cell cycle genes can drive cell clustering and IR is known to affect the distribution of cells within the cell cycle.

To explore the relationship between cell cycle state and X-ray response in our data, we applied a cell cycle centric clustering approach. We performed dimensionality reduction and clustering on a manually curated list of 175 cell cycle genes (Table S6\_T1). We note that separating cells into distinct phases of the cell cycle based on transcriptional profile alone is a notoriously difficult task for which several approaches have been developed (comprehensively reviewed in Guo & Chen, 2024). One type of approach, like the one used here, relies upon manually selected cell cycle marker genes to classify cells into different cell cycle phases. Importantly, the accuracy of these approaches, including ours, is dependent on the quality of selected marker genes. The 175 cell cycle genes used here are drawn from several sources (see methods), and represent our best guess at genes with core functions in different phases of the cell cycle.

For clustering, we applied the Louvain algorithm with a resolution parameter of 0.5, using the first 30 PCs (cell embeddings transformed with CCA based integration) of the 175 cell cycle genes as variables, resulting in 6 total clusters. For visualization of

clusters, we ran UMAP on these same 30 PCs (Fig. 6A-6C'). Of the 175 cell cycle genes used for clustering, cluster 3 was high in S-phase genes including *PCNA*, *Ts*, *Claspin*, and *Mcm5*. Cluster 5 was also high in many of the same S-phase genes albeit to a lesser extent, including *PCNA*, but was also marked by three M-phase genes, *aurA*, *aurB*, and *bora* (Fig 6D, Table T6\_1). The high S-phase markers of cluster 3 (hereafter "High-*PCNA* Cluster-a") are consistent with this cluster containing cells in the G1/S phase of the cell cycle. The high but slightly lower levels of these S phase markers including *PCNA* in cluster 5, along with the expression of *aurA*, *aurB*, and *bora*, which are required for entry into mitosis, is consistent with this cluster containing cells in late S/G2 (hereafter "High-*PCNA* Cluster-b"). There was a notable reduction in the proportion of cells belonging to the High-*PCNA* Cluster-a from 0 rad (~21% of cells) to 4000 rad (~8% of cells) (Fig. 6E), indicating a reduction in the proportion of cells in this putative G1/S phase transcriptional state after X-ray exposure.

Cluster 4 was marked by the expression of *trbl*, which encodes a kinase-like protein that generates a G2/M cell cycle arrest by inducing the degradation of the mitosis promoting *Cdc25* proteins String (*Stg*) and Twine (*Twe*) (Mata et al., 2000). Cluster 4 (hereafter "High-*trbl* Cluster") had the highest expression of *p53*, high levels of genes involved in both DNA synthesis and repair, such as *RPA1*, *RPA2*, *RPA3* and *Spn-a*, and relatively low expression of *Stg* (See Table T7\_1 for complete list of cell cycle markers). High *trbl* and low *Stg* expression are consistent with this cluster containing cells arrested, or entering arrest, at the G2/M phase of the cell cycle. The High-*trbl* Cluster contained exceptionally few cells at 0 rad (~2%) with markedly increased representation at 4000 rad (~18%) (Fig. 6E). The large increase in the number of cells in this transcriptional state after irradiation is compatible with the large increase in G2/M cells after irradiation observed in vivo by other groups using the cell cycle reporter Fucci and DNA content quantification using FACS (Ruiz-Losada et al., 2022). For cluster stability at different clustering resolutions, see Fig. S6\_1. For cluster relationships, see Fig. S6\_2.

To see how cells belonging to the High-*PCNA* and High-*trbl* Clusters were distributed amongst clusters that were previously generated at a global level from the 2000 most variable genes in the dataset, we transferred cell cycle-based cluster annotations onto our previously clustered data. We found that cells belonging to the High-*PCNA* and the High-*trbl* clusters were distributed among each of the seven broad PD regions (Fig. 6D-6D'). As expected, *PCNA* and *trbl* expression matched the distribution of High-*PCNA* and High-*trbl* Cluster identities (Fig. 6G-6I').

Next we focused on differences in highly induced genes ("HIGs", defined as X-ray induced genes  $>\log_2FC$  1 between conditions,  $n=359$ ) between cell cycle clusters. At 4000 rad, both High-*PCNA* Clusters had relatively low levels of many X-ray induced genes including those involved in apoptosis (*rpr*, *hid*, *Corp*, *egr*). This was a general

trend, with the average scaled expression across HIGs being slightly lower in the High-PCNA Clusters than in other clusters (Fig. 7A). Both of these clusters had few positive X-ray induced markers (Table S7\_T1). In comparison, the High-*trbl* Cluster showed a strong enrichment for many HIGs, having the highest average scaled expression across all of these genes (303/359) compared to other clusters in the 4000 rad condition (Fig 7A).

The High-*trbl* cluster was enriched in HIGs involved in apoptosis (*rpr*, *hid*, *Corp*, *egr*), DNA damage repair (e.g. *rad50*, *lrbp18*, *Ku80*, *mre11*) and ROS related genes (*GstE6*, *GstE7*, *GstD1*). Additionally, this cluster was enriched in HIGs encoding a subset of TFs (*Ets21C*, *dysf*, and *Dif*), and secreted proteins (*Pvf2*, *upd2*, *upd3*, and *spz*) (For complete list of markers, see Table T7\_1). Most of these gene categories were represented among the top 24 HIGs with highest expression in the High-*trbl* Cluster (Fig. 7B). Though the majority of HIGs were highest in the High-*trbl* cluster, 56/309 were generally more homogenous across clusters (Fig. 7C), with none having relative expression in other clusters as high as those enriched in the High *trbl* cluster (Fig. 7A, 7C). These results suggest that a High-*trbl* transcriptional cell cycle state, which accounts for approximately 18% of cells, is associated with the bulk of X-ray induced gene expression.

The high *trbl* cluster was also enriched in two noteworthy secreted HIGs: *Swim* and *Arc1*. *Swim* is a secreted protein that binds to *wg* and has been proposed to aid in its spreading, though this point is contended (McGough et al., 2020; Mulligan et al., 2012; Simões et al., 2022). *Arc1* is a retroviral gag protein primarily described as a regulator of neural plasticity in *Drosophila*, but was recently shown in a *RasV12* tumor model to be expressed in tumor associated hemocytes, with a loss of function being associated with larger tumors, decreased pJNK, and decreased Dcp-1 activity in tumors (Khalili et al., 2023).

In conclusion, our results are consistent with transcriptional states that likely correspond to early and late S-phase being reduced in proportion after X-ray exposure, and cells accumulating in what might be a normally uncommon transcriptional state that could correspond to a G2/M arrest. Cells in the putative G1/S and S/G2 states have relatively low expression of many HIGs. In contrast, cells in the putative M/G2 stalled state show relatively high expression of many HIGs and seem to be responsible for the bulk of X-ray induced gene expression.

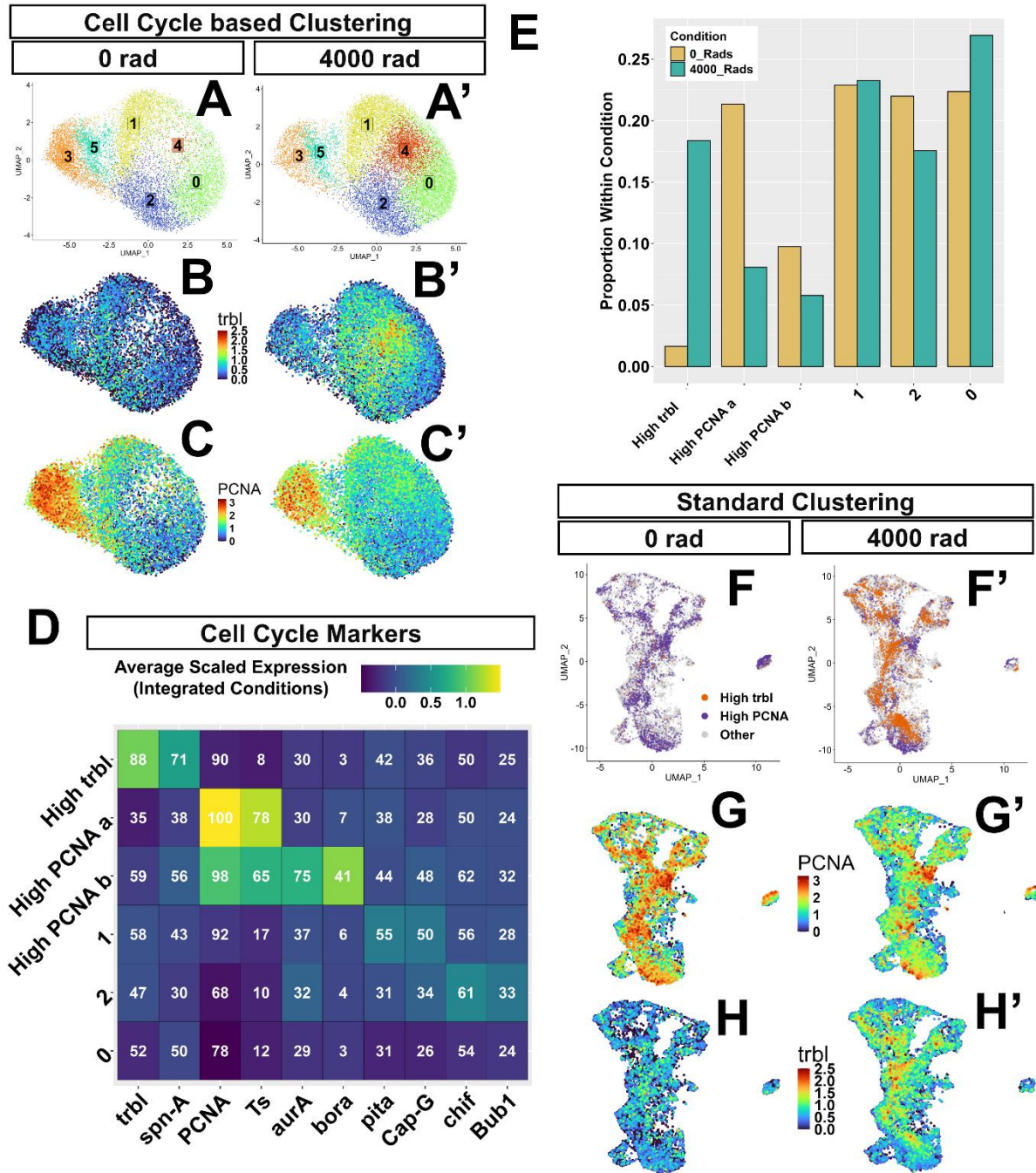
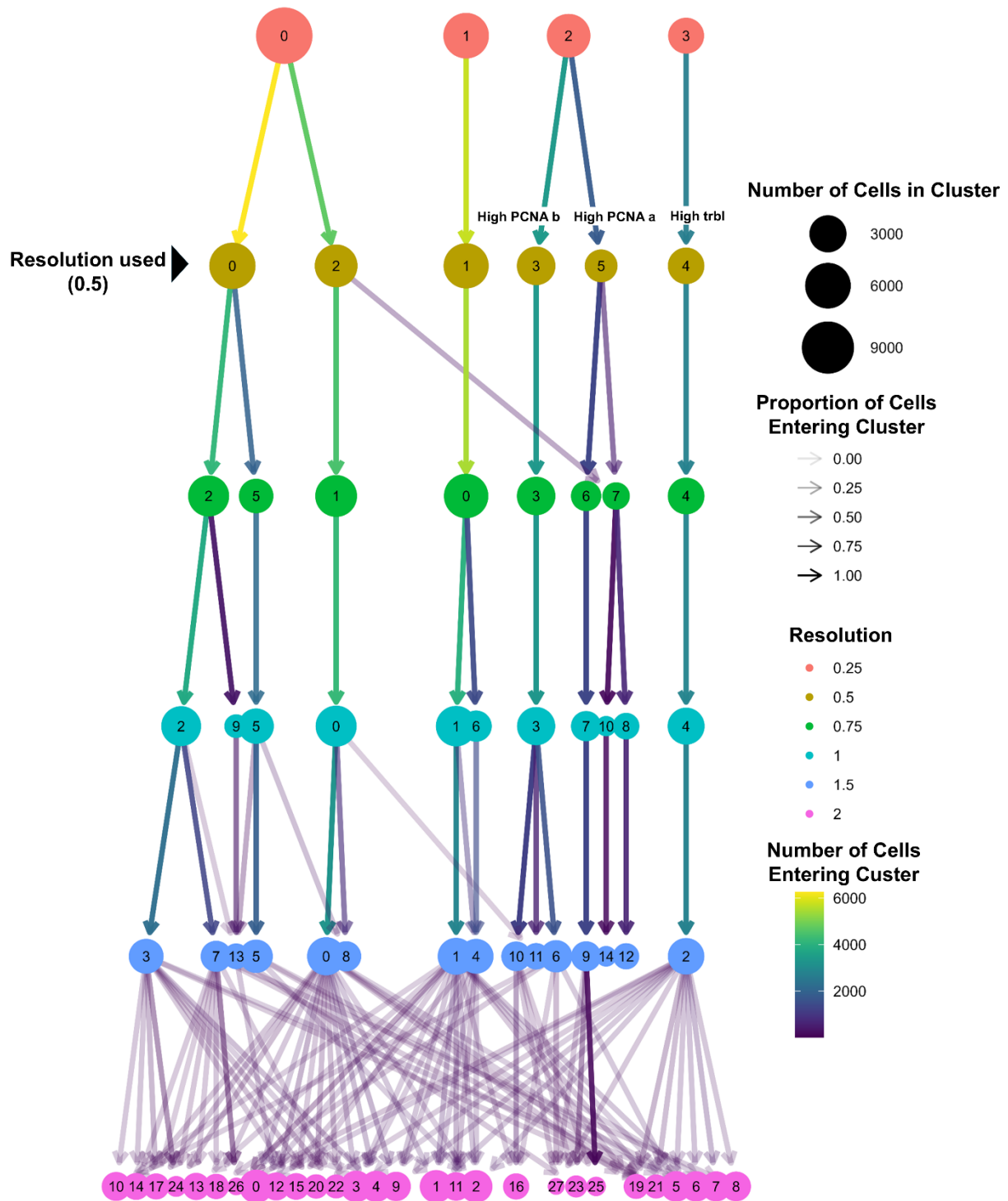


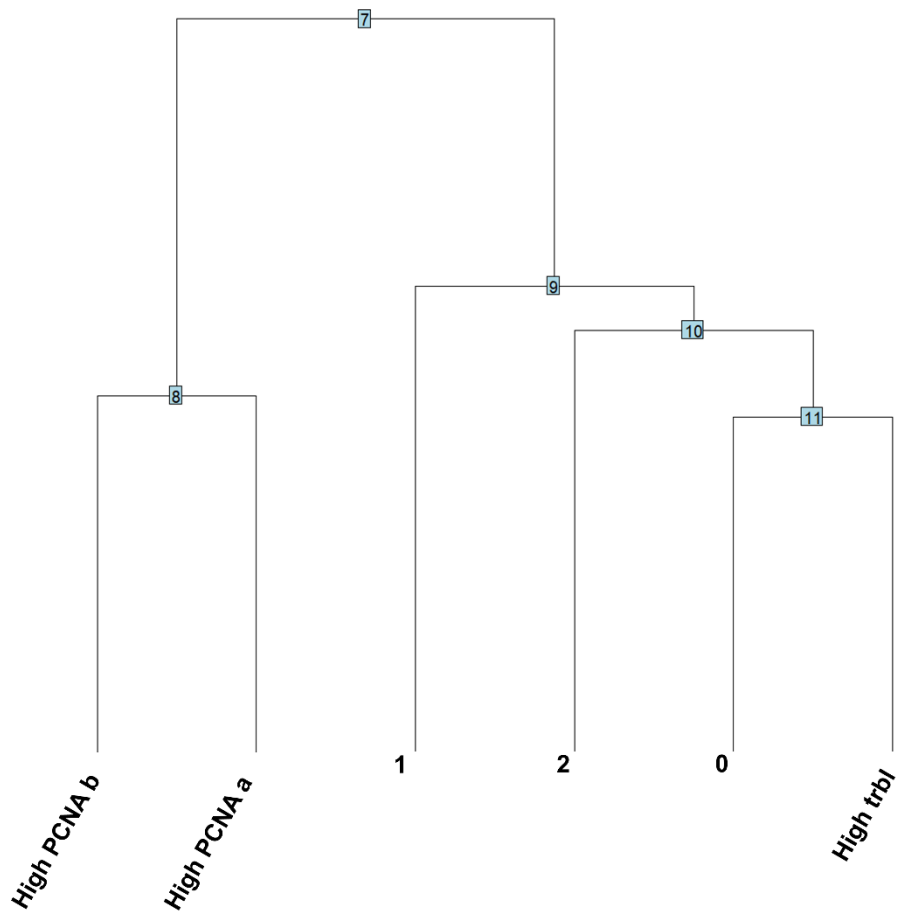
**Figure 6. Visualization of expression changes using cell-cycle-based clustering** (A - A') Cluster UMAPs of data processed and clustered on cell cycle genes at 0 rad (A) and 4000 rad (A'). (B-C') Expression in this UMAP object of *trbl* and *PCNA* at 0 rad (B, C) and 4000 rad (B', C'). (D) Heatmap showing average scaled expression of cell cycle marker genes in each cell cycle cluster. Numbers are the percent of cells expressing each gene in each cluster. (E) Bar plot showing the proportion of cells each cluster contributes to 0 rad (cream) and 4000 rad (teal) conditions. (F-H') High *trbl* cluster 4 (in orange) and high *PCNA* clusters 3 and 5 (in purple) from panels A-A' mapped onto the

standard UMAP at 0 rad (**F**) and 4000 rad (**F'**). (**G-H'**) Standard expression UMAPs of *PCNA* and *trbl* at 0 rad (**G, H**) and 4000 rad (**G', H'**).



### **Supplement S6\_1. Cluster tree showing cluster stability at different clustering resolutions**

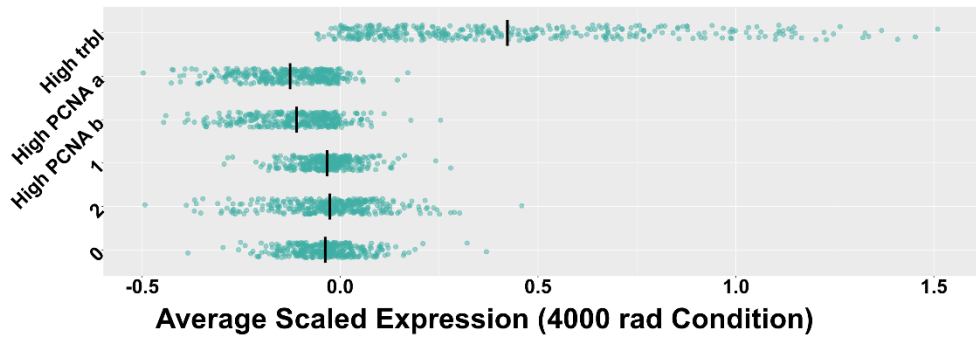
Tree showing clusters generated using different Louvain clustering resolution parameters on the integrated dimensions derived from 175 cell cycle genes. Each node is a cluster (cluster numbers are in order of decreasing cluster size but otherwise arbitrary). Each row of clusters from top to bottom are derived from increasing resolutions. Arrows represent cells moving from one cluster identity at a lower resolution to a different cluster identity at the next resolution. Arrow color represents the number of cells making the transition, and arrow transparency represents the proportion contribution of those cells to the new cluster.



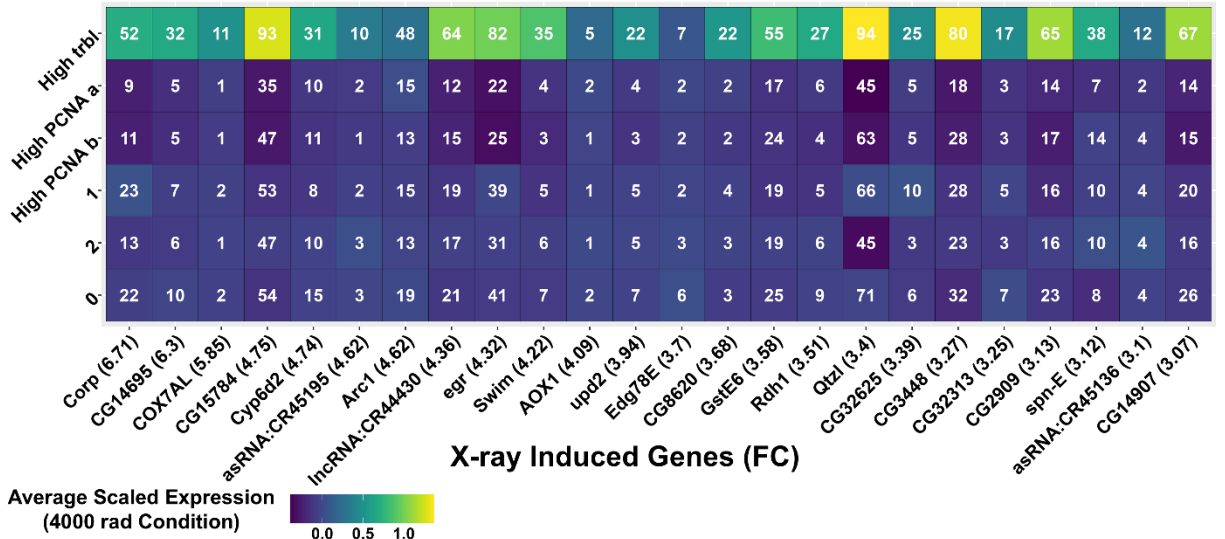
### Supplement S6\_2. Dendrogram of cell cycle based cluster relationships

Dendrogram showing the relationship of cell-cycle based clusters to one another in integrated PCA space. Shorter lines represent a closer relationship; Longer lines a more distant relationship.

**A** X-Ray Induced Genes, log2FC ≥ 1, n=359



**B** Max Expression: High trbl Cluster



**C** Max Expression: Other Cluster

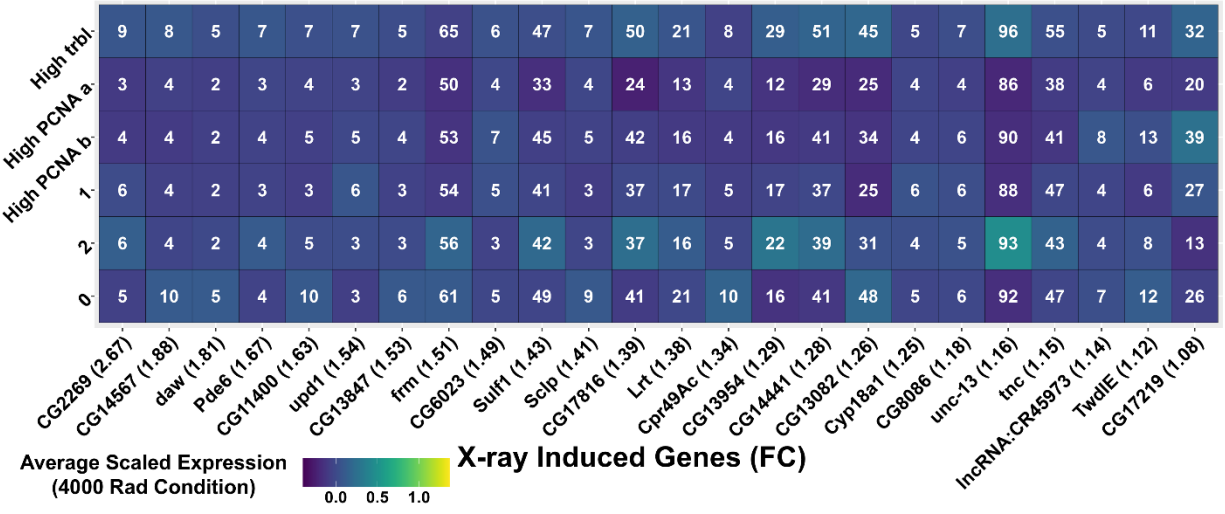


### Figure 7. Differences in gene expression between cell cycle clusters

**(A)** Mean scaled expression of X-ray induced genes  $\geq$  avg  $\log_2$ FC 1 between conditions. Values calculated using the 4000 rad condition on cell-cycle-based clusters. Each row contains the same genes. **(B)** Heatmap showing average scaled expression of the top 24 X-ray-induced genes with highest expression in the *trbl* cluster. **(C)** 24 of the genes expressed maximally in one of the other clusters. Numbers are the percent of cells expressing each gene in each cluster. Only genes with  $\geq$  5% expression in any cluster at 4000 rad were selected from the initial 359.

### 2.3-7 Simultaneously visualizing two levels of heterogeneity

To compare the level of heterogeneity that was observed using the two clustering approaches for individual genes, we plotted their two HHI scores on a two dimensional plot where the X-axis shows the score obtained using cell-cycle-based clustering and the Y-axis shows the score obtained from the clusters obtained with the standard Seurat pipeline (Fig. 8). For these plots we used transformed HHI scores where the original HHI scores which ranged from  $1/N$  to 1 (where N represents the number of clusters) were mapped to a range from 0 to 1 using a linear transformation. Importantly, the two parameters cannot be considered to be truly orthogonal since the cell-cycle state likely makes some contribution to the clustering using the standard pipeline and because a cell's location in the disc might affect its behavior with respect to the cell cycle. Additionally, the distribution HHI scores with respect to any parameter changes with the number of clusters being analyzed - thus the values on the two axes are not directly comparable. With these caveats in mind, these plots provide us with a sense of the extent of heterogeneity of expression that each gene displays when assessed in each of these two ways.

As can be seen from the plots, genes encoding components of the DNA-damage response and regulators of ROS levels, apoptosis and cell-cycle progression are expressed broadly in the disc since their HHI scores are low when the standard clustering pathway is used. However, genes in each of these categories have a diversity of HHI values when the cell-cycle-based clustering is used, indicating that some of these genes show variations between cells that correlate with their cell-cycle state (Fig. 8A - D). Genes encoding transcription factors (Fig. 8E) or ligands (Fig. 8H) display a variety of HHI scores along both axes indicating that they have both inter-regional and intra-regional heterogeneity. Signaling proteins such as phosphatases, kinases and receptors (Fig. 8F, G, I) show an intermediate level of variation with respect to both parameters.

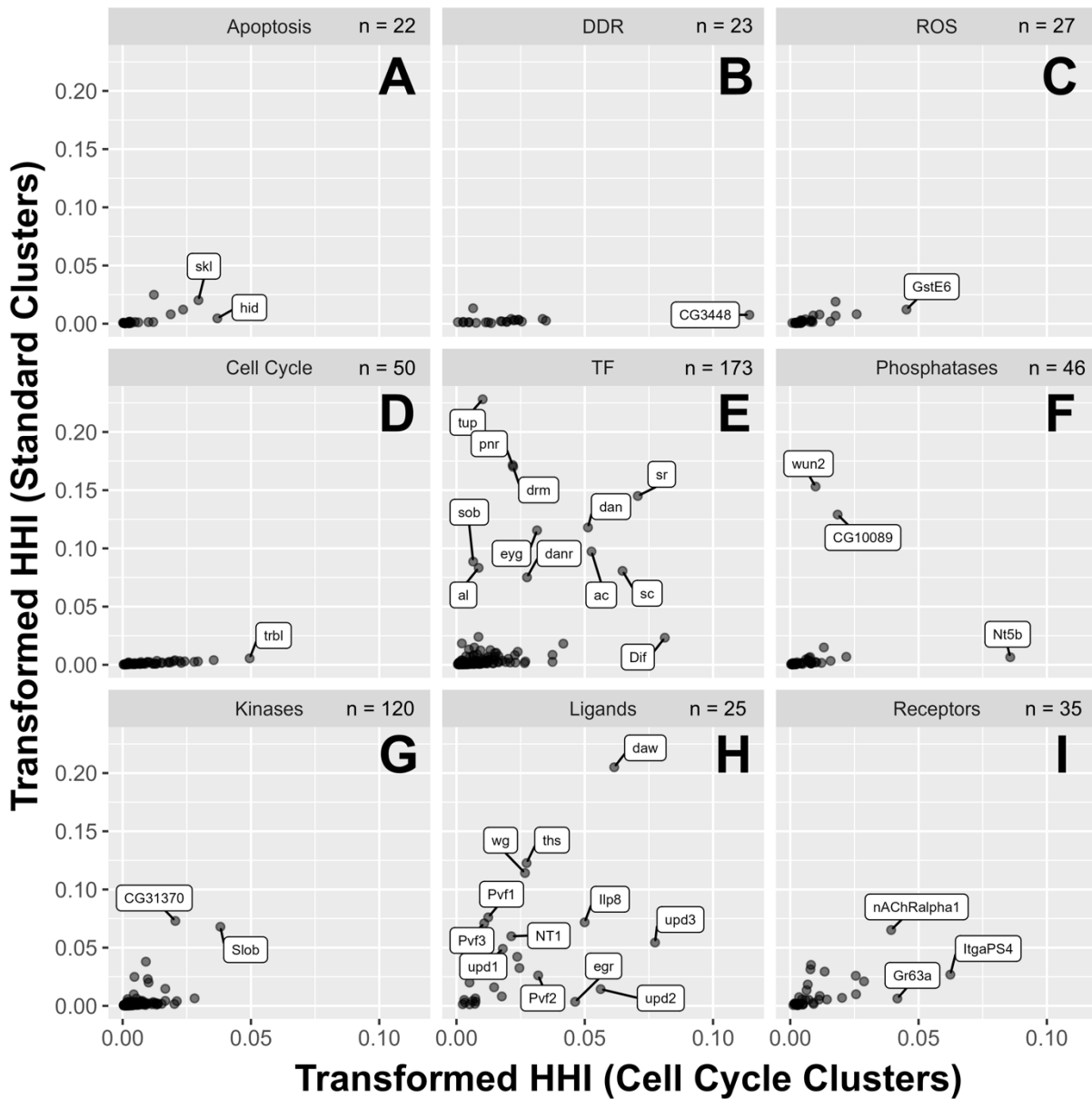


**Figure 8. HHI scoring of categorical genes in standard clusters vs cell cycle clusters.**

(A-I) Transformed HHI scores calculated using the 35 standard clusters (y-axis) and the 6 cell cycle based clusters (x-axis). Genes used were the 521 categorical genes used previously in Fig. 3A. Scores were calculated using the 4000 rad condition only. Genes displayed encode for proteins involved in apoptosis (A), DDR (B), ROS (C), cell cycle (D), TFs (E), Phosphatases (F), Kinases (G), Ligands (H), and Receptors (I). Genes are labeled where space permits, but were otherwise chosen arbitrarily.

## 2.4 Discussion

An important shift in our understanding of biological systems in recent decades has been an increasing awareness of heterogeneity. This applies at multiple levels – from molecules to cells. At the level of cells, even individual cells in microbial communities have considerable phenotypic diversity, especially in response to changes in environmental conditions (Ackermann, 2015). Thus, it is likely that cells in mammalian tissues, which are often composed of many different types of cells, will display diverse responses to external stressors such as ionizing radiation. Only recently have single-cell approaches been used to study the effects of ionizing radiation on complex tissues, for example (Lu et al., 2023; Mills et al., 2025; Morral et al., 2024; Mukherjee et al., 2021; Sheng et al., 2020; Yuan et al., 2023). These studies have mostly focused on changes in cellular composition following radiation, or in characterizing particular subpopulations, rather than attempting to address the overall types of heterogeneity in response within and between cell types.

To make the study of heterogeneity of cellular responses to radiation more tractable, we have used a relatively simple and homogenous tissue, the *Drosophila* wing disc which is mostly composed of two different cell types (reviewed by Tripathi & Irvine, 2022). Each wing disc is composed of a little over 30,000 epithelial cells (Martín et al., 2009) and approximately 2,500 myoblasts (Gunage et al., 2014). This has allowed us to look for differences in the way cells in different parts of the wing disc respond to radiation without the complication of a diversity of cell types. Our studies have uncovered two kinds of heterogeneity (Fig. 9). The first kind, inter-regional heterogeneity, is where some genes are upregulated far more in some territories of the wing disc than in others (Fig 9A). The other kind of heterogeneity, intra-regional heterogeneity, is manifest in all regions of the wing disc. Here cells with different types of radiation-responsive transcriptomes are interspersed among each other (Fig 9B).

### **Using the Herfindahl-Hirschman Index to assess heterogeneity of single-cell datasets**

Studies that use single-cell RNAseq or multiomics frequently characterize differences in gene expression between clusters, but they typically do not use quantitative approaches to examine the extent of heterogeneity between clusters on a genome-wide level. To develop a means of ranking genes with respect to heterogeneity of expression between clusters, we have used a simple mathematical tool, the Herfindahl-Hirschman Index (HHI), which is most typically used by economists to study market concentration (Herfindahl, 1950; Hirschman, 1945). This and other mathematical ways of calculating heterogeneity are summarized by (Steele et al., 2022). In the context of our application,

a low HHI index value indicates a lower level of concentration or more homogenous expression, while a higher value indicates that most of the expression occurs in one or a few clusters. While the value of the index for any given gene is not particularly useful in isolation, ranking genes has allowed us to identify those genes that are expressed more homogeneously among clusters as opposed to those that are expressed primarily in a few clusters. When we have used the conventional Seurat pipeline, a higher HHI typically identifies genes that are expressed in a subset of territories in the wing disc i.e. inter-regional heterogeneity. When applied to clusters generated using a curated set of cell-cycle genes, a high HHI indicates that that gene is preferentially expressed in a subset of cells that have a particular transcriptome state of cell cycle genes. This type of intraregional heterogeneity is observed in most, if not all, parts of the disc. Thus, these two types of heterogeneity can be shown simultaneously using a two-dimensional plot (Fig. 8). Given that the same tissue can be analyzed using a variety of cellular parameters (e.g. chromatin accessibility, proteomic approaches), cells can be clustered using each of these approaches, and an HHI score for each gene could be calculated with respect to that parameter. In principle, each gene could then be assigned a multi-dimensional HHI score that reflects its heterogeneity with respect to each parameter.

### **Characterization of inter-regional heterogeneity**

Since DNA damage, as assessed by p-H2Av immunofluorescence, is uniformly distributed throughout the disc, it is unsurprising that most genes that are upregulated in response to DNA damage are also expressed relatively uniformly. These include genes encoding proteins that repair DNA damage, inactivate ROS as well as those that regulate cell-cycle responses and apoptosis in response to DNA damage. This also applies to the key transcription factor considered to regulate many of the transcriptional responses to DNA damage, p53. We find that heterogeneous expression with respect to geographical territories in the wing disc is most evident among some genes encoding transcription factors and secreted ligands and found occasionally among receptors and signal transducers such as kinases and phosphatases.

Why are these genes expressed heterogeneously? By manually inspecting gene expression we find that in many cases, the expression pattern following irradiation is similar to that in unirradiated discs. Like our approach with the HHI, we have used a Euclidean distance measure in seven-dimensional space to rank the difference in expression pattern with respect to the seven major regions of the disc under the two conditions (unirradiated versus irradiated) (Fig. 3C). Genes with an especially low Euclidean distance have more similar patterns of expression between the two conditions. Clear examples are *dawdle* (*daw*) which encodes a ligand for an activin

receptor, and *upd1* which encodes a ligand upstream of the JAK/STAT pathway, which have similar patterns of expression under the two conditions but are expressed at higher levels in the same regions after irradiation. Why might this happen? One possibility is that the expression of this gene requires both a region-specific transcription factor and a transcription factor induced by irradiation. An alternative possibility is that the chromatin state of such genes might reflect their pattern of expression in the unirradiated disc; a radiation-induced transcription factor might bind more readily to genes that already have more accessible chromatin. Both explanations are consistent with our observation that the non-uniform upregulation of several radiation induced genes including *upd2*, *upd3* and *Ets21* require the function of *p53* which is induced by X-ray irradiation yet expressed in all territories of the disc.

For some genes such as the JAK/STAT ligands *upd2* and *upd3*, expression is clearly non-uniform after radiation. Yet in the unirradiated condition, expression is not detected. This pattern of induction is more difficult to explain. It is possible that *upd2* and *upd3* might be expressed at extremely low levels in unirradiated discs in patterns similar to their induction. Also possible is that the chromatin state of these genes, even if they are not expressed in the unirradiated disc, shows inter-regional heterogeneity. This phenomenon was also observed with the transcription factor *Ets21C* which is known to be necessary for regeneration of the wing pouch after its ablation (Worley et al., 2022). Identification of many such examples of interregional differences in the induction of genes that likely play an important role in response to radiation indicate that this phenomenon is relatively widespread and that its mechanistic basis merits further investigation.

### **Intraregional heterogeneity: cells with a particular cell-cycle transcriptome show the highest levels of upregulation of damage-responsive genes**

Since the standard Seurat pipeline, when applied to the wing disc, generated clusters that most reflect a cell's location in the wing disc, we tried alternative approaches that could separate cells into clusters that were agnostic to their location in the disc. Using a curated set of cell-cycle genes, we were able to separate cells into six clusters. One cluster accounted for only 2% of cells in the unirradiated state but 18% of cells following irradiation. This cluster was marked by high expression of the *trbl* gene which encodes a pseudokinase that promotes the degradation of the Cdc25 ortholog String (Mata et al., 2000). Based on their transcriptome, cells in this cluster are likely to be in G2 and prevented from entering mitosis. Unexpectedly, *p53*, as well as genes involved in DNA repair, apoptosis and inactivation of ROS were all most highly expressed in this cluster at 4000 rad as were the majority of radiation-induced genes. Thus, rather than being

expressed uniformly in all cells, expression of many radiation-induced genes shows strong intra-regional heterogeneity with the highest expression found in a subpopulation that occupies a particular cell-cycle transcriptomic state. This same high-*trbl* cluster also expresses higher levels of the transcription factor *Ets21C* as well as genes encoding a variety of secreted ligands such as *Pvf2*, *upd2*, *upd3* and *spz*. Studies of regeneration in recent years have identified situations where subsets of cells function to organize regenerative proliferation by secreting factors that promote the survival and proliferation of other cells (Aztekin et al., 2019;). Indeed, following ablation of the wing pouch, a localized subpopulation of cells likely arrested in G2 (Cosolo et al., 2019) promotes the proliferation of surrounding cells (Worley et al., 2022). In the case of diffuse damage, such as that elicited by X-ray exposure, the analogous population of organizing cells could be dispersed throughout the disc and interspersed with other cells. Cells belonging to the high-*trbl* cluster could potentially represent such a population.

### **Functional consequences of heterogeneity**

Many of the genes that display intraregional heterogeneity have been implicated previously in regulating cell survival and proliferation as well as in activating mechanisms that function during regeneration. These include the *upd2* and *upd3* genes, and the transcription factor *Ets21C*. Previous work has shown that a region of the wing disc, the dorsal hinge, has less apoptosis following irradiation that is dependent upon increased JAK/STAT signaling in that region (Verghese & Su, 2016). It is therefore likely that many of the examples that we have observed of interregional heterogeneity have functional consequences. A systematic disruption of all genes that display heterogeneous patterns of expression would give us a more complete view of this phenomenon.

The observation that many of the highly inducible genes are expressed in a subset of cells that have a particular cell-cycle state was an unexpected finding of our analysis. This could imply that cells must be in this state to most effectively turn on these genes. Alternatively, the suite of genes that are expressed most after irradiation could push the cells to a particular cell-cycle state. Such a state might be more conducive to the repair of cellular damage and to promote local and systemic responses to radiation that facilitate recovery. Further study of this phenomenon could enable ways of using cell cycle manipulations to alter radiosensitivity.

## Concluding remarks

Our studies have focused on one time point at one developmental stage in a relatively simple tissue. The levels of heterogeneity that we have uncovered here show that heterogeneity in response to radiation must be far more widespread and complex in tissues such as mammalian organs that are composed of many different types of cells. The approach and the methods of analysis that we have used here should be applicable, with appropriate modifications, to these more complex situations.

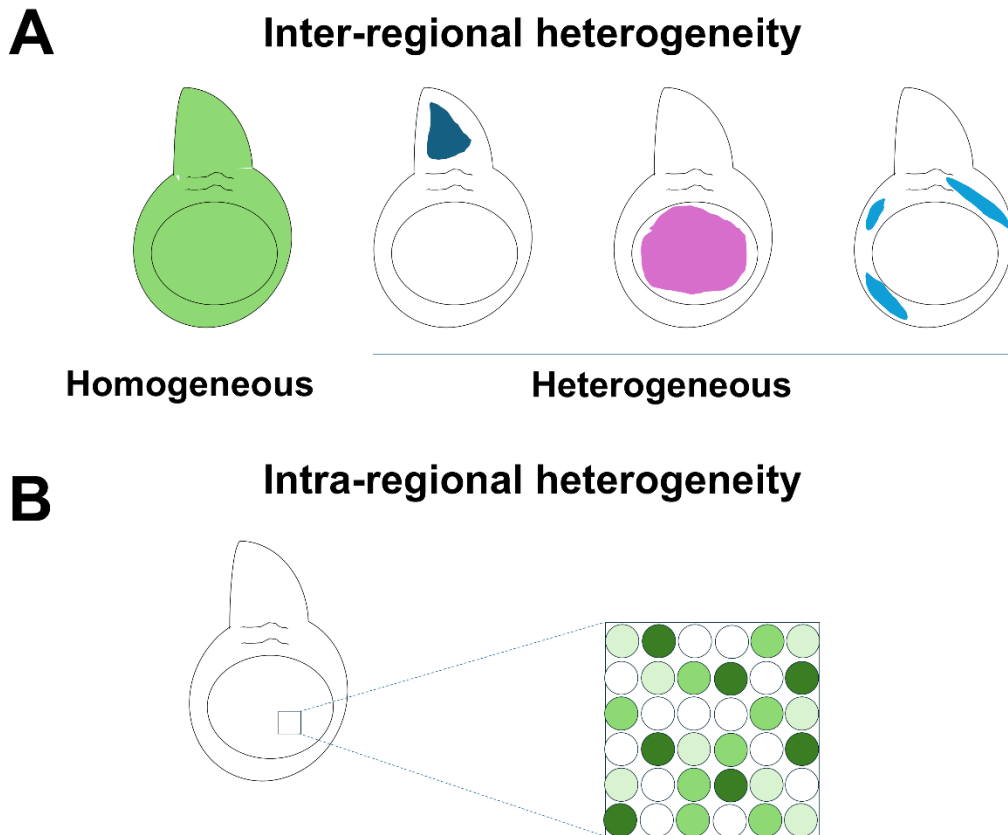


**Figure 9. Two types of heterogeneity following X-ray irradiation**

(A) Inter-regional heterogeneity. Many genes are expressed uniformly while some are expressed in specific territories following irradiation.

(B) Intra-regional heterogeneity. In the example shown, a gene is expressed at high levels in some cells, intermediate levels in some, and no expression in others. Cells with different levels of expression are interspersed.

## 2.5 Materials and Methods

### Fly strains used

Oregon R was used for wildtype experiments and p53[5A-1-4] (BDSC #6815) was used for p53 mutant experiments.

### Antibodies used

*Primaries:* Rabbit anti-H2AvD-pS13 (#600-401-914, Rockland), 1:250; Rabbit anti-Dcp-1 (#9578S, Cell Signaling), 1:250 ; Rabbit anti-PHH3 (#06-570, Millipore), 1:500 ; Rat anti-Zfh2 (), 1:200; *Secondaries:* Goat anti-rat Alexa Fluor 555 (A21434, Invitrogen), 1:500; Goat anti-rabbit Alexa Fluor 555 (A21428, Invitrogen), 1:500;

### Single-Cell Sequencing Experiments

#### *Preparation of Petri Dish Food Plates for Rearing and Irradiation*

For scRNA-seq experiments: Fly food prepared using the Bloomington *Drosophila* Stock Center (BDSC) formula was melted in the microwave and poured to a height of 10 +/- 2 mm into clear 15 mm x 60 mm petri dishes. After cooling, condensation was wiped from the lid, and ~1/8th tsp of dry active yeast was added on top of the food. Plates were stored at room temperature for 1-2 days before use.

#### *Egg Collections and Rearing*

All single-cell experiments were performed using the "Oregon R" wildtype fly strain. Egg lays and rearing were performed at 25C. Groups of 15 males and 35-40 females were sorted into food vials and allowed to recover from CO<sub>2</sub> incapacitation. Flies were then tapped into egg lay bottles containing a grape agar plate topped with a dollop of yeast paste and pre-incubated for 1-2 days to increase egg yield. On the day of egg collection, flies were tapped into egg-lay bottles containing fresh grape agar plates and yeast paste, and incubated for 4 hours. After the egg lay period, grape plates were collected and yeast paste was removed. Eggs were incubated for 24 hours, after which 1st instar larvae were picked using a poker tool dipped in yeast paste for adhesion. 50 larvae were deposited into each petri dish food plate, and incubated until their time of irradiation/dissection.

#### *Dissections, Tissue Dissociations, and FACS*

All microcentrifugations between washes were performed at 5,000 RPM (~2,000 g) at room temperature. All samples and media were stored on ice unless otherwise noted. Larvae were collected into 1X PBS and dissected in supplemented schneider's media (SSM) at room temperature over one hour. Wing discs were collected into SSM on ice, pooled into 1.5 ml Eppendorf tubes, and washed with Rinaldini solution. Wing discs were dissociated at 37C in 0.25% Trypsin EDTA (Sigma T4049) for 10 minutes. Dissociated cells were washed once in PBS-10% FBS and twice in PBS-1% FBS. Cells were pooled together in a final suspension of 500 ul PBS-1% FBS and passed through a 35 uM filter into a FACS tube. Cell suspensions were sorted on a BD FACSAria

Fusion. Forward scatter and side scatter were used to sort out debris and doublets. Propidium iodide (PI) was added to the sample and a Texas Red filter was used to remove low quality/dead cells: PI fluorescence intensity revealed a bimodal distribution of cells, and a gate was drawn between the two distributions. The upper distribution was sorted out. Cell concentrations were determined using a hemocytometer, and brought to an appropriate final concentration in accordance with 10X Genomics v3.1 guidelines.

#### *Library Preparation, Sequencing, and Alignment*

cDNA libraries were generated using 10X Genomics v3.1 chemistry and hardware. All libraries were sequenced at a depth of around 1 billion paired end reads. Sequences were aligned to *Drosophila* transcriptome v6.55 using Kallisto-Bustools v0.28.2 (Kallisto v0.50.1, Bustools v0.43.2) with default settings. FlyBase gene IDs were translated to gene symbols using org.Dm.eg.db v3.18.0 R package. A table containing all gene symbols used in this dataset, their Flybase IDs, and their annotation symbols are included as a supplement.

#### *Data Processing and Analysis*

After alignment, all datasets were individually filtered in the same manner before integrated analysis.

1) Genes which were captured in 3 or less cells, and cells which contained less than 200 unique genes were removed.

2) Unique genes captured per cell were visualized with a density plot (typically used for continuous data, but used here heuristically), revealing roughly bimodal distributions in each sample. One maxima was near zero (representing “low quality” cells) and the other maxima was between 2000 and 5000 unique genes. A cutoff was drawn at the lowest density value between the two maxima, and the lower half of cells were removed.

3) Cells which were in the 98.5 percentile of unique features and above (potential doublets) were removed

#### **Immunofluorescence**

All larvae were reared at 25C. For each experiment, wandering L3 larvae were picked from non-synchronized stocks and placed into separate vials. They were then irradiated with 4000 rad, or left outside of the irradiator for control. At the end of irradiation, larvae were allowed 4 hours of recovery at 25C. After recovery, 9-15 larvae were picked, dissected in 1x PBS, and fixed. After fixing for 20 minutes in 4% PFA in PBS, carcasses then washed 3x in 0.1% PBST for 10 minutes. Then carcasses were blocked in 10% NGS in 0.1% PBST. After blocking, samples were incubated with primary antibodies in blocking solution overnight at 4C. The next day, samples were washed 3x in PBST for 15 minutes and then incubated with secondary antibodies in blocking solution at 1:500

for 2.5 hours at 25C or overnight at 4C. Samples were washed once in PBST for 5 minutes and then incubated with 1:1000 DAPI in PBST for 20 minutes. Afterwards, samples were washed 2x in PBS for 10 minutes and wing discs were mounted. Wing discs were imaged on an epifluorescent microscope with apotome attachment.

### **EdU Assays**

Larvae were dissected and incubated in Schnieder's *Drosophila* Medium (Thermo Fisher 21720024) at room temperature. Discs were incubated in EdU for 30 minutes. After incubation, discs were fixed in 4% PFA for 15 minutes. EdU staining protocol followed the Click-iT EdU Cell Proliferation Kit, Alexa Fluor 647 (Thermo Fisher C10340).

### **Hybridization Chain Reaction**

All larvae were reared at 25C. For each experiment, about 50 third instar larvae for each condition were placed into vials containing bloomington food for irradiation. Half of the vials were then irradiated at a dose of 4000 rad while the other half were left outside of the irradiator. Larvae were given a four hour recovery time at 25C after irradiation before the beginning of dissection. Dissection took approximately one hour to complete and carcasses were kept on ice until fixation. Our HCR protocol was adapted from Molecular Instruments for use on larval carcasses and used Molecular Instruments reagents. In brief, after fixing in formaldehyde, samples were permeabilized in detergent solution and pre-hybridized in "Probe Hybridization Buffer" for 30 minutes at 37°C. Probe sets for any given gene were made against mRNA sequences conserved between all predicted gene isoforms. After pre-hybridization, samples were incubated in a probe solution consisting of "Probe Hybridization Buffer" and probesets overnight (14-17 hours) at 37°C. Following hybridization, samples were washed using "Probe Wash Buffer" and SSCTween. Samples were then pre-incubated in "Amplification Buffer" for 30 minutes. After pre-incubation in "Amplification Buffer", samples were left in hairpin solution consisting of "Amplification Buffer" and complementary hairpins in the dark at room temperature overnight (12-15 hours). Samples were then washed, incubated with DAPI, and mounted using Invitrogen's Diamond Antifade Mountant. Slides were imaged using a confocal microscope and images were processed using Fiji. For image processing, a max-projection was generated of all images and the signal from each channel of the irradiated samples were auto-adjusted. These adjustments were propagated to all other wing-disc images of the same genotype.

### **Supplementary Tables**

#### **Supplementary Table S2\_T1. Top Markers for each cluster.**

Contains the following columns (**Column**; description): **Subregion**; cluster name  
**Marker\_Integrated\_Global**; Top marker gene when comparing cluster to all other cells

in the integrated data. **Pct\_Diff\_Integrated\_Global**; Percent of cells expressing top marker in cluster of interest minus percent of cells expressing in all other cells in the integrated data. **Marker\_R4K\_Global**; Top marker gene when comparing cluster to all other clusters in the 4000 rad condition. **Pct\_Diff\_R4K\_Global**; Percent of cells expressing top marker in cluster of interest minus percent of cells expressing in all other cells in the 4000 rad condition. **Marker\_R0K\_Global**; Top marker gene when comparing cluster to all other clusters in the 0 rad condition. **Pct\_Diff\_R0K\_Global**; Percent of cells expressing top marker in cluster of interest minus percent of cells expressing in all other cells in the 0 rad condition. **Marker\_Integrated\_Region**; Top marker gene when comparing cluster to all other clusters within its broad PD region in the integrated data. **Pct\_Diff\_Integrated\_Region**; Percent of cells expressing top marker in cluster of interest minus percent of cells expressing in all other cells within its broad PD region in the integrated condition. **Marker\_R4K\_Region**; Top marker gene when comparing cluster to all other clusters within its broad PD region in the 4000 rad condition. **Pct\_Diff\_R4K\_Region**; Percent of cells expressing top marker in cluster of interest minus percent of cells expressing in all other cells within its broad PD region in the 4000 rad condition. **Marker\_R0K\_Region**; Top marker gene when comparing cluster to all other clusters within its broad PD region in the 0 rad condition. **Pct\_Diff\_R0K\_Region**; Percent of cells expressing top marker in cluster of interest minus percent of cells expressing in all other cells within its broad PD region in the 0 rad condition. Markers were only considered if (1) they were expressed in at least 10% of cells in the cluster being considered or its comparison group, (2) there was minimum difference of 10% between the cluster being considered or its comparison group, and (3) there was an enrichment of at least  $\log_2FC=1$  in the cluster being considered. Ties were broken by taking the marker with the higher  $\log_2FC$ .

#### **Supplementary Table S3\_T1. DEG 4000 rad vs 0 rad.**

Contains the following columns (**Column**; description): **gene\_name**; Gene name. **p\_val**; unadjusted p-value of Wilcoxon rank-sum test. **avg\_log2FC**; average  $\log_2FC$  of all cells in 4000 rad condition versus all cells in 0 rad condition. **pct.1**; Percent of cells expressing given gene in 4000 rad condition. **pct.2**; Percent of cells expressing given gene in 0 rad condition. **p\_val\_adj**; Bonferroni corrected p-value from p\_val column (corrected on total genes captured = 13,384). Genes were only included in this table if they were present in at least 1% of cells in either condition, had an adjusted p-value <0.05, and had an average  $\log_2FC$  of  $\geq 0.1$ . This table was produced using the FindMarkers() function in Seurat v5.

**Supplementary Table S3\_T2. Apoptosis, DNA damage response (DDR), response to reactive oxygen species (ROS), cell cycle regulation, transcription factors (TFs), phosphatases, kinases, ligands, and receptors genes considered for HHI comparison (pre-filter).**

Contains the following columns (**Column**; description): **genes\_this\_data**; All genes captured in this data belonging to the considered categories, 1716 total. **Category**; Category each gene is classified into.

**Supplementary Table S3\_T3. Apoptosis, DNA damage response (DDR), response to reactive oxygen species (ROS), cell cycle regulation, transcription factors (TFs), phosphatases, kinases, ligands, and receptors genes considered for HHI comparison (post-filter).**

Contains the following columns (**Column**; description): **gene\_name**; Gene name. Includes all 521 genes used in 3A. **HHI\_4KR**; HHI score in the 4000 rad condition. **max\_logFC**; Maximum log<sub>2</sub>FC when looking at the change in expression within a cluster between conditions. **max\_pct**; Maximum percentage of cells expressing in any cluster. **Group**; Gene category. **Broad\_Group**; Gene category where DDR, ROS, Apoptosis, and Cell Cycle are condensed into a category called “D/R/A/C.”

**Supplementary Table S6\_T1. Cell Cycle Gene Markers for Cell Cycle Based Clusters.**

Contains the following columns (**Column**; description): **gene**; Gene name. **avg\_scaled\_...**; Average scaled expression in each cell cycle cluster (integrated). 6 columns. **Percent\_Expressed\_...**; Percentage of cells expressing given gene in each cell cycle cluster (integrated). 6 columns. This table includes all 175 genes used in cell cycle based clustering.

**Supplementary Table S7\_T1. Highly Induced Gene Markers for Cell Cycle Based Clusters.**

This table includes the 359 genes that are highly induced after irradiation. These genes are expressed in at least 1% of cells in either condition, have an average log<sub>2</sub>FC  $\geq 1$ , and an adjusted p-value  $< 0.05$ . Contains the following columns (**Column**; description): **gene**; Gene name. **avg\_scaled\_...**; Average scaled expression in each cell cycle cluster in the 4000 rad condition. 6 columns. **Percent\_Expressed\_...**; Percentage of cells expressing given gene in each cell cycle cluster in the 4000 rad condition. 6 columns.

## **2.6 Acknowledgements**

We are grateful to Nitya Mani for educating us on mathematical approaches to the study of heterogeneity, especially the Herfindahl-Hirschman Index. We thank Karthik Shekhar, Peter Sudmant, and Nicholas Everetts for their input on computational analyses. We thank Rebecca Chang for assistance in single-cell sample collection. We thank past and present members of the Hariharan Lab for their help dissecting larvae for scRNA-seq: Allie Cho, Nick Everetts, Sophia Friesen, Triny Ravindran, Danielle Spitzer, Melanie Worley, Ishita Srivastava, and Edgar Zepeda. We also thank Stephan Uwe Gerlach for his help with dissections. We thank Justin Choi for his preparation of 10x libraries. We thank Twinkle Bansal for proofreading the manuscript. We thank Gary Karpen for the p-H2Av antibody, the Developmental Studies Hybridoma Bank for antibodies and the Bloomington Drosophila Stock center for fly stocks and FlyBase for hosting an invaluable compilation of information. This work was funded by an NIH grant R35 GM122490 (to IKH) and an NSF GRFP to JC.

## 2.7 Chapter 2 References

- Ackermann, M. (2015). A functional perspective on phenotypic heterogeneity in microorganisms. *Nature Reviews Microbiology*, 13(8), 497–508.  
<https://doi.org/10.1038/nrmicro3491>
- Akdemir, F., Christich, A., Sogame, N., Chapo, J., & Abrams, J. M. (2007). P53 directs focused genomic responses in *Drosophila*. *Oncogene*, 26(36), 5184–5193.  
<https://doi.org/10.1038/sj.onc.1210328>
- Bageritz, J., Willnow, P., Valentini, E., Leible, S., Boutros, M., & Teleman, A. A. (2019). Gene expression atlas of a developing tissue by single cell expression correlation analysis. *Nature Methods*, 16(8), 750–756. <https://doi.org/10.1038/s41592-019-0492-x>
- Blanco, E., Ruiz-Romero, M., Beltran, S., Bosch, M., Punset, A., Serras, F., & Corominas, M. (2010). Gene expression following induction of regeneration in *Drosophila* wing imaginal discs. Expression profile of regenerating wing discs. *BMC Developmental Biology*, 10(1), 94. <https://doi.org/10.1186/1471-213X-10-94>
- Brodsky, M. H., Nordstrom, W., Tsang, G., Kwan, E., Rubin, G. M., & Abrams, J. M. (2000). *Drosophila* p53 Binds a Damage Response Element at the reaper Locus. *Cell*, 101(1), 103–113. [https://doi.org/10.1016/S0092-8674\(00\)80627-3](https://doi.org/10.1016/S0092-8674(00)80627-3)
- Brodsky, M. H., Weinert, B. T., Tsang, G., Rong, Y. S., McGinnis, N. M., Golic, K. G., Rio, D. C., & Rubin, G. M. (2004). *Drosophila melanogaster* MNK/Chk2 and p53 Regulate Multiple DNA Repair and Apoptotic Pathways following DNA Damage. *Molecular and Cellular Biology*, 24(3), 1219–1231.  
<https://doi.org/10.1128/MCB.24.3.1219-1231.2004>

- Brown, J., Bush, I., Bozon, J., & Su, T. T. (2020). Cells with loss-of-heterozygosity after exposure to ionizing radiation in *Drosophila* are culled by p53-dependent and p53-independent mechanisms. *PLoS Genetics*, *16*(10), e1009056. <https://doi.org/10.1371/journal.pgen.1009056>
- Butler, M. J., Jacobsen, T. L., Cain, D. M., Jarman, M. G., Hubank, M., Whittle, J. R. S., Phillips, R., & Simcox, A. (2003). Discovery of genes with highly restricted expression patterns in the *Drosophila* wing disc using DNA oligonucleotide microarrays. *Development*, *130*(4), 659–670. <https://doi.org/10.1242/dev.00293>
- Capilla, A., Karachentsev, D., Patterson, R. A., Hermann, A., Juarez, M. T., & McGinnis, W. (2017). Toll pathway is required for wound-induced expression of barrier repair genes in the *Drosophila* epidermis. *Proceedings of the National Academy of Sciences*, *114*(13). <https://doi.org/10.1073/pnas.1613917114>
- Carvalho, L., Jacinto, A., & Matova, N. (2014). The Toll/NF- $\kappa$ B signaling pathway is required for epidermal wound repair in *Drosophila*. *Proceedings of the National Academy of Sciences*, *111*(50). <https://doi.org/10.1073/pnas.1408224111>
- Córdoba, S., & Estella, C. (2018). The transcription factor Dysfusion promotes fold and joint morphogenesis through regulation of Rho1. *PLoS Genetics*, *14*(8), e1007584. <https://doi.org/10.1371/journal.pgen.1007584>
- Cosolo, A., Jaiswal, J., Csordás, G., Grass, I., Uhlirova, M., & Classen, A.-K. (2019). JNK-dependent cell cycle stalling in G2 promotes survival and senescence-like phenotypes in tissue stress. *eLife*, *8*, e41036. <https://doi.org/10.7554/eLife.41036>
- Deng, M., Wang, Y., Zhang, L., Yang, Y., Huang, S., Wang, J., Ge, H., Ishibashi, T., & Yan, Y. (2019). Single cell transcriptomic landscapes of pattern formation,

- proliferation and growth in *Drosophila* wing imaginal discs. *Development*, dev.179754. <https://doi.org/10.1242/dev.179754>
- Dong, Y.-L., Vadla, G. P., Lu, J.-Y., Ahmad, V., Klein, T. J., Liu, L.-F., Glazer, P. M., Xu, T., & Chabu, C.-Y. (2021). Cooperation between oncogenic Ras and wild-type p53 stimulates STAT non-cell autonomously to promote tumor radioresistance. *Communications Biology*, 4(1), 374. <https://doi.org/10.1038/s42003-021-01898-5>
- Everetts, N. J., Worley, M. I., Yasutomi, R., Yosef, N., & Hariharan, I. K. (2021). Single-cell transcriptomics of the *Drosophila* wing disc reveals instructive epithelium-to-myoblast interactions. *eLife*, 10, e61276. <https://doi.org/10.7554/eLife.61276>
- Floc'hlay, S., Balaji, R., Stanković, D., Christiaens, V. M., Bravo González-Blas, C., De Winter, S., Hulselmans, G. J., De Waegeneer, M., Quan, X., Koldere, D., Atkins, M., Halder, G., Uhlirova, M., Classen, A.-K., & Aerts, S. (2023). Shared enhancer gene regulatory networks between wound and oncogenic programs. *eLife*, 12, e81173. <https://doi.org/10.7554/eLife.81173>
- Gunage, R. D., Reichert, H., & VijayRaghavan, K. (2014). Identification of a new stem cell population that generates *Drosophila* flight muscles. *eLife*, 3, e03126. <https://doi.org/10.7554/eLife.03126>
- Guo, X., & Chen, L. (2024). From G1 to M: A comparative study of methods for identifying cell cycle phases. *Briefings in Bioinformatics*, 25(2), bbad517. <https://doi.org/10.1093/bib/bbad517>
- Harper, J. W., & Elledge, S. J. (2007). The DNA Damage Response: Ten Years After. *Molecular Cell*, 28(5), 739–745. <https://doi.org/10.1016/j.molcel.2007.11.015>
- Harris, R. E., Stinchfield, M. J., Nystrom, S. L., McKay, D. J., & Hariharan, I. K. (2020).

Damage-responsive, maturity-silenced enhancers regulate multiple genes that direct regeneration in *Drosophila*. *eLife*, 9, e58305.

<https://doi.org/10.7554/eLife.58305>

Harrison, D. A., McCoon, P. E., Binari, R., Gilman, M., & Perrimon, N. (1998).

*Drosophila unpaired* encodes a secreted protein that activates the JAK signaling pathway. *Genes & Development*, 12(20), 3252–3263.

<https://doi.org/10.1101/gad.12.20.3252>

Haynie, J. L., & Bryant, P. J. (1977). The effects of X-rays on the proliferation dynamics of cells in the imaginal wing disc of *Drosophila melanogaster*. *Wilhelm Roux's Archives of Developmental Biology*, 183(2), 85–100.

<https://doi.org/10.1007/BF00848779>

Hendzel, M. J., Wei, Y., Mancini, M. A., Van Hooser, A., Ranalli, T., Brinkley, B. R., Bazett-Jones, D. P., & Allis, C. D. (1997). Mitosis-specific phosphorylation of histone H3 initiates primarily within pericentromeric heterochromatin during G2 and spreads in an ordered fashion coincident with mitotic chromosome condensation. *Chromosoma*, 106(6), 348–360.

<https://doi.org/10.1007/s004120050256>

Herfindahl, O. (1950). *Concentration In The Steel Industry*. Columbia University.

Herrera, S. C., & Bach, E. A. (2019). JAK/STAT signaling in stem cells and regeneration: From *Drosophila* to vertebrates. *Development*, 146(2), dev167643.

<https://doi.org/10.1242/dev.167643>

Hirschman, A. O. (1945). *National Power and the Structure of Foreign Trade*. University of California Press.

- Ip, Y. (1993). Dif, a dorsal-related gene that mediates an immune response in *Drosophila*. *Cell*, 75(4), 753–763. [https://doi.org/10.1016/0092-8674\(93\)90495-C](https://doi.org/10.1016/0092-8674(93)90495-C)
- James, A. A., & Bryant, P. J. (1981). A Quantitative Study of Cell Death and Mitotic Inhibition in  $\gamma$ -Irradiated Imaginal Wing Discs of *Drosophila melanogaster*. *Radiation Research*, 87(3), 552. <https://doi.org/10.2307/3575520>
- Jiang, L., & Crews, S. T. (2003). The *Drosophila dysfusion* Basic Helix-Loop-Helix (bHLH)–PAS Gene Controls Tracheal Fusion and Levels of the Trachealess bHLH-PAS Protein. *Molecular and Cellular Biology*, 23(16), 5625–5637. <https://doi.org/10.1128/MCB.23.16.5625-5637.2003>
- Katsuyama, T., Comoglio, F., Seimiya, M., Cabuy, E., & Paro, R. (2015). During *Drosophila* disc regeneration, JAK/STAT coordinates cell proliferation with Dilp8-mediated developmental delay. *Proceedings of the National Academy of Sciences*, 112(18). <https://doi.org/10.1073/pnas.1423074112>
- Khalili, D., Mohammed, M., Kunc, M., Sindlerova, M., Ankarklev, J., & Theopold, U. (2023). Single-cell sequencing of tumor-associated macrophages in a *Drosophila* model. *Frontiers in Immunology*, 14, 1243797. <https://doi.org/10.3389/fimmu.2023.1243797>
- Khan, C., & Baker, N. E. (2022). *The DNA Damage response and cell competition are p53- and Xrp1-dependent processes that suppress hyperplastic aneuploidy*. <https://doi.org/10.1101/2022.06.06.494998>
- Kurtz, P., Jones, A. E., Tiwari, B., Link, N., Wylie, A., Tracy, C., Krämer, H., & Abrams, J. M. (2019). *Drosophila* p53 directs nonapoptotic programs in postmitotic tissue. *Molecular Biology of the Cell*, 30(11), 1339–1351.

<https://doi.org/10.1091/mbc.E18-12-0791>

- Ledru, M., Clark, C. A., Brown, J., Verghese, S., Ferrara, S., Goodspeed, A., & Su, T. T. (2022). Differential gene expression analysis identified determinants of cell fate plasticity during radiation-induced regeneration in *Drosophila*. *PLOS Genetics*, *18*(1), e1009989. <https://doi.org/10.1371/journal.pgen.1009989>
- Lee, C.-Y., Clough, E. A., Yellon, P., Teslovich, T. M., Stephan, D. A., & Baehrecke, E. H. (2003). Genome-Wide Analyses of Steroid- and Radiation-Triggered Programmed Cell Death in *Drosophila*. *Current Biology*, *13*(4), 350–357. [https://doi.org/10.1016/S0960-9822\(03\)00085-X](https://doi.org/10.1016/S0960-9822(03)00085-X)
- Levine, A. J. (2020). p53: 800 million years of evolution and 40 years of discovery. *Nature Reviews Cancer*, *20*(8), 471–480. <https://doi.org/10.1038/s41568-020-0262-1>
- Lu, H., Yan, H., Li, X., Xing, Y., Ye, Y., Jiang, S., Ma, L., Ping, J., Zuo, H., Hao, Y., Yu, C., Li, Y., Zhou, G., & Lu, Y. (2023). Single-cell map of dynamic cellular microenvironment of radiation-induced intestinal injury. *Communications Biology*, *6*(1), 1248. <https://doi.org/10.1038/s42003-023-05645-w>
- Martín, F. A., Herrera, S. C., & Morata, G. (2009). Cell competition, growth and size control in the *Drosophila* wing imaginal disc. *Development*, *136*(22), 3747–3756. <https://doi.org/10.1242/dev.038406>
- Mata, J., Curado, S., Ephrussi, A., & Rørth, P. (2000). Tribbles Coordinates Mitosis and Morphogenesis in *Drosophila* by Regulating String/CDC25 Proteolysis. *Cell*, *101*(5), 511–522. [https://doi.org/10.1016/S0092-8674\(00\)80861-2](https://doi.org/10.1016/S0092-8674(00)80861-2)
- McBride, W. H., & Schaeue, D. (2020). Radiation-induced tissue damage and response.

- The Journal of Pathology*, 250(5), 647–655. <https://doi.org/10.1002/path.5389>
- McGough, I. J., Vecchia, L., Bishop, B., Malinauskas, T., Beckett, K., Joshi, D., O'Reilly, N., Siebold, C., Jones, E. Y., & Vincent, J.-P. (2020). Glypicans shield the Wnt lipid moiety to enable signalling at a distance. *Nature*, 585(7823), 85–90. <https://doi.org/10.1038/s41586-020-2498-z>
- McNamee, L. M., & Brodsky, M. H. (2009). P53-Independent Apoptosis Limits DNA Damage-Induced Aneuploidy. *Genetics*, 182(2), 423–435. <https://doi.org/10.1534/genetics.109.102327>
- Mills, M., Emori, C., Kumar, P., Boucher, Z., George, J., & Bolcun-Filas, E. (2025). Single-cell and bulk transcriptional profiling of mouse ovaries reveals novel genes and pathways associated with DNA damage response in oocytes. *Developmental Biology*, 517, 55–72. <https://doi.org/10.1016/j.ydbio.2024.09.007>
- Moon, N.-S., Frolov, M. V., Kwon, E.-J., Di Stefano, L., Dimova, D. K., Morris, E. J., Taylor-Harding, B., White, K., & Dyson, N. J. (2005). Drosophila E2F1 Has Context-Specific Pro- and Antiapoptotic Properties during Development. *Developmental Cell*, 9(4), 463–475. <https://doi.org/10.1016/j.devcel.2005.08.015>
- Morral, C., Ayyaz, A., Kuo, H.-C., Fink, M., Verginadis, I. I., Daniel, A. R., Burner, D. N., Driver, L. M., Satow, S., Hasapis, S., Ghinnagow, R., Luo, L., Ma, Y., Attardi, L. D., Koumenis, C., Minn, A. J., Wrana, J. L., Lee, C.-L., & Kirsch, D. G. (2024). P53 promotes revival stem cells in the regenerating intestine after severe radiation injury. *Nature Communications*, 15(1), 3018. <https://doi.org/10.1038/s41467-024-47124-8>
- Mukherjee, A., Epperly, M. W., Shields, D., Hou, W., Fisher, R., Hamade, D., Wang, H.,

- Saiful Huq, M., Bao, R., Tabib, T., Monier, D., Watkins, S., Calderon, M., & Greenberger, J. S. (2021). Ionizing irradiation-induced Fgr in senescent cells mediates fibrosis. *Cell Death Discovery*, 7(1), 349.  
<https://doi.org/10.1038/s41420-021-00741-4>
- Muller, H. J. (1927). Artificial Transmutation of the Gene. *Science*, 66(1699), 84–87.  
<https://doi.org/10.1126/science.66.1699.84>
- Mulligan, K. A., Fuerer, C., Ching, W., Fish, M., Willert, K., & Nusse, R. (2012). Secreted Wingless-interacting molecule (Swim) promotes long-range signaling by maintaining Wingless solubility. *Proceedings of the National Academy of Sciences*, 109(2), 370–377. <https://doi.org/10.1073/pnas.1119197109>
- Ogura, K., Magae, J., Kawakami, Y., & Koana, T. (2009). Reduction in Mutation Frequency by Very Low-Dose Gamma Irradiation of *Drosophila melanogaster* Germ Cells. *Radiation Research*, 171(1), 1–8. <https://doi.org/10.1667/RR1288.1>
- Ollmann, M., Young, L. M., Di Como, C. J., Karim, F., Belvin, M., Robertson, S., Whittaker, K., Demsky, M., Fisher, W. W., Buchman, A., Duyk, G., Friedman, L., Prives, C., & Kopczynski, C. (2000). *Drosophila* p53 Is a Structural and Functional Homolog of the Tumor Suppressor p53. *Cell*, 101(1), 91–101.  
[https://doi.org/10.1016/S0092-8674\(00\)80626-1](https://doi.org/10.1016/S0092-8674(00)80626-1)
- Pizzul, P., Casari, E., Gnugnoli, M., Rinaldi, C., Corallo, F., & Longhese, M. P. (2022). The DNA damage checkpoint: A tale from budding yeast. *Frontiers in Genetics*, 13, 995163. <https://doi.org/10.3389/fgene.2022.995163>
- Rajan, A., & Perrimon, N. (2012). *Drosophila* Cytokine Unpaired 2 Regulates Physiological Homeostasis by Remotely Controlling Insulin Secretion. *Cell*,

151(1), 123–137. <https://doi.org/10.1016/j.cell.2012.08.019>

Romão, D., Muzzopappa, M., Barrio, L., & Milán, M. (2021). The Upd3 cytokine couples inflammation to maturation defects in *Drosophila*. *Current Biology*, *31*(8), 1780–1787.e6. <https://doi.org/10.1016/j.cub.2021.01.080>

Ruiz-Losada, M., González, R., Peropadre, A., Gil-Gálvez, A., Tena, J. J., Baonza, A., & Estella, C. (2022). Coordination between cell proliferation and apoptosis after DNA damage in *Drosophila*. *Cell Death & Differentiation*, *29*(4), 832–845. <https://doi.org/10.1038/s41418-021-00898-6>

Salic, A., & Mitchison, T. J. (2008). A chemical method for fast and sensitive detection of DNA synthesis *in vivo*. *Proceedings of the National Academy of Sciences*, *105*(7), 2415–2420. <https://doi.org/10.1073/pnas.0712168105>

Seimiya, M., & Gehring, W. J. (2000). The *Drosophila* homeobox gene *optix* is capable of inducing ectopic eyes by an *eyeless*-independent mechanism. *Development*, *127*(9), 1879–1886. <https://doi.org/10.1242/dev.127.9.1879>

Sekelsky, J. (2017). DNA Repair in *Drosophila*: Mutagens, Models, and Missing Genes. *Genetics*, *205*(2), 471–490. <https://doi.org/10.1534/genetics.116.186759>

Sheng, X., Lin, Z., Lv, C., Shao, C., Bi, X., Deng, M., Xu, J., Guerrero-Juarez, C. F., Li, M., Wu, X., Zhao, R., Yang, X., Li, G., Liu, X., Wang, Q., Nie, Q., Cui, W., Gao, S., Zhang, H., ... Yu, Z. (2020). Cycling Stem Cells Are Radioresistant and Regenerate the Intestine. *Cell Reports*, *32*(4), 107952. <https://doi.org/10.1016/j.celrep.2020.107952>

Shlevkov, E., & Morata, G. (2012). A dp53/JNK-dependant feedback amplification loop is essential for the apoptotic response to stress in *Drosophila*. *Cell Death &*

- Differentiation*, 19(3), 451–460. <https://doi.org/10.1038/cdd.2011.113>
- Simões, A. R., Neto, M., Alves, C. S., Santos, M. B., Fernández-Hernández, I., Veiga-Fernandes, H., Brea, D., Durá, I., Encinas, J. M., & Rhiner, C. (2022). Damage-responsive neuro-glial clusters coordinate the recruitment of dormant neural stem cells in *Drosophila*. *Developmental Cell*, 57(13), 1661-1675.e7. <https://doi.org/10.1016/j.devcel.2022.05.015>
- Song, Z., McCall, K., & Steller, H. (1997). DCP-1, a *Drosophila* Cell Death Protease Essential for Development. *Science*, 275(5299), 536–540. <https://doi.org/10.1126/science.275.5299.536>
- Steele, L. G., Bostic, A., Lynch, S. M., & Abdelaaty, L. (2022). Measuring Ethnic Diversity. *Annual Review of Sociology*, 48(1), 43–63. <https://doi.org/10.1146/annurev-soc-030420-015435>
- Toggweiler, J., Willecke, M., & Basler, K. (2016). The transcription factor Ets21C drives tumor growth by cooperating with AP-1. *Scientific Reports*, 6(1), 34725. <https://doi.org/10.1038/srep34725>
- Tripathi, B. K., & Irvine, K. D. (2022). The wing imaginal disc. *Genetics*, 220(4), iyac020. <https://doi.org/10.1093/genetics/iyac020>
- Tsai, C.-R., Wang, Y., Jacobson, A., Sankoorikkal, N., Chirinos, J. D., Burra, S., Makthal, N., Kumaraswami, M., & Galko, M. J. (2022). Pvr and distinct downstream signaling factors are required for hemocyte spreading and epidermal wound closure at *Drosophila* larval wound sites. *G3 Genes/Genomes/Genetics*, 12(1), jkab388. <https://doi.org/10.1093/g3journal/jkab388>
- Van Bergeijk, P., Heimiller, J., Uyetake, L., & Su, T. T. (2012). Genome-Wide

- Expression Analysis Identifies a Modulator of Ionizing Radiation-Induced p53-Independent Apoptosis in *Drosophila melanogaster*. *PLoS ONE*, 7(5), e36539. <https://doi.org/10.1371/journal.pone.0036539>
- Verghese, S., & Su, T. T. (2016). *Drosophila* Wnt and STAT Define Apoptosis-Resistant Epithelial Cells for Tissue Regeneration after Irradiation. *PLoS Biology*, 14(9), e1002536. <https://doi.org/10.1371/journal.pbio.1002536>
- Wells, B. S., & Johnston, L. A. (2012). Maintenance of imaginal disc plasticity and regenerative potential in *Drosophila* by p53. *Developmental Biology*, 361(2), 263–276. <https://doi.org/10.1016/j.ydbio.2011.10.012>
- Wells, B. S., Yoshida, E., & Johnston, L. A. (2006). Compensatory Proliferation in *Drosophila* Imaginal Discs Requires Dronc-Dependent p53 Activity. *Current Biology*, 16(16), 1606–1615. <https://doi.org/10.1016/j.cub.2006.07.046>
- Wichmann, A., Jaklevic, B., & Su, T. T. (2006). Ionizing radiation induces caspase-dependent but Chk2- and p53-independent cell death in *Drosophila melanogaster*. *Proceedings of the National Academy of Sciences*, 103(26), 9952–9957. <https://doi.org/10.1073/pnas.0510528103>
- Withers, H. R. (1975). The Four R's of Radiotherapy. In *Advances in Radiation Biology* (Vol. 5, pp. 241–271). Elsevier. <https://doi.org/10.1016/B978-0-12-035405-4.50012-8>
- Worley, M. I., Everetts, N. J., Yasutomi, R., Chang, R. J., Saretha, S., Yosef, N., & Hariharan, I. K. (2022). Ets21C sustains a pro-regenerative transcriptional program in blastema cells of *Drosophila* imaginal discs. *Current Biology*, 32(15), 3350-3364.e6. <https://doi.org/10.1016/j.cub.2022.06.040>

- Worley, M. I., Setiawan, L., & Hariharan, I. K. (2013). TIE-DYE: A combinatorial marking system to visualize and genetically manipulate clones during development in *Drosophila melanogaster*. *Development*, *140*(15), 3275–3284.  
<https://doi.org/10.1242/dev.096057>
- Xie, H. B., & Golic, K. G. (2004). Gene Deletions by Ends-In Targeting in *Drosophila melanogaster*. *Genetics*, *168*(3), 1477–1489.  
<https://doi.org/10.1534/genetics.104.030882>
- Yuan, T., Zhang, J., Zhao, Y., Guo, Y., & Fan, S. (2023). Single-cell RNA sequencing of intestinal crypts reveals vital events in damage repair and the double-edged sword effect of the Wnt3/ $\beta$ -catenin pathway in irradiated mice. *Redox Biology*, *68*, 102942. <https://doi.org/10.1016/j.redox.2023.102942>
- Zappia, M. P., De Castro, L., Ariss, M. M., Jefferson, H., Islam, A. B., & Frolov, M. V. (2020). A cell atlas of adult muscle precursors uncovers early events in fibre-type divergence in *Drosophila*. *EMBO Reports*, *21*(10), e49555.  
<https://doi.org/10.15252/embr.201949555>
- Zhang, Y., Lin, N., Carroll, P. M., Chan, G., Guan, B., Xiao, H., Yao, B., Wu, S. S., & Zhou, L. (2008). Epigenetic Blocking of an Enhancer Region Controls Irradiation-Induced Proapoptotic Gene Expression in *Drosophila* Embryos. *Developmental Cell*, *14*(4), 481–493. <https://doi.org/10.1016/j.devcel.2008.01.018>